BIODEGRADABLE POLY(ESTER-URETHANE) SCAFFOLDS FOR BONE TISSUE ENGINEERING

A THESIS SUBMITTED TO
THE GRADUATE SCHOOL OF NATURAL AND APPLIED SCIENCES
OF
MIDDLE EAST TECHNICAL UNIVERSITY

BY

AYSEL KIZILTAY

IN PARTIAL FULFILLMENT OF THE REQUIREMENTS
FOR
THE DEGREE OF DOCTOR OF PHILOSOPHY
IN
BIOTECHNOLOGY

SEPTEMBER 2011

Approval of the thesis:

BIODEGRADABLE POLY(ESTER-URETHANE) SCAFFOLDS FOR BONE TISSUE ENGINEERING

submitted by **AYSEL KIZILTAY** in partial fulfillment of the requirements for the degree of **Doctor of Philosophy in Biotechnology Department, Middle East Technical University** by,

Prof. Dr. Canan Özgen _____
Dean, Graduate School of **Natural and Applied Sciences**

Prof. Dr. İnci Eroğlu _____
Head of Department, **Biotechnology**

Prof. Dr. Nesrin Hasırcı _____
Supervisor, **Chemistry Dept., METU**

Prof. Julio San Roman _____
Co-Supervisor, **CSIC, SPAIN**

Examining Committee Members:

Prof. Dr. Aşkın Tümer _____
Dept. of Biology, Hacettepe University

Prof. Dr. Nesrin Hasırcı _____
Dept. of Chemistry, METU

Prof. Dr. Meral Yücel _____
Dept. of Biological Sciences, METU

Prof. Dr. İnci Eroğlu _____
Dept. of Chemical Engineering, METU

Assoc. Prof. Dr. Ayşen Tezcaner _____
Dept. of Engineering Sciences, METU

Date: 14.09.2011

I hereby declare that all information in this document has been obtained and presented in accordance with academic rules and ethical conduct. I also declare that, as required by these rules and conduct, I have fully cited and referenced all material and results that are not original to this work.

Name, Last name: Aysel Kızıltay

Signature:

ABSTRACT

BIODEGRADABLE POLY(ESTER-URETHANE) SCAFFOLDS FOR BONE TISSUE ENGINEERING

Kızıltay, Aysel
Ph.D., Department of Biotechnology
Supervisor: Prof. Dr. Nesrin Hasırcı

September 2011, 128 pages

During last decade, polyurethanes (PUs) which are able to degrade into harmless molecules upon implantation have received a significant level of attention as a biomaterial in tissue engineering applications. Many studies are focused especially on development of PUs based on amino acid derivatives; however, there are only few applications of amino acid based PUs in tissue engineering. In this study, a biocompatible and biodegradable thermoplastic poly(ester-urethane) (PEU) based on L-lysine diisocyanate (LDI) and polycaprolactone diol (PCL) was synthesized and used for the preparation of two dimensional (2D) films and three dimensional (3D) scaffolds. The resulting polymer was casted as 2D films for full characterization purpose and it was found that it is highly elastic with modulus of elasticity ~12 MPa. Surfaces of 2Ds were modified via micropatterning and fibrinogen coating to check the material-cell interaction. The 3D scaffolds were obtained by salt leaching and rapid

prototyping (bioplotting) techniques. The 3D scaffolds had various pore size and porosity with different mechanical strength. The bioplotted scaffolds had uniform pore size of ~450 μm and exhibited higher compressive modulus (~4.7 MPa) compared to those obtained by salt leaching (~147 kPa). Salt leached 3D scaffolds had inhomogenous pore size distribution in the range of 5 μm - 350 μm and demonstrated greatest degradation profile compared to 2D films and 3D bioplotted samples under enzymatic condition. Rat bone marrow stem cells (BMSCs) were used to investigate the biocompatibility of the polymer and suitability of fabricated scaffolds for osteogenesis. Presence of micropatterns on 2D matrices did not show any influence on osteoblastic function, but presence of fibrinogen enhanced cell attachment and proliferation. All of the fabricated 3D PEU matrices supported proliferation, osteoblastic differentiation and extracellular matrix (ECM) deposition with highest osteoblastic activity on bioplotted scaffolds which confirmed by von Kossa staining and EDX analysis. The results indicated that the synthesized PEU based scaffolds were able to induce osteoblastic differentiation and mineralization of BMSC and therefore these scaffolds can be good candidates to be used in bone tissue engineering.

Keywords: Bone tissue engineering, Polyurethane, Lysine, Rapid prototyping, Salt leaching

ÖZ

KEMİK DOKU MÜHENDİSLİĞİ İÇİN BİYOBOZUNUR POLİ(ESTER-ÜRETAN) DESTEK YAPILAR

Kızıltay, Aysel
Doktora, Biyoteknoloji Bölümü
Tez Yöneticisi: Prof. Dr. Nesrin Hasırcı

Eylül 2011, 128 sayfa

Son on yılda, vücut içine yerleştirildikten sonra zararsız bileşenlere parçalanabilen poliüretanlar (PU) biyomalzeme olarak doku mühendisliği uygulamalarında oldukça dikkat çekmiştir. Birçok çalışma özellikle amino asit temelli PU'ların geliştirilmesine odaklanmış olduğu halde, amino asit bazlı PU'ların doku mühendisliğine yönelik uygulamaları çok azdır. Bu çalışmada, lisin diizosiyanat (LDI) ve polikaprolakton diol (PCL) temelli biyouyumlu ve biyobozunur termoplastik bir poli(ester-üretan) (PEU) sentezlenmiş, iki boyutlu (2D) ve üç boyutlu (3D) destek yapıların hazırlanmasında kullanılmıştır. Elde edilen polimer tam karakterizasyon için 2D film olarak elde edilmiş ve polimerin ~12 MPa'lık bir elastik modulüs değeriyle birlikte oldukça elastik bir yapıya sahip olduğu bulunmuştur. 2D yapıların yüzeyleri, malzeme-hücre etkileşimini incelemek amacıyla mikrodesenleme ve fibrinojen kaplama ile değiştirilmiştir. 3D

iskele yapılar tuz uzaklaştırma ve hızlı prototiplendirme (bioplotting) teknikleriyle elde edilmiştir. 3D iskele yapılar farklı gözenek boyutu ve mekanik dayanım göstermiştir. Bioplotting tekniğiyle elde edilen iskele yapılar ~450 μm büyüklükte homojen gözenek boyutuna sahip olup tuz uzaklaştırma tekniğiyle elde edilen yapılardan (~147 kPa) daha büyük basma modulüsü (~4.7 MPa) göstermiştir. Tuz uzaklaştırma ile elde edilen 3D iskele yapılar, 5 μm - 350 μm aralığında eşit olmayan gözenek boyutu dağılımına sahip olup enzimli ortamda film ve bioplotting ile elde edilen yapılara göre daha hızlı bozunma profili göstermiştir. Polimerin biyouyumluluğu ve elde edilen destek yapıların osteogenesis için uygunluğunun araştırılmasında fare kemik iliği kök hücreleri (BMSC) kullanılmıştır. 2D yapılar üzerinde mikrodesen varlığı, osteoblastik işlev üzerinde bir etki göstermezken fibrinojen varlığı hücre yapışmasını ve çoğalmasını arttırmıştır. von Kossa boyama ve EDX analiziyle doğrulanan sonuçlara göre, üretilen bütün 3D PEU destek yapılar hücre çoğalmasını, osteoblastik farklılaşmayı ve hücre dışı matrisin (ECM) birikmesini desteklemiştir ve en yüksek osteoblastik aktivite, bioplotting ile elde edilen yapılar üzerinde görülmüştür. Sonuçlar, sentezlenen PEU temelli iskele yapıların BMSC'lerin osteoblastik hücreye farklılaşmasını ve mineralizasyonunu uyarabildiğini göstermiştir ve bu nedenle, bu iskele yapılar kemik doku mühendisliğine yönelik kullanım için uygun adaylar olabilirler.

Anahtar Kelimeler: Kemik doku mühendisliği, Poliüretan, Lizin, Hızlı prototip, Tuz uzaklaştırma

To my family...

ACKNOWLEDGEMENTS

I would like to express my special thanks to my supervisor Prof. Dr. Nesrin Hasırcı for her continuous guidance, encouragement, motivation and support during all the stages of my thesis. I sincerely appreciate the time and effort she has spent to improve my experience during my graduate years.

I am also deeply thankful to Prof. Dr. Vasıf Hasırcı for his support, leadership and guidance in METU-BIOMAT Biomaterials and Tissue Engineering Research Group.

My sincere acknowledgements go to my thesis progress committee members, Prof. Dr. Aşkın Tümer and Prof. Dr. Meral Yücel for their helpful comments and suggestions throughout this thesis.

I am grateful to Prof. Dr. Julio San Roman, Dr. Angel M. Fernandez and for their guidance during the stage of polymer synthesis and characterization studies at CSIC, Madrid. Also, I am thankful to Dr. Alberto Gallardo for his endless help and company in laboratory and outlife in Madrid. I am grateful to all people in polymer department in CSIC.

I wish to thank Prof. Dr. Rui Reis for providing me a good opportunity to work in his research laboratory. I would like to acknowledge Dr. Rui Amandi de Sousa for his help during my experiments. I also would like to thank to all members of 3B's Research Group for their support during my stay in Portugal.

I deeply thank to special lab mates Tuğba Endoğan, Eda Ayşe Aksoy, Cantürk Özcan, İsmail Doğan Günbaş, Taylan Özerkan, Elif Vardar, Cansel Işıklı, Aysun Güney, Şeniz Uçar, Filiz Kara and other lab members of D-148 for the good memories, continuous help and support during my experiments. I also would like to thank my roommates, especially to Eylem Yalçınkaya, Mine Kalkancı and Aydan Bahadır for their support and friendship during graduate years.

I am thankful to Dr. Deniz Yücel and Dr. Halime Kenar who teached me cell culture techniques and supported me throughout all the stages of my graduate years.

I deeply thank all the members of METU-BIOMAT group, especially Dr. Pınar Yılgör, Arda Büyüksungur, Albana Ndreu, Beste Kınıkoğlu and Hayriye Özçelik. I also would like to thank Mr. Zeynel Akın for his endless technical support throughout my research.

I would like to thank to METU Central Laboratory for characterization analyses.

This study was supported by METU-BAP 2005-07-02-00-92 and FP6 European Network of Excellence project EXPERTISSUES and these grants are gratefully acknowledged. I also would like to acknowledge the support from TUBITAK through projects TBAG 105T508 and 108T805, 104M432.

Finally, I would like to thank to my mother Fatma Kızıltay, my father Hilmi Kızıltay and my brothers Murat and Şenol Kızıltay, for the love and patience they have shown throughout all my life.

TABLE OF CONTENTS

ABSTRACT iv
ÖZ……. vi
ACKNOWLEDGEMENTS ix
TABLE OF CONTENTS xi
LIST OF TABLES xv
LIST OF FIGURES xvi
ABBREVIATIONS xix
CHAPTERS
1. INTRODUCTION 1
1.1 Bone Physiology 1
1.1.1 Bone Composition and Structure 1
1.1.2 Extracellular Bone Matrix 4
1.1.2.1 Mineral (Inorganic) Phase 5
1.1.2.2 Organic Phase 6
1.1.3 Dependence of Bone Architecture on Anatomical Locations, Age and Gender 7
1.1.4 Bone Regeneration and Remodeling 8
1.1.5 Bone Grafts (Autologous, Allografts, Xenografts) 9
1.1.6 Classification of Tissue Response 10
1.1.7 Bone Graft Substitutes (BGS) 12
1.1.7.1 Human Bone Matrix and Demineralized Bone Matrix. 12
1.1.7.2 Ceramic Biomaterials (Calcium Orthophosphates). 13
1.1.7.3 Natural Coral and Other Marine Biomaterials. 14
1.2 Tissue Engineering of Bone 15

1.3 Biomaterials Used for Tissue Engineering Scaffolds 16
1.4 Engineered Cells 21
1.4.1 Bone Morphogenetic Proteins and Osteogenic Supplements 22
1.5 Fabrication Techniques in Scaffold Development 23
1.5.1 Fiber Bonding Technique 25
1.5.2 Solvent Casting and Particulate Leaching Techniques 25
1.5.3 Gas-Foaming Technique 26
1.5.4 Freeze Drying 26
1.5.5 Electrospinning 27
1.5.6 Melt Based Fabrication Techniques 27
1.6 Scaffold Fabrication with Designed Architecture 28
1.6.1 Rapid Prototyping (RP) 28
1.6.1.1 Melt-Dissolution Technique. 29
1.6.1.2 Particle Bonding Technique. 29
1.7 Surface Modification of Tissue Engineered Constructs 32
1.8 The Aim of This Study 35
2. EXPERIMENTAL 37
2.1 Materials 37
2.2 Synthesis of Lysine Based Polyurethane 37
2.3 Preparation of PEU Matrices 39
2.3.1 Preparation of PEU Films 40
2.3.2 Preparation of PEU Sponges 41
2.3.3 Fabrication of PEU Scaffolds by 3-D Plotting 42
2.3.4 Modification of PEU Matrices with Oxygen Plasma 45
2.4 Characterization of Matrices 45
2.4.1 Composition and Molecular Weight 45
2.4.2 Thermal Characterization 45

2.4.3 Determination of Porosity and Pore Size Distribution of PEU Matrices 46
2.4.4 Mechanical Properties of PEU Matrices 47
2.4.5 Dynamical Mechanical Analysis (DMA) of PEU Films 48
2.4.6 Evaluation of In situ Degradation 48
2.4.7 Water Contact Angle Measurements 49
2.5 In Vitro Studies 49
2.5.1 Isolation and Culture of Mesenchymal Osteoprogenitor Cells 49
2.5.2 Cell Seeding and Culturing on PEU Matrices 50
2.5.3 Microscopy and Image Analysis 51
2.5.3.1 Scanning Electron Microscopy. 51
2.5.3.2 Fluorescent Microscopy. 51
2.5.4 Cell Proliferation 51
2.5.5 Determination of Osteoblastic Differentiation 52
2.5.5.1 Alkaline Phosphatase (ALP) activity. 52
2.5.5.2 Matrix Mineralization. 52
3. RESULTS AND DISCUSSION 54
3.1 Characterization of PEU Matrices 54
3.2 Liquid State NMR, FTIR-ATR, GPC and Contact Angle Analyses 54
3.3 Thermal Properties of PEU Matrices 57
3.3.1 Tensile Test Results of PEU Films 60
3.3.2 Dynamical Mechanical Analysis (DMA) of PEU Films 62
3.4 Morphology of 3D PEU Matrices 65
3.5 Porosity and Pore Size Distribution of 3D PEU Matrices 68
3.5.1 Determination of Porosity 68
3.5.2 Pore Size Distribution 71
3.6 In situ Degradation Profiles of PEU Matrices 74
3.7 Compressive Modulus of 3D PEU Matrices 76

3.8 In Vitro Studies 79
3.8.1 In Vitro Cell Culture on 2D PEU Films 79
3.8.1.1 Cell Morphology. 79
3.8.1.2 Cell Proliferation. 82
3.8.1.3 Osteoblastic Differentiation. 84
3.8.2 In Vitro Cell Culture on 3D Scaffolds 86
3.8.2.1 Surface Modification of 3D Scaffolds. 86
3.8.2.2 Cell Morphology on 3D Scaffolds. 87
3.8.2.3 Cell Proliferation on 3D Scaffolds. 90
3.8.2.4 von Kossa Staining. 91
3.8.2.5 SEM/EDX Imaging of Mineralization on 3D Scaffolds. 95
3.8.3 Effect of Cell Proliferation on Compressive Properties of 3D PEU Matrices 100
4. CONCLUSIONS 103
REFERENCES 103
APPENDIX A Calibration Curve 125
CURRICULUM VITAE 126

LIST OF TABLES

TABLES

Table 1.1 Biochemical composition of bone 3
Table 1.2 Mechanical properties of various human bone tissues 4
Table 1.3 Matrix proteins of bone 7
Table 1.4 Classification of implant material with respect to tissue response they evoke 12
Table 2.1 Designation of 2D and 3D matrices prepared from PEU 39
Table 3.1 The molecular weight, heterogeneity index (HI) and water contact angle values of SF 56
Table 3.2 Thermal data for different PEU matrices 59
Table 3.3 Tensile test parameters of PEU 61
Table 3.4 Tan δ peak magnitude and Tg values for PEU at different frequencies 63
Table 3.5 Porosity of 3D scaffolds 70
Table 3.6 Compressive modulus values of 3D scaffolds 70
Table 3.7 Weight percentage of C, O, P and Ca elements on different scaffolds seeded with BMSCs 98
Table 3.8 Change in compressive moduli of seeded 3D scaffolds by time 101

LIST OF FIGURES

FIGURES

Figure 1.1 Schematic drawing of hierarchical structure of bone. 2
Figure 1.2 Illustration of urethane linkage formation 20
Figure 2.1 Synthesis of poly(ester-urethane) from PCL diol and LDI.....38
Figure 2.2 Summary of experimental study 40
Figure 2.3 Schematic presentation of micropatterned polymeric film preparation 41
Figure 2.4 Steps of salt leaching for porous foam fabrication. 42
Figure 2.5 Bioplotter instrument 44
Figure 2.6 Plotting of melted PEU a) layer by layer, b) BP-B, c) BP-O.....44
Figure 3.1 ^{13}C-NMR spectrum of PEU and PCL diol.....55
Figure 3.2 FTIR-ATR spectra of PEU film and PCL diol. 57
Figure 3.3 DSC thermograms of PEU matrices. 59
Figure 3.4 TGA curves of PEU smooth film (SF) and bioplotted (BP-B) scaffold. 60
Figure 3.5 Representative stress–strain curve of the synthesized PEU film 61
Figure 3.6 Tan δ versus temperature curve of PEU film at different frequency. 64
Figure 3.7 Temperature dependency of the storage modulus for PEU film at different frequency. 64
Figure 3.8 Shifting of Tg at different frequencies.....65
Figure 3.9 SEM images of PEU scaffolds fabricated by Bioplotter. 66
Figure 3.10 SEM images of PEU scaffolds prepared by freeze drying and salt leaching. 67

Figure 3.11 Pseudo-coloured μ-CT images of PEU scaffolds produced by Bioplotter a) Isometric, b) Side view. 71
Figure 3.12 Pore size distributions of freeze dried spongy scaffolds. a) Freeze dried (SP0), b) Low salt leaching ratio (SP5), c) High salt leaching ratio (SP10). 73
Figure 3.13 Degradation profiles of 2D films and 3D scaffolds in PBS with 0.18 U/mL of lipase (n=3).....75
Figure 3.14 Representative load-deformation curves of freeze dried and salt leached spongy scaffolds.....77
Figure 3.15 Representative load-deformation curve of bioplotted scaffolds 77
Figure 3.16 Fluorescence images of BMSCs seeded on a) MF-Fn, b) MF. Actin microfilaments (green) were visualized by FITC-labeled phalloidin. Cell nuclei were visualized by DAPI (blue). 81
Figure 3.17 SEM images of BMSCs seeded on a) SF, b) MF. c) and d) Closer views of alignment within the groove (day 3). 82
Figure 3.18 Cell proliferation of BMSCs on PEU films and tissue culture plate (control) quantified using Alamar Blue assay on days 1, 7, 14 and 21 (n=3).....84
Figure 3.19 ALP activity of BMSCs per sample at the end of three weeks (n=3).....85
Figure 3.20 Fluorescence microscopy images showing mineralization achieved by osteoblasts on polymeric films at the end of three weeks. 85
Figure.3.21 Fate of drop of cell suspension on a) untreated and b) plasma treated scaffolds. Photo was taken right after the dropping. 87
Figure 3.22 Cell attachment and spreading on salt leached spongy scaffolds on day 1. a) SP5 b) SP10. Images on the right colons are the high magnification of corresponding images. 88
Figure 3.23 SEM micrographs of the seeded bioplotted scaffolds showing the interaction between the cells and scaffold fibers on a) day 1, b)

day 3, c) day 7. Images on the right colons are the high magnification of the corresponding images. 89
Figure 3.24 Proliferation of BMSCs on 3D scaffolds (n=3). 91
Figure 3.25 von Kossa staining of mineralization on salt leached scaffold after 5weeks of culture a) Unseeded negatif control b) SP5 and b) SP10 (Scale bar = 100 μm). Arrow indicates mineralized nodules. 93
Figure 3.26 von Kossa staining of mineralization on bioplotted scaffolds after 5 weeks of culture. a) Unseeded negatif control b) Focus on upside fiber surface, b) Focus on underside fiber surface (Scale bar = 200 μm, insets =100 μm). 94
Figure 3.27 SEM micrographs showing ECM deposition and mineralisation on salt leached scaffolds after 5 weeks of culture. a-b) on SP5, c-d) on SP10. Arrows indicate mineral deposits. 96
Figure 3.28 SEM micrographs showing ECM deposition and mineralisation on bioplotted scaffolds after 35 days of culture. a) Top view, b) and c) Side view of ECM deposition. 97
Figure 3.29 EDX measurement for the detection of mineralization on a) SP5, b) SP10), c) BP-O on day 1 (left column) and on day 35. 99
Figure 3.30 Compressive moduli of seeded salt leached scaffolds on day 1 and on day 35 under wet conditions.....102
Figure 3.31 Compressive moduli of seeded bioplotted scaffolds on day 1 and on day 35 under wet conditions.....102

ABBREVIATIONS

2D	Two Dimensional
3D	Three Dimensional
ALP	Alkaline Phosphatase
ATR	Attenuated Total Reflectance
BGS	Bone Graft Substitute
BSA	Bovine Serum Albumin
BMSC	Bone Marrow Stem Cell
DMA	Dynamic Mechanical Analysis
E	Young's Modulus
E′	Storage Modulus
EAB	Elongation at Break
SEM	Scanning Electron Microscope
ECM	Extracellular Matrix
Fn	Fibrinogen
FTIR	Fourier Transform Infrared Spectroscopy
GPC	Gel Permeation Chromatography
Mn	Number Average Molecular Weight
Mw	Weight Average Molecular Weight
MW	Molecular Weight
NMR	Nuclear Magnetic Resonance
PBS	Phosphate Buffer Saline
PEU	Poly (ester-urethane)
SEM	Scanning Electron Microscope
Tg	Glass Transition Temperature
Tm	Melting temperature

CHAPTER 1

INTRODUCTION

1.1 Bone Physiology

Bone tissue is responsible for various functions in the body, including structural support, mineral storage, and physiological functions such as the formation of blood vessels [1]. Normal bone formation is a prolonged process which is regulated carefully and involves sequential growth-regulatory steps. The physiology of bone involves a complex interrelation of cellular, molecular and systemic components. Bone is continuously remodeled tissue where mineral resorption and deposition take place within a balance as a response to mechanical and molecular influences [2].

1.1.1 Bone Composition and Structure

Bone is a composite material, composed of extracellular matrix (inorganic and organic components) and cells, which are osteoblasts (bone-forming cells), osteoclasts (bone-destroying cells) and osteocytes, (bone-maintaining cells). Bone is a hierarchically structured tissue where its mechanical properties depend on its architecture at all levels of hierarchy (Figure 1.1). At the macroscopic level, human and mammalian bones are classified into two types of osseous tissue, namely cortical bone (also known as compact bone) and cancellous or spongy bone (also known as trabecular bone). Compact bone tissue is dense and looks smooth and homogenous with canals and passageways, while spongy bone composed of trabeculae with much open space between the trabeculae filled with bone marrow [3]. Cortical bone is found primarily in the shaft of long bones and the outer shell around cancellous bone. Cancellous bone is found within cortical tissue, in medullary cavities at the ends of long bones, in the

interior of short bones mainly in the vertebrae [4]. Cancellous and cortical bone have different anatomical features but identical cell types and a similar remodeling cycle [5]. At the sub-microscopic level, layers of parallel collagen fibrils (lamellae) surround a central hole in a structure known as an osteon where bone undergoes remodelling. This lamellar structure of the bone matrix gives fracture toughness. At the lowest level, mineralized collagen fibrils gather into bundles named as fibril arrays where calcium phosphate (hydroxyapatite) nanocrystals are embedded into these collagen fibrils increasing their stiffness, but decreasing their fracture strain. Mechanical properties of collagen fibrils depend on the amount of mineral particles and their arrangement within the fibrils [6]..

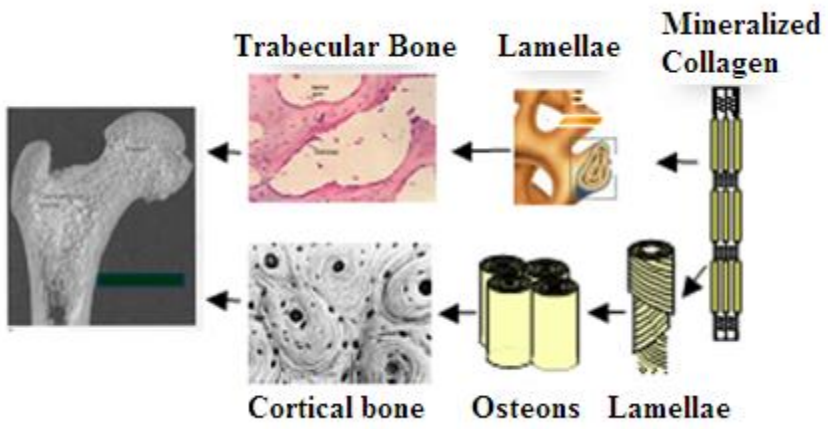

Figure 1.1. Schematic drawing of hierarchical structure of bone [4].

Structurally, the hard tissue is composed of four phases: collagen fibers, calcium-phosphate rich mineral, organic substances and water: 60% inorganic elements, 5% minerals, 9% water and 25% organic bone matrix and ground substances (proteins, polysaccharides and mucopolysaccharides), where the relative fractions of each vary from bone to bone, as well as on age, sex and anatomical location within the body [7,8]. Biochemical composition of bone is given in Table 1.1. Beside the main bone cells, other cell types like endothelial cells, fibroblasts, lining cells and stem cells are present in bone tissue.

The mineral homeostasis of the body is regulated by the action of bone cells together via hormonal and mechanical stimuli. Osteoblasts are present in the interior and the periphery surface of the bone. They activate the mineralization process by synthesizing alkaline phosphatase enzyme. Osteoblasts are the final form of cells as a result of stem cell differentiation in the bone marrow. After three months, they become flat in shape and turn into lining cells which are metabolically inactive and very few of them (~15%) turn into osteocytes.[9].

Table 1.1. Biochemical composition of bone

Inorganic part	**Organic part**
Hydroxyapatite [HAp-$Ca_{10}(PO_4)_6(OH)_2$]	Collagen type I
Minerals (sodium, magnesium, other traces)	Non-collagenous proteins, morphogenetic proteins, serum proteins
Carbonates	Polysaccharides, lipids, cytokines
Citrates	Primary bone cells (osteoblasts, osteocytes, osteoclasts)
Water	-

The cortical bone differs from cancelleous bone by structurally and functionally. The cortical part of bone is responsible for mechanical and protective functions, whereas cancellous bone mostly takes part in metabolic functions. Both structural and metabolic aspects are related to the properties of mineralised extracelluar matrix [10]. Thus, it is important to understand hard tissue formation and mineralization processes in bone in order to mimic the natural bone tissue in vitro by tissue engineering attempt.

As mentioned before, the composition of bone differs between bone types, where cancellous bone is much weaker than cortical bone. The enamel of teeth is the hardest material in the human body due to its high mineral content (~95%) [8]. The mechanical properties of various bone tissues are included in Table 1.2.

Table 1.2. Mechanical properties of various human bone tissues

Osseous tissue	Elastic modulus (GPa)	Tensile strength (MPa)
Cortical bone	17.7	133
Cancellous bone	0.30	15
Enamel	85	11.5 transverse, 42.2 parallel
Dentine	32.4	44.4

1.1.2 Extracellular Bone Matrix

Mesenchymal tissues like cartilage, bone, tendon, ligament and other connective tissues are fabricated by highly differentiated cells which produce unique extracellular matrices (ECMs) that finally predominate and give the characteristics of a tissue. Cells are organized in the ECM which provides structural support and cope with different loads via various mechanisms. In elder people collagen and proteoglycan structure of

the ECMs are comparatively denser which are responsible for mechanical and functional characteristics of tissues [11]. The extracellular matrix is essential for some type of cells for their specific functions.

The major solid components of human bone are collagen, mainly type I collagen (organic matrix), and hydroxyapatite (inorganic matrix) (a natural ceramic, also found in teeth) [12]. Collagen, apatite mineral and water are responsible for the main structure of the bone. Collagen fibrils form a microenvironment which favours apatite nucleation [13]. The composition of the mineral phase is mainly calcium ($Ca^{2+)}$ and phosphate (PO_4^{3-}) and a low amount of carbonates (CO_3^{2-}), sodium (Na) and magnesium (Mg) [14]. Mineral part of bone is similar to hydroxyapatite [$(Ca_{10}(PO_4)_6(OH)_2$], as shown by X-ray diffraction analysis.

1.1.2.1 Mineral (Inorganic) Phase

Calcium hydroxyapatite (HAp) is a mineral salt of mostly calcium phosphates in a crystalline structure and constitute the inorganic part of bone. It is responsible for the hardness of the bones. Hydroxyapatite crystals are organized within collagen fibrils. In mature bone, minerals are associated with collagen fibrils; HAp crystals are aligned in the direction of collagen fibrils as well as they are located in an ordered manner in channels or grooves formed by neigboring gaps within the collagen network [15,16]. The mineral phase is important in the sense of mechanical properties, since mineral part provide stiffness and strength to the bone. Therefore, mineral loss would lead to decrease of modulus and strength of bone, which increase the risk of bone fracture. In addition, orientation of crystals within ECM determines the anisotropy property of the bone [17], the property of being directionally dependent that is physical and mechanical properties differ with orientation.

1.1.2.2 Organic Phase

Type I collagen protein is the major component (over 90%) of organic matrix. It provides strength and flexibility, as well as space for nucleotion of apatite crystals. Collagen molecules are arranged as fibrils in a staggered fashion where crosslinks connecting the C-terminal of a molecule to the N-terminal of neighboring one. These crosslinks affect the mechanical behavior of bone by organizing fibrillation and involving in mineralization process. Beside collagen type I, organic phase of bone contains other structural proteins, proteoglycans and hyaluronan; and specialized multiadhesive proteins. Types of bone matrix proteins are tabulated in Table 1.3. Every tissue contains its own type of ECM specialized for its particular function [18]. The amount of specific components varies according to the function of the tissue. The ECM has received attention because of its importance in cell-to-cell signaling [19], wound repair [20], and tissue functions [21]. It is an active and dynamic structure that conducts vital regulatory signals between the cells, , influence gene expression at the cellular level [22]. ECM components regulate mineralization, stock growth factors and protect them against deactivation or destruction [23].

Table 1.3. Matrix proteins of bone

Collagen Types	Non-collagenous proteins	Proteoglycans
Major components		
Collagen Type I	Osteocalcin	Decorin
Collagen Type III	Matrix Gla protein	Biglycan
Collagen Type X	Protein S	Fibromodulin
Minor components		
Collagen Type V		
Collagen Type VI		
Collagen Type XIII		
Collagen Type XIV		

1.1.3 Dependence of Bone Architecture on Anatomical Locations, Age and Gender

Histomorphometry studies have shown that the bone architecture, especially of the trabecular bone is site dependent. For example, bone volume fraction (ratio of the bone volume to the specimen volume of interest) of trabecular in femoral neck is much higher than that in the lumbar spine. Eckstein et al. (2007) showed that the trabeculae are thickest in the femoral neck and thinnest in the iliac crest [24].

Over age 45, a decrease in bone volume fraction and connectivity density (a measure of unconnected trabeculae) for trabecular bone, a decrease in the thickness and an increase in the porosity for cortical bones have been reported [4]. These architectural changes may influence the mechanical properties of bone; decrease the strength and toughness

off the bone tissue. The most age-related structural change is decrease of bone volume fraction in trabecular bone [25] and increase of porosity in cortical bone [26].

Architectural differences have been indicated between men and women; women being more susceptible to osteoporosis. Architectural differences are more severe in women with increasing age than in men. In postmenopausal women, trabecular matrix show higher tendency to disconnect than men at same age. In addition, women usually have thinner trabeculae at younger ages; therefore have higher risk of microstructural damages with increasing age than men [27].

1.1.4 Bone Regeneration and Remodeling

One of the unique aspects of bone is that old tissue is continually being replaced with the new tissue; this process is called bone remodeling. Bone is one of the body's tissues that have the ability to regenerate itself after a partial damage. However, bone itself cannot heal a serious break or tumor lesions. Thus, a bone substitute is required to fill defected bone tissue area. Bone failure is commonly seen in elder people. Joint diseases and osteoporosis related fractures display important chronic conditions in people over 65 and women over 50, respectively. It is indicated that 25% of health espending in developing countries will be spent on trauma-related care by the end of the 2010. Beside, many children are suffering from crippling diseases and skeletal deformities [28] and large bone defects, as observed after bone tumor resections require surgical treatment [29]. Currently, bone grafting procedures are employed to promote the healing of fracture and the repairing of other bone defects. Autografts (tissue graft within the same individual), allografts (tissue graft between two individuals of same species) and synthetic biomaterials like metallic, ceramic, polymer or composite are the preferred bone substitutes in clinical practice.

Osteoblasts and osteocytes (differentiated osteoblasts) are bone forming cells originated from pluripotent mesenchymal progenitor cells. Osteoblasts secrete bone matrix and organic proteins such as collagen type I, osteopontin, osteocalcin etc. and alkaline phosphatase (an indicator of bone cell function). Osteocytes are osteoblasts which entrapped within the bone matrix. They secrete osseous growth factors such as insulin like growth factor and tissue growth factor β which promote osteoblastic differentiation. Immature osteoblasts do not secrete calcium, but mature osteoblasts do [30]. It has been shown that three different growth phases undergo after osteoblasts adhere to a material surface in vitro which are proliferation and synthesis of ECM, development and maturation of ECM and ECM mineralization.

1.1.5 Bone Grafts (Autologous, Allografts, Xenografts)

Bone tissue failure like bone fractures and damages come out as a result of various situations like trauma, surgery, infection, defects and aging. Bone grafts are bone material that is isolated from another part of the body in order to help healing of defective bone tissue or promote its function. Bone materials may be obtained from the patient himself, from a donor or from an animal source. Bone grafts that are taken directly from another skeletal part of the patient and transferred into another site of his or her own bones are called autologous bone grafts (autografts), or bone autografts. A portion of bone is usually harvested from iliac crest, tibia, fibula, and scapula or, in the case of craniomaxillofacial reconstruction, the symphysis, maxillary tuberosity, mandibular retro-molar area, or zygoma [31]. Generally, autografts are gold standard for bone grafts due to their advantages like excellent incorporation of the graft, lack of disease transmission, and absence of an immune rejection response. They are more tolerable and effective, since they contain high amount of the patient's own osteoblast progenitor cells and bone morphogenetic proteins (BMPs). Autograft bone provides a strong framework for the new bone to grow into. The drawbacks of autografts are the need of an additional surgery (extra pain and discomfort for the patient), hematoma,

infection, increased operation time and cost, morbidity at the donor site and limited availability of sufficient bone [32,33]. Bone graft that comes from another person is called allograft bone. Allograft bone usually comes from bone banks that harvest the bone from cadavers. Allografts, like autografts, provide a matrix for the new bone to grow through it. The advantages of allograft bone are availability in high amount, the elimination of second surgery, lack of pain and donor site morbidity and relatively less time consuming. Disadvantages of allograft bone are the slight risk of disease transmission, tissue rejection and a less potency since they do not contain proteins and live cells which are removed during the cleaning and disinfecting processes [34].

Despite the benefits of autografts and allografts, the limitations and drawbacks of each required the development of alternatives. Especially, there is an increasing demand for synthetic bone graft products free from the limitations of supply, consistency, and disease.

Various materials have been examined for their potential uses in place of the autografts or allografts. Natural and synthetic polymers, ceramics, and composites either alone or in combination with other materials have been widely investigated for this purpose. In some strategies, growth factors and/or cells are incorporated to the material(s). Although most of the available substitutes provide an alternative solution, none of them yet possess all the benefits of one's own bone. For the last decades, investigators have focused on the development of novel bone graft substitutes which stimulate bone healing and provide a strong and biocompatible matrix for the new bone formation [35-37].

1.1.6 Classification of Tissue Response

All materials intended for use in humans as biomaterials, medical devices, or prostheses undergo tissue responses when implanted into the body [38]. When

developing new material(s), it is important to have idea about the host response of the material(s). Materials that evoke minimum response when contact with tissues or body liquids are called biomaterials. Ideally, biomaterials should be biocompatible, meaning do not provoke any undesired reaction within the body. Biocompatibility of an implant is defined as the ability of a biomaterial to perform with an appropriate host response in a specific application. Several factors influence an implantable material's biocompatibility. Surgical procedure, material-cell interfacial interactions, toxicology, biodegradation, implant movement, mechanical properties, site of implantation, sterilization and design, and construction are some of them [39]. An important issue of host response is the formation of a structural and biological bond between the material and host tissue. If the material is not biocompatible, systemic or local tissue reactions will occur [8]. Implant materials are generally categorized according to their potential risk of biological response that they induce when implanted (Table 1.4). The series of tissue response initiated by the surgical procedure, as well as by the introduced material. If the material is toxic, it causes death of the surrounding cells and tissue mostly due to the release of soluble products. Bioinert materials are biocompatible materials and do not induce formation of biological bond between implants and the tissue. Bioactive materials can form biological and chemical bonds in the early stages of implantation period. Bioresorbable materials are the ones which gradually resorbed before they totally disappear and eventually replaced by the new coming tissue. There is no material that behaves as totally inert. When a material is implanted, it is recognized as a foreign matter and tried to be eliminated by the body. If the foreign body could not be eliminated by macrophages, then the next step of this process is the isolation of the implant by surrounding it with a capsule. Depending on the surface area, shape and physicochemical properties of the material, blood cells of the immune system and/or coagulation system are activated in order to protect the body against the foreign matter. Most biomaterials display fibrous encapsulation where initially a thin 1–3 mm-thick loosely organized capsule-like fibrous layer is formed on the surface of the implant in order to isolate the implant from the living part of the body. The thickness of

the fibrous layer formed depends on chemical reactivity (inertness) and the relative motion between the implant and tissue [40]. A thicker layer formation is induced by more reactive materials, such as metals that undergo corrosion or polymer containing residual monomers that may be leached under physiological conditions in order to isolate the source of irritation. The immune responses to nonresorbable (nondegradable) or resorbable (degradable) materials are similar initially; but as tissue interacts with the degrading material surface and/or released degradation products, the responses start to differ from each other. Nonresorbable biomaterials barely induce inflammatory response or cause clot formation, where resorbable ones left the body after a mild inflammation, generally via hydrolysis [41].

Table 1.4. Classification of implant material with respect to tissue response they evoke

Classification	**Tissue response**
Toxic	Surrounding tissue dies
Biologically inactive (Bioinert/biotolerant)	Fibrous tissue with various thickness forms
Bioactive	An interfacial bond with the implant forms
Bioresorbable	Newly forming tissue replaces the implant as it degrades

1.1.7 Bone Graft Substitutes (BGS)

1.1.7.1 Human Bone Matrix (BM) and Demineralized Bone Matrix (DBM)

Mineralized and demineralized bone matrix is obtained by processing (e.g. freeze drying, disinfection) allograft bones. Allograft bone matrix has osteoinductive activity and compatibility with the surrounding blood cells, since it contains collagen, proteins and growth factors [42]. It is available as powder, crushed granules, paste and gel [43]

and can be injected through a syringe [44]. Mineralized allograft contains hydroxyapatite which provides osteoconductivity and mechanical strength. DBM is less immunogenic compare to BM [45]; but has lower mechanical strength since it does not contain minerals [46]. Because of their osteoconductive and osteoinductive properties, BM and DBM have been used for the regeneration of orthopedic, dental and craniofacial injuries, defects or abnormalities [45]; mostly combined with other carrier materials like calcium sulfate, hyaluronic acid and glycerol [47,48]. There are various commercially available DBMs which have been demonstrated to have different biological properties for a specific application [49].

1.1.7.2 Ceramic Biomaterials (Calcium Orthophosphates)

Calcium phosphate based ceramic materials seem to be noticeable as bone substitutes due to their excellent strength, biocompatibility and osteoinductive properties. This is because inorganic part of mammalian calcified tissues (bone and teeth) consists of calcium orthophosphates [50]. Materials such as Bioglass, β tricalcium phosphate (β-TCP), calcium sulphate (CS), hydroxyapatite (HAp) and biphasic calcium phosphate or mixtures of these have been developed in bulk form or as granules as bone substitutes in dentistry as well as orthopedic and reconstructive surgery [51]. This group of materials exhibit high level of biocompatibility and osteoconductivity and binds directly to bone tissues. Of the various calcium phosphates, HAp has received considerable attention because its mineral composition [$Ca_{10}(PO_4)_6(OH)_2$] is close to natural bone. However, due to its less solubility compared to other calcium phosphates (e.g. β-TCP), it remains in the body longer and impedes new bone replacement [52]. Different calcium based compounds have various Ca/P ratio. For example, Ca/P ratio for TCP and HAp is 1.5 and 1.67, respectively. Ca/P ratio of less than 1.0 is not biomedically important. It has been stated that nonstoichiometric HAp shows better osteoconduction property [53]. The bioceramics have also been used to coat the gliding surfaces of artificial joints with the aim of providing bonding between the implant and

the native bone to enhance implant integration. Other ceramics like alumina and zirconia are used for wear applications in joint replacements. When implanted, bioceramics are not encapsulated by fibrous tissue as many others do [40]. However, their mechanical and elastic properties do not resemble of the natural tissue properties, since scaffolds made of calcium orthophosphates have a low elasticity, high brittleness, poor mechanical strength especially in load-bearing sites, and low mechanical reliability and fracture toughness. Moreover, generally it is difficult to form calcium orthophosphates into the desired shape [54]. In the last decade, researchers have developed biocomposites or biphasic calcium phosphate (BCP) by combining the HAp with bioinert ceramics like alumina and zirconia to improve toughness and strength of HAp. In some studies, BCP was formed with various ratio of HAp: TCP to obtain desired properties. Nevertheless, none of these HAp-based composites showed superior mechanical, physical and degradability properties.

1.1.7.3 Natural Coral and Other Marine Biomaterials

Marine biomaterials like coral, chitosan and sponge skeleton etc. are among the bone substitutes. Corals are a broad group of marine invertebrate animals consist of a mineral skeleton, mainly calcium carbonate in the structural form of aragonite with impurities such as Sr, Mg and F ions, and an organic matrix [55]. The skeletons of certain corals have been used as bone graft substitutes to treat various bone related problems in humans [56] and in scaffolding for bone tissue engineering due to their porous, osteoconductive and biodegradable properties [57]. Properties like 3D structure, porosity, pore interconnections, and inorganic composition make the natural coral suitable for bone tissue regeneration; however lack of osteoinductivity and osteogenesis is major drawback to its use [56].

Chitosan is an amino-polysaccharide obtained by alkaline deacetylation of chitin which is natural component of naturally found in shrimp or crab shells. It has a wide use in

biomedical field due to its biocompatible, biodegradable, osteoconductive and antibacterial properties. Alone chitosan is not useful as a bone substitute due to its very low mechanical strength. Thus, it has been used in combination with inorganic materials like HAp and calcium phosphate in order to enhance biologic activity, and decrease the inflammation caused by the leakage or migration of inorganic particles [58].

1.2 Tissue Engineering of Bone

To overcome the limitations faced with conventional therapies used to treat bone tissue defects or diseases, bone tissue engineering has been promoted as a new alternative to regenerate bone tissue. In bone tissue engineering approach, cells capable of osteogenic activity and osteoinductive signal molecules are combined with an appropriate material [59]. For bone regeneration; a morphogenetic signal, responsive host cells that will respond to the signal, a suitable carrier that can deliver the signal to specific locations and can serve as matrix for the growth of the host cells, and a viable well vascularized host bed are needed [60]. Two concepts are important for regeneration: osteoconduction and osteoinduction. An osteoconductive material is one which allows growth of bone on its surface or within its structure (e.g. down into pores, channels). Osteoinduction is defined as the ability to cause pluripotential cells, from a nonosseous environment to differentiate into chondroctyes and osteoblasts. Osteoinduction is the ability of a material to allow repair in a location that would normally not heal if left untreated [61]. The current trend in bone tissue engineering is to develop biodegradable materials which temporarily support the bone tissue at the same time stimulating its regeneration in such a way that this, temporary matrix disappears as the bone renew itself. The biodegradable materials act as cell carriers and generally referred as scaffolds [62]. For bone tissue engineering to succeed, there are some key factors which the scaffolding biomaterials should provide [63]. These are summarized as follows:

- *Biocompatability*: Lack of immnune response. Neither material itself nor the degradation products should not be toxic, allergic or carcinogenic,

- *Osteoconductivity*: Material should have sufficient porous interconnected structure for the cells to attach proliferate and migrate through the scaffold structure, for the delivery of nutrients, growth factors, for penetration of new vessels and removal of wastes,

- *Osteoinductivity*: Material should possess essential proteins and growth factors that induce mesenchymal stem cells and other osteoprogenitor cells toward the osteoblast lineage,

- *Osteointegrity*: Newly constituted mineralized tissue should be able to form an intimate bond with the implant material,

- *Mechanical match*: Material should have similar mechanical properties that are consistent with the tissue they are replacing.

Additionally, the material should:

- Have the desired surface properties to allow cell attachment, proliferation and differentiation,

- Degrade with a certain rate proportional to the regrowth of new tissue,

- Be easily processed into 3D constructs in a well-controlled and reproducible manner.

1.3 Biomaterials Used for Tissue Engineering Scaffolds

Scaffolds are main components of tissue engineering policies since they provide an architectural texture in which extracellular matrix, cell–cell and growth factor interactions take place to provide matrices for tissue regeneration [64]. In the sense of bone tissue engineering, osteogenesis is highly dependent on the substrate carrier used, which has to provide a suitable environment into which bone cells can migrate before proliferating, differentiating and depositing bone matrix [65]. The substrate must have specific physicochemical characteristics (e.g. surface free energy, charge,

hydrophobicity, etc.) and specific geometry (e.g. three dimensional and interconnected porosity). Choosing the suitable materials for scaffold fabrication is very critical. The materials used must be safe, not cause excessive immune responses, the bulk and degradable products must be biocompatible and clearable by the body (resorption rate must meet with the new bone formation rate) [66]. Besides, the scaffolds must be osteoconductive, suitable for manufacturing techniques that generate high surface area porous structures and sterilizable and handable during operation [67]. Generally, it has been stated that scaffolds designed for bone tissue engineering purposes should possess good mechanical properties in order to bear mechanical loading [68,69]. However, some investigators believe that this requirement is not necessary, since the main function of a scaffold is to support bone ingrowth and not to sustain mechanical loading [70].

Polymers (macromolecules) are the main materials used for scaffold preparation in various tissue engineering applications. Polymers can be obtained with different molecular weight, polydispersity, crystallinity and thermal transitions which provide various mechanical strength and flexibility. The surface hydrophobicity and crystallinity of the polymers can affect cell morphology. Change of surface chemistry will affect cell spreading or cell affinity for the surface, which can also cause changes in phenotypic expression.

Polymers used for scaffold fabrication are either synthetic polymers or derived from natural sources. Natural polymers are advantegous in the sense of having biological recognition sites which enhance initial cell attachment and function. Most commonly used natural polymers for bone tissue engineering include polysaccharides (e.g. chitosan, alginate and hyaluronan) and proteins (e.g. collagen, gelatin, silk fibroin and elastin). However, certain disadavantages of natural polymers restricted their use in tissue engineering, which are weak mechanical properties, biodegradability, limited availability, possible immunogenicity and risk of pathogenic impurities [63]. Generally,

natural polymers are combined with other synthetic polymers or ceramics to form a composite material [71] having the advantageous of both natural and synthetic materials or used in preparation of drug delivery systems [72].

Synthetic polymers are very attractive materials for bone tissue engineering applications due to their advantegous properties like mechanical strength, degradability, batch to batch consistency and microstructure. In contrast to metals and ceramics which are also widely used as bone substitutes, polymers offer an extend design flexibility since their composition and structure can be easily tailored for a specific application [72]. Their biodegradation rate can be controlled through molecular design. Some polymers are susceptible to hydrolytic degradation while some others can degrade by cellular or enzymatic activity. The most commonly used synthetic polymers for bone tissue engineering are listed below:

- Aliphatic (α-hydroxy) polyesters including poly(glycolic acid) (PGA), poly(L-lactic acid) (PLLA), and their copolymers poly(lactic acid-co-glycolic acid) (PLGA).
- Poly(ε-caprolactone) (PCL)
- Poly(hydroxy butyrate) (PHB)
- Poly(1,4-butanediol succinate) (PBS)
- Poly(propylene fumarate) (PPF), degrade through hydrolysis of the ester bonds similar to glycolide and lactide polymers
- Polyurethanes
- Polyphosphazenes
- Polyanhidrides
- Poly(ortho esters)

The aliphatic (α-hydroxy) polyesters have FDA approval for certain human use. They degrade through hydrolysis of ester bonds. Their degradation rate can be altered to last from several weeks to several years by changing the chemical composition,

crystallinity, molecular weight and molecular weight distribution. Although they are widely used in bone tissue engineering, there are still ongoing researchs to enhance their functionality.

Among the wide polyester family, polyurethanes are one of the most popular group of biomaterials used for the development of medical devices [73]. Due to their versatility in chemical, physical and mechanical properties, and moderately good biocompatibility, they have a broad range of uses and applications varying from textiles [74] to medical products like blood-contact materials [75,76], heart valves [77], cardiac pacing leads [78], ureteral stents [79], bone implants [80], controlled release devices [81] and so on.

Traditionally, PUs have been aimed as long-term implant materials for which biodegradation was not desired [73]. Since toxic products can be released upon degradation of polyamines associated with conventional isocyanates, their use as absorbable biomaterials have been limited [82]. Degradation products of polyurethanes based on diisocyanates such as 4,4'methylenediphenyl diisocyanate (MDI) and toluene diisocyanate (TDI) are reported to be carcinogenic and mutagenic [83,84]. Therefore, in the synthesis of degradable PUs, aromatic isocyanates have been replaced with isocyanates like lysine ethyl ester diisocyanate (LDI, 2,6- or 1,4-diisocyanatobutane (BDI) [85,86] which degrade into non-toxic products (i.e. lysine) and as well as support the cell migration and new tissue formation [87,88]. Their cationic properties due to amine groups made them an interesting candidate for gene delivery. Cationic polymers condense DNA into nanoparticles small enough to enter a cell, and protect negatively charged strands of DNA from nuclease degradation. Beside cationic properties, lysine based PUs eliminate the long-term safety concerns like cytotoxicity and nonbiodegradability in delivery systems [89]. During last two decades, PUs were investigated for their in vivo biodegradation as biomaterials for tissue engineering [90]. PUs have been studied as scaffolding material for tissue engineering of bone [91],

cartilage [92], nerve [93] and skeletal muscle [94]. Degradable PUs can be obtained by incorporating ester linkages into the polymer backbone. The soft segments of biodegradable polyurethanes are generally either polyethylene glycol (PEG) or polycaprolactone diol (PCL) [95]. Polycaprolactone (PCL) is a highly processible semicrystalline linear polyester with a low melting point (ca. 60^{o}C) and extensively investigated as scaffold for tissue engineering because of its soft [96] and hard [97] tissue compatibility. It is an FDA approved material due to its safe application in human body [98] and especially interesting for the preparation of long term implantable devices owing to its slow degradation [97].

PUs are block copolymers with alternating soft and hard blocks or segments. Polyether or polyester polyol are responsible for the formation of soft segments and whereas the diisocyanates form the hard segments. The urethane linkage (–NH–COO–) is obtained when a diisocyanate's isocyanate (NCO) group reacts with polyol's hydroxyl group (OH). PUs are produced by the polyaddition reaction of a polyisocyanate with a polyol in the presence of a catalyst and/or other additives as shown in Figure 1.2.

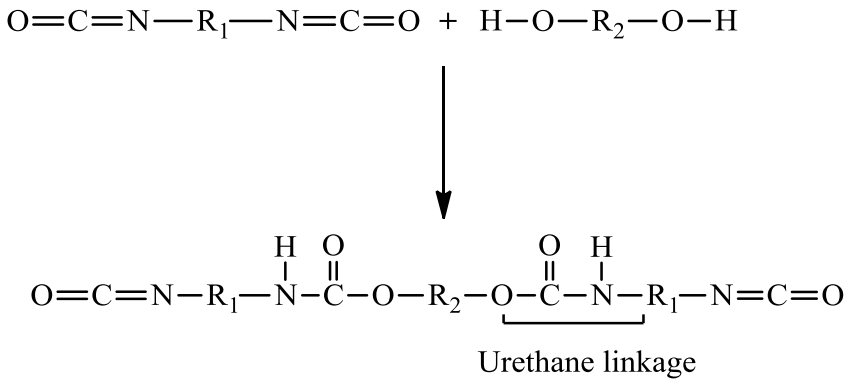

Figure 1.2. Illustration of urethane linkage formation.

In literature, studies related to various tissue engineering applications have been done with lysine based polyesters, containing mostly polycaprolactone as diol [85,99]. Degradation rate of synthetic polyesters can be modified from several weeks to several years by changing crystalline property, molecular weight and monomer ratio. Since these polymers are thermoplastic they can be easily fabricated as a 3D scaffold with a desired microstructure, shape and dimension by using different techniques.

1.4 Engineered Cells

Many tissue engineering and regenerative medicine strategies are based on cells obtained from exogenous source. These cells are expected to provide effective, long-lasting and stable repair of damaged or diseased tissues. There are some important criteria to be considered:

Bone is formed by osoteoblasts, which originate from mesenchymal stem cells (MSCs) in a multi-step lineage cascade. The stem cells are found in the bone surface and in the bone marrow. Bone marrow stem cells (BMSCs) have received enormous interest in clinical applications, due to their plasticity and potential use for treatment of various diseases. In regenerative medicine, stem cells have been extensively used for bone healing since they display high potential for differentiation into osteogenic cells [100,101].

The number of MSCs in freshly isolated bone marrow cells is very small and therefore, their expansion by in vitro culture is needed before seeding on scaffolds. The cultured MSCs can be differentiated into osteoblast in vitro in the presence of vitamin C, β-glycerophosphate and dexamethasone (Dex). After 3-4 weeks of culturing, bone like tissue formation can be observed.

1.4.1 Bone Morphogenetic Proteins and Osteogenic Supplements

Bone morphogenetic proteins (BMPs) are members of the transforming growth factor-β (TGF-β) family that are potent stimulators of bone regeneration. BMPs produced in our bodies and regulate bone formation and healing. BMPs like BMP-2, BMP-4 and BMP-7 have been shown that they are capable to heal bone in vitro and in vivo. BMPs regulate a set of downstream target genes during the early stages of osteogenic differentiation [102]. Scientists have discovered how to extract growth factors substances from human or cow bones and even produce them in the laboratory. Despite the use of BMPs as potential inductors of osteogenic differentiation, the amount of BMPs needed vary in humans and animal studies. Currently, these therapies have not yet approved by the United States Food and Drug Administration (FDA); but their safety and effectiveness are investigated by extended studies in both humans and animals. In tissue engineering applications, these growth factors are generally administrated in tissue engineered constructs (scaffolds) to induce bone formation. Although BMPs are useful as osteogenic inductors, their delivery from material constructs is a problem, because of that growth factors are easily degrade and they could be destroyed during material processing. Thus, currently there is no gold standard in terms of optimal dose for growth factors to be incorporated. Various delivery strategies have been developed for these active molecules in order to prolonged their availability and biologic activity [103]. Yilgor et al. (2008) developed PLGA and PHBV based controlled release systems in nano size for the sequential release of several BMPs. Their results indicated successful sequential delivery of BMPs with the achievement of higher osteoblastic activity on BMPs (in nanocapsules) incorporated scaffolds [104].

In cell culture experiments, dexamethasone, L-ascorbic acid, β-glycerophosphate, 1,25-dihydroxyvitamin D3 are used as supplements in order to facilitate osteogenic differentiation of mesenchymal stem cells (MSCs), progenitor cells or osteoblasts

[105]. Dexamethasone stimulates proliferation and assists osteogenic differentiation by binding to regulatory proteins and modulating the transcription of osteogenic genes [106]. Ascorbic acid and 1,25-dihydroxyvitamin D3 are used for osteogenic induction, increasing alkaline phosphatase (ALP) activity and matrix deposition, and osteocalcin production. L-ascorbic acid, also known as vitamin C, is an essential cofactor for the hydroxylation of proline and lysine residues in collagen, which is the most abundant protein in the body [107]. Thus, it has a very important role in differentiation of various cell types in culture including osteogenesis through formation of the collagen matrix [108]. β-glycerophosphate takes place in mineralization and osteoblastic processes by acting as a phosphate supply.

1.5 Fabrication Techniques in Scaffold Development

In the body, tissues are organized into three-dimensional structures as functional organs and organ systems. Human tissues exhibit different and complex geometries, hierarchical structures and mechanical properties. Scaffolds are the tissue engineered constructs that must meet these features until regenerated tissue matures [109]. To engineer functional tissues and organs successfully, the scaffolds have to be designed to facilitate cell distribution and guide tissue regeneration in three dimensions. Tissue engineering constructs are typically in 3D. However, 2D scaffolds have been also prepared in various forms like films, and fibers [110].

To maintain precise control over the desired structural properties like external geometry, density, pore size, porosity, pore interconnectivity, mechanical strength, surface topography etc. is technical challenge of scaffold fabrication. Macro and microstructure of scaffolds depend mostly on fabrication techniques, but the underlying material should also be considered since natural and synthetic underlying material have different processing requirements to form a scaffold. For example inorganic materials are fabricated with techniques commonly used in ceramic technology, whereas for

synthetic and natural polymeric materials various techniques have been developed [111]. Conventional methods for manufacturing polymer based scaffolds include fiber meshes and fiber bonding, solvent casting, particulate leaching, membrane lamination, gas foaming, phase separation, melt molding, extrusion, solvent casting and freeze drying [110]. Many applications in tissue engineering often require a scaffold with high porosity and ratio of surface area to volume. The conventional methods may have some limitations such as low capability to control pore size, pore geometry, pore interconnectivity, spatial distribution of pores and construction of internal channels within the scaffold [112]. Cells seeded on these scaffolds cannot migrate deep into the scaffold because of the lack of nutrients and oxygen and insufficient removal of waste products. Cells are colonized at the scaffold periphery and consumed or act as a barrier to the diffusion of oxygen and nutrients into the interior of the scaffold. Thus, cells can only survive on the surface of the scaffold. Furthermore, for bone tissue engineering the high rates of nutrient and oxygen transfer at the surface promote the mineralization of the scaffold surface which limits the further mass transfer to the interior of scaffold [113]. In the last decade, new fabrication techniques like rapid prototyping have been introduced in tissue engineering to overcome the limitations of conventional processing techniques. Rapid prototyping, also expressed as solid free-form fabrication, offers production of 3D scaffolds with ordered external and internal structure.

Currently employed conventional and advanced fabrication techniques for polymers are detailed below. A wide variety of produced scaffolds were applied for the engineering of bone and cartilage tissues [114]. Choose of fabrication technique depends mostly on the bulk and surface properties of the underlying material and the intended function of the scaffold. Each method has its own advantages and disadvantages, thus the appropriate technique must be selected to meet the requirements for the specific type of tissue.

1.5.1 Fiber Bonding Technique

The first tissue engineering constructs had been fabricated in the form of nonbonded tassels or felts. However, these constructs lacked the mechanical integrity. To overcome this, fiber bonding technique was developed to join the fibers physically at the intersection points. PGA and PLLA are good example for this technique. Briefly, PLLA, dissolved in methylene chloride (not a solvent for PGA), is cast over the PGA fibers which are in a nonwoven mesh form. After removal of solvent, the resulting PGA-PLLA composite matrix is heated over melting temperature of PGA to bond the PGA fibers at their cross-points. Then PLLA is removed by dissolving it in methylene chloride and the solvent is evaporated by vacuum drying [115]. Similar method is applied by rotating a nonwoven PGA fiber mesh while spraying it with an atomized PLLA or PLGA solution. The polymer solution builds up on the PGA fibers and bonds them at contact points. The advantages of fiber-bonding technique are its simplicity, the maintenance of the original fiber properties, and the use of only biocompatible materials like PGA and PLLA. However, obtaining a scaffold with a defined pore size, availability of suitable solvents, and immiscibility of the two polymers in the melt state and the required relative melting temperatures of the polymers are encountered problems with this method [66].

1.5.2 Solvent Casting and Particulate Leaching Techniques

Solvent casting and particulate leaching is a simple and most commonly used method for fabricating scaffolds for tissue engineering. Scaffolds produced by this technique have been used in many studies for bone and cartilage tissue engineering with promising results [116]. The technique involves mixing a water soluble porogen (e.g. sodium chloride, sodium citrate, sugar) with a biodegradable polymer solution in an organic solvent [110]. Then the solvent is evaporated and porogen is removed by immersing in water yielding an interconnected porous polymer scaffold. In this

method, the control of porosity and pore size is more likely compared to most conventional techniques. Porosity and pore connectivity are controlled by the ratio of polymer/porogen and the size of the porogen particulates.

1.5.3 Gas-Foaming Technique

In gas foaming technique high pressure CO_2 gas is applied to compressed polymer disks in order to prepare porous matrices. The porosity and pore structure depend on the amount of gas dissolved in the polymer, the rate and type of gas nucleation, and the diffusion rate of gas molecules through the polymer to the pore nuclei. In this method the use of organic solvents and high temperatures is avoided. However, the resultant matrices have closed pore structure and a solid skin of polymer remains on the surface of the matrices which are disadvantages in many tissue engineering applications. Combination of this method with salt leaching technique has been shown to create an open-pore network in scaffolds with enhanced compressive and tensile modulus compared to scaffolds prepared with salt leaching technique only [117].

1.5.4 Freeze Drying

Freeze drying is a simple and rapid scaffold fabrication method also called lyophilization. It is a frequently used technique and can be applied to both natural and synthetic polymers. Briefly, polymer solution is frozen within a mold and then the solvent is removed by vacuum sublimation leaving behind porous foam. Depending on viscosity of the polymer solution and freezing temperature, various pore size and porosity can be obtained within the foam structure. As viscosity and freezing temperature decrease, the pore size also decreases [118]. Closed-pore morphology and low mechanical properties are encountered disadvantages with this technique.

1.5.5 Electrospinning

Electrospinning is a modern fabrication method for producing fibrous networks with fiber diameters ranging from several microns down to several hundred nanometers. The process uses an electric field to control the formation and deposition of polymer fibers onto a target substrate. In this technique, a polymer solution (e.g. PHBV in chloroform) is loaded into a syringe and then expelled through a metal capillary at a constant rate via syringe pump. A high voltage (10 - 15 kV) is applied to the capillary, charging the polymer and ejecting it toward a grounded collecting surface. As the thin fibers assemble on the plate, the solvent evaporates, leaving a nonwoven porous scaffold. Fiber thickness and scaffold diameter depend on polymer concentration, used solvent, ejection rate, and applied voltage, capillary diameter, collecting material**.** A variety of natural materials such as silk fibroin, collagen, polypeptides and synthetic polymers such as PLGA, PHBV, PCL, PVA, and PEO can be processed through electrospinning [119,120].

1.5.6 Melt Based Fabrication Techniques

Melt moulding/particulate leaching, extrusion and injection moulding are among the melt based fabrication techniques. In melt moulding/particulate leaching, polymer is mixed with a porogen and loaded into a mould. Then, the mould is heated above the glass transition temperature of the polymer. When the glass transition temperature is reached, the mould is immersed in water to dissolve porogen. The technique allows fabrication of scaffolds with defined shapes by using predefined mold geometry. Extrusion and injection moulding also provide generation of highly porous and interconnected scaffolds as with melt moulding/particulate leaching. However, the control of pore distribution is difficult [121].

1.6 Scaffold Fabrication with Designed Architecture

1.6.1 Rapid Prototyping (RP)

Although permitting for the fabrication of scaffolds readily, the conventional methods discussed above have limitations in controlling interconnectivity and geometry of the 3D pore structure. Additionally, these methods often rely on the use of toxic organic solvents that are damaging to cells or tissues. To overcome this problem, rapid prototyping techniques have been adopted. Rapid prototyping (RP) is a common name for a group of techniques that can generate a 3D precise structure with fully interconnected pores directly from computer-aided design data [112]. These methods require a computer model of the desired scaffold architecture from computer-assisted design (CAD) or computed tomography (CT). Such a technique was initially explored at Massachusetts Institute of Technology [63]. It is an additive process in which each part is constructed in a layer-by-layer manner. The main advantages of this technique over conventional ones are fabrication of scaffolds with defined internal and external structure; computer controlled processing, and plotting of scaffolds with cells. Moreover, with this technique it is possible to visualize the defect geometry and it seems likely to fabricate very soon a complex scaffold having macroscopic, microscopic and nanoscopic structural properties in different areas resembling the natural complex tissue like bone. The 3D structure is generated layer by layer via defined processing techniques. Rapid prototyping techniques have been used mostly for the engineering of bone tissue [122-125]. There are several rapid prototyping (RP) techniques such as fused deposition modeling (FDM) and stereo lithography being explored for scaffold fabrication [126,127].

1.6.1.1 Melt-Dissolution Technique

In a melt-dissolution technique, molten polymers are extruded through an orifice which merges the material on the previous layer. Each layer is created by extrusion of a strand of material while it moves across the plane of the layer cross-section. Some common systems using this technique are; fused deposition modeling (FDM), 3D fiber-deposition technique, 3D bioplotter and rapid prototyping robotic dispensing system. This technique has been applied for the production of 3D scaffolds using many PCL, PLGA, high-density polyethylene, chitosan and composites like PCL/hydroxyapatite [128]. By using FDM processing, scaffolds with pore sizes ranging from 160 - 700 μm with porosities between 50 - 70% can be created [129]. Main advantage of this technique is that it allows fabrication of scaffolds with controlled pore size. The disadvantages are limited material types that can be processed and limited control in z direction. Suitable materials that can be processed by this method are only thermoplastic materials.

1.6.1.2 Particle Bonding Technique

In this technique particles are selectively bonded in a thin layer of powder material. The thin 2D layers are bonded one upon another to form a complex 3D solid object. 3D printing (3DP) and selective laser sintering (SLS) are the mostly used particle bonding techniques.

3DP utilizes a simple inkjet printing system directed by the CAD program. Briefly, a thin layer of polymer powder (e.g. PLGA) is spread over a piston surface. The inkjet dispenses a binding liquid, which is a solvent for the polymer, in the desired pattern of the scaffold layer. After a short bonding time, the piston is lowered by the thickness of a single layer and the subsequent layers of powder and binding liquid are applied. Unbound polymer remains in the network during the fabrication process to support

disconnected sections in the layer. Giordano et al. (1996) produced PLLA based scaffolds by 3D-printing and analyzed the effects of printing conditions on mechanical and physical properties of the scaffolds. They stated that 3D-printed scaffolds had mechanical properties similar to those made by compression molding [130]. Moreover, study of Kim et al. (1998) showed that hepatocytes cocultured with nonparenchymal cells were able to attach and survive on the 3D polymer scaffolds in both static and flow conditions [131].

Various RP technologies have been applied to process biodegradable and bioresorbable materials into three-dimensional (3D) polymeric scaffolds with controllable and reproducible porosity and well-defined 3D microstructures. Ang et al. (2004) fabricated chitosan and chitosan-hydroxyapatite scaffolds with a fully interconnected channel architecture using a robotic dispensing system and their results demonstrates that this system allows fabrication of 3D scaffolds with regular and reproducible macropore architecture [132].

In spite of the increasing interest in the use of RP, there are several challenges: The limited range of materials, the optimal scaffold design, the bioactivity of the scaffold, as well as the issues of cell seeding and vascularization [132]. Each RP technique has its shortcomings. For example, 3DP requires post processing to improve the mechanical properties of the scaffold. Fused deposition modeling, on the other hand, allows only the application of thermoplastic polymers and prevents the application of biological agents and natural polymers [133].

Material processability, degradation rate, degradation product and mechanical strength of scaffolds are important during the selection of materials for a selected RP process. Each technique requires a specific form of input material such as filament, powder, solid pellet or solution. For a scaffold; architecture, design, pore size, scaffold morphology, surface topography are important factors to be considered. Different types

of tissue require different optimal pore size. There are many studies indicating the existence of an optimal range of pore size for different cell types. Bingon et al. (2003) have cultured human osteoblasts and fibroblasts on materials with different porous morphologies and investigated influences of porosity and interconnectivity on penetration of cells. In their study they showed that an interconnection size of 15 μm seems to support the invasion of cells without decreasing the required mechanical strength [134]. Zeltinger et al. (2001) fabricated scaffolds with various pore sizes (38 - 150 μm) and void fractions (75% and 90%) using 3DP technology and salt leaching technique and they investigated the cellular reactions (adhesion, proliferation and matrix deposition) to pore size and void fractions [135]. Their results suggest that scaffolds with 75% void fraction are not suitable for tissue formation.

The surface roughness of the scaffold is important in cell–matrix interactions. A rough surface might enhance cell adhesion, but too rough surfaces might prevent the cells to form focal adhesions. In some type of RP systems, smooth surfaces are obtained as a result of melt process which might not be favorable for the cells and therefore might require further surface modification or coating.

The ease of scaffold fabrication using RP provides a way to investigate the cell-scaffold interaction. The effects of several factors like material rigidity, surface topography and roughness, pore size and architecture can be investigated to understand cell behavior.

Tissue engineering strategies offer artificial and biological solutions in order to meet various necessities of tissue reconstruction. There are many processing techniques and no one is unique for all tissue-engineering applications. Each method has distinctive advantages and limitations. An ideal scaffold is desired to have a high porosity, adequate pore size for cell migration and nutrient/waste exchange, biocompatibility, biodegradability, and mechanical integrity [136]. Depending on the tissue type and

extent of regeneration, scaffold properties must be ordered in order to select the most appropriate manufacturing method. Currently, researchers attempt to incorporate bioactive molecules into the scaffolds, develop new materials for scaffolding and produce constructs with mechanical properties that resemble those of the targeted tissue, and improve the time and costs of scaffold production.

1.7 Surface Modification of Tissue Engineered Constructs

Understanding of cell-substrate interactions and control of cellular environment are important in the development of scaffolds for tissue engineering. It has been stated that cell-substrate interaction may give explanation to differences in cell behavior in vivo and in vitro [137]. In order to clarify some fundamental biological phenomena like cell interactions with each other in tissues, cell response to stimuli, abnormal stimuli that give rise to pathological conditions, understanding the behavior of cells in a well-controlled microenvironment is needed. The nature of the surface can directly influence cellular response. Surface chemistry, as well as surface topography determines whether protein molecules can adsorb to the surface and how cells attach and align themselves. Attachment of cells depends on the cues present on the matrix for cell attachment, motility, differentiation, dedifferentiation and apoptosis. Cells are sensitive to their surroundings. In literature, several types of surface modification have been described in order to understand and manipulate cell behavior. Scaffold materials have been modified via protein coating [138], peptide immobilization, micropatterning [139] and plasma treatment [140] to alter cell attachment characteristics.

Many studies were performed to evaluate the influence of surface topography on cell attachment, alignment, proliferation, cytoskeleton arrangement, differentiation and gene expression [139,141,142]. These studies have shown that surface roughness may affect cell response. There are several techniques to create synthetic micro- and nano-structured surfaces [143-146]. Microfabrication and micropatterning techniques (e.g.

soft litography) using stamps or molds fabricated from elastomeric polymers have been applied for generating patterns of proteins and ligands on surfaces and microscale channels in the range of 0.1 - 100 μm for culturing the cells. Soft lithography techniques are inexpensive and relatively simple procedures. An elastomeric polymer, polydimethylsiloxane (PDMS) is used for prodution of stamps to form patterns on the surfaces of various substrates. There are various soft lithographic techniques like microcontact printing, micromolding, patterning with microfluidic channels, and laminar flow patterning.

Micro-scale featuring of material surfaces enable the studies of cell behaviour. The patterns on a material surface restrict the anchorage dependent cells (most normal cells in multicellular organisms are anchorage dependent) to specific regions and allow the precise control of the size and shape of the cells. Microtopographies like microholes, microwells, microgrooves, micropillars on surfaces have been created in order to investigate influence of topography on cell function. Mcbeath et al. (2004) showed that stem cells have differentiated into osteoblasts when allowed to adhere flattened and spread, whereas they became adipocytes when their spreading was prohibited by micro patterns on the surface [147]. It has been stated that local cues present on the surface influence differentiation of human mesenchymal stem cells.

The topography of the scaffolds affects the adhesion and migration of cells. The surface roughness of the scaffold is important in cell-matrix interactions [120]. Some cell types prefer smooth surfaces while some are prefer rough surfaces. Too sharp surfaces are not desired because the cells could be damaged physically. Su et al. (2006) seeded fibroblasts on pillared silicon substrates and investigated the influence of geometry of pillars on the cells' behaviour. They showed that fibroblasts have different morphology on the various surface patterns and that is their architecture was affected strongly by the heights of pillars [148].

Lack of biological recognition and possesing a hydrophobic surface are disadvantages of most synthetic biodegradable polymers used in tissue engineering[149]. In order to enhance cell function on these biomaterials, introduction of functional groups or molecules onto biomaterial surfaces is important. Surface modifications like plasma treatment and protein coating are effective techniques which provide chemical and biological cues to the cells, respectively. Coating of polymer surface with biologically active molecules (e.g. RGD sequence, fibronectin, fibrinogen, fibrin, hyaluronic acid etc.) via adsorption or chemical bonding have been applied in order to enhance bioactivity of the underlying material. Cells express specific integrins which bind to proteins of ECM. Thus, by coating the material surface with the correct protein cell attachment to the material can be enhanced. Even binding between the cells and proteins is temporary, it can at least provide anchorage points for the cells on the material. It has been showed that fibronectin adsorption onto polymer scaffold increased the initial cell attachment and proliferation compared to uncoated controls [150]. Moreover, hydrophobic surfaces have higher affinity for protein adsorption than less hydrophobic surfaces [151]. Following protein adsorption, cells can then bind to those proteins on the scaffold surface. Type of protein can affect the cell specific attachment. Body proteins like collagen, thrombospondin, osteopontin, bone sialoprotein, fibronectin, vitronectin, fibrinogen, laminin, entactin, and tenascin have been used for surface coating to facilitate cell adhesion. Proteins coated via adsorption will eventually lose their biological activity due to dissociation from the scaffold. For long term applications this is an disadvantage. However, for short-term purpose such as cell seeding, it is not a problem [152].

There is no a certain hydrophobicity value which is optimum for all cell types. But generally, cells do not prefer too hydrophobic surfaces. Plasma treatment is an effective and widely used method which changes the physicochemical properties of biomaterials' surfaces. Plasma treatmet can be used for surface etching, protein immobilization or increase of surface hydrophilicity. Modification of a hydrophobic

surface with oxygen plasma leads to a hydrophilic surface due to increase of oxygen-containing functional groups on the polymer surface [153]. It has been reported that oxygen plasma modification increased the wettability and enhanced cell attachment and cell proliferation on PLGA films [140].

1.8 The Aim of This Study

During last decade, a considerable development was achieved in bone tissue engineering which demonstrates a great potential for improved treatment or replacement of damaged bone as an alternative to conventional therapies. It is known that bone is a dynamic organ with highly capacity for growth, regeneration and remodelling. Therefore, bone tissue engineering should involve mimicking and creating a complex biomechanical environment for cell-cell and cell-matrix interactions which should also promote development of the cell-scaffold construct in vitro. Although extensive studies have been performed for the development of porous scaffolds for bone regeneration, with promising results, all have a common limitation that is the inherent lack of strength associated with porosity. In recent years, considerable attention has been given to the development of fabrication methods to prepare porous scaffolds for osseous tissue regeneration. Development of tissue-engineered constructs for bone tissue regeneration requires use of a suitable cell source and optimization of scaffold properties.

The ultimate goal of this study was to develop a biomaterial which supports osteogenic activity. For this purpose, a biocompatible and biodegradable poly(ester-urethane) based on polycaprolactone diol and lysine diisocyanate was synthesized. Incorporation of lysine amino acid into the polymer structure expected to show favorable biological properties. Synthesized polymer was used to prepare cell carriers (either two dimensional, 2D or three dimensional, 3D) for bone tissue engineering. The resulting scaffolds were examined by FTIR-ATR, NMR, GPC, DSC, TGA, mechanical tests,

contact angle measurements, SEM and fluorescence microscopy. For 2D structures, micropatterns were created on the surface in order to investigate the physical effects on osteoblastic cell function. Additionally, smooth and micropatterned 2D surfaces were coated with fibrinogen to compare the effect of biological modification with untreated surfaces in terms of cell attachment, proliferation and differentiation. To fabricate 3D scaffolds two techniques were used: rapid prototyping and conventional salt leaching. The resulting scaffolds had different compression moduli and porosities. For cell culture tests, all 3D scaffolds were treated with oxygen plasma in order to enhance penetration of cells within the structure. In 3D scaffolds, the influence of porosity and matrix stiffness on osteoblastic activity was investigated.

CHAPTER 2

EXPERIMENTAL

2.1 Materials

Polycaprolactone diol (MW=1250, PCL1250) and stannous 2-ethylhexanoate (stannous octoate) were obtained from Aldrich (Germany). PCL1250 was dried at 70^{o}C and stored in a vacuum desiccator until used. L-lysine diisocyanate (LDI, diisocyanate of the L-lysine methyl ester) was kindly donated by Kyowa Hakko Kogyo Co., Ltd (Japan). Absolute ethanol and 1,2-dichloroethane (DCE) were from Scharlau (Spain). Dexamethasone, β-glycerophosphate disodium salt and L-ascorbic acid were purchased from Sigma-Aldrich (Germany). Bovine serum albumin (BSA) was obtained from Fluka (USA). Dulbecco's Modified Eagle Medium (DMEM, high glucose) and fetal bovine serum (FBS) were obtained from Hyclone (USA). Penicillin/Streptomycin (Pen/Strep) solution was the product of HQClone. Trypsin-EDTA (0.25%), glutaraldehyde and cacodylic acid (sodium salt) were obtained from Sigma (USA). Fibrinogen was the product of Roche (Germany). Alexa Fluor 488 phalloidin and 4′-6-diamidino-2-phenylindole (DAPI) were obtained from Chemicon (USA). Nucleocounter reagents were supplied by Chemometec (Denmark) and Alamar Blue cell proliferation assay was from Biosource (USA). For the determination of ALP enzyme activity, alkaline phosphatase kit (Randox, USA) was used.

2.2 Synthesis of Lysine Based Polyurethane

Poly(ester-urethane) (PEU) synthesis from polycaprolactone diol and lysine diisocyanate was performed in DCE solution (0.39 M) at 80^{o}C for 3 h and then at room

temperature overnight under magnetic stirring and nitrogen flow. The molar ratio of polyol to diisocyanate was kept constant as 1:1. Stannous octate was used as catalyst with a concentration of 0.2% w/w. The resulting polymer was dissolved in chloroform, precipitated in water and dried under vacuum. The polymer was labeled as PEU and the chemical, thermal and mechanical properties were determined by nuclear magnetic resonance spectroscopy (NMR), Fourier Transform Infrared - Attenuated Total Reflectance (FTIR-ATR), gel permeation chromatography (GPC), differential scanning calorimetry (DSC), thermogravimetric analysis (TGA), dynamic mechanical analyses (DMA) and mechanical testing. The surface hydrophilicity was studied by water contact angle measurements using a goniometer. Synthesis of PEU and the urethane bonds are represented schematically in Figure 2.1.

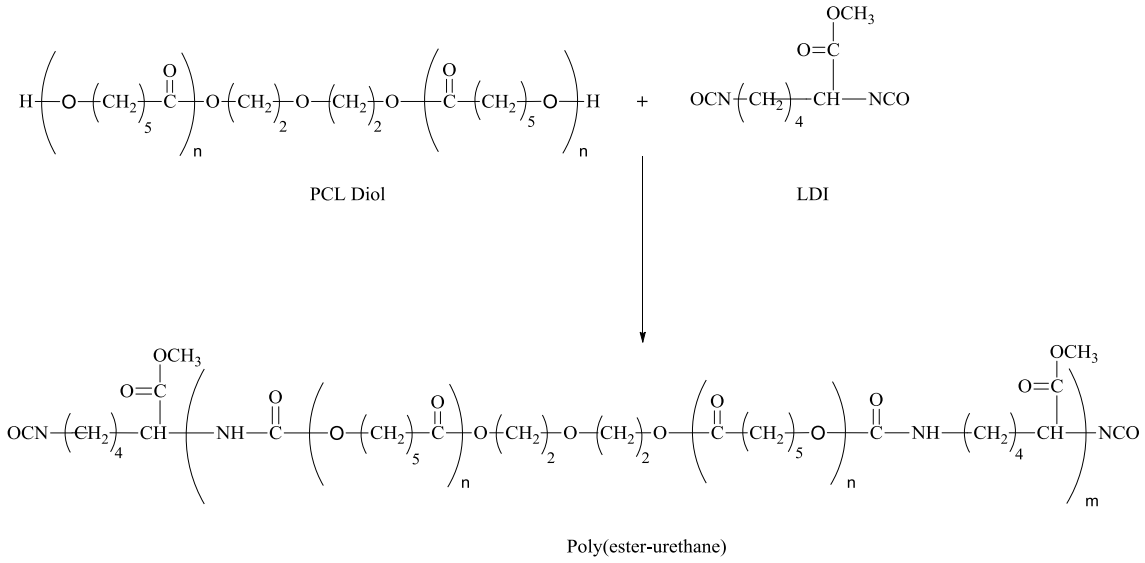

Figure 2.1. Synthesis of poly(ester-urethane) from PCL diol and LDI.

2.3 Preparation of PEU Matrices

Cells exist in a three-dimensional (3D) extracellular matrix in vivo. Therefore, biomaterials are generally fabricated into 3D scaffolds for tissue engineering applications to mimic the cell behavior in vivo. In this study, 2D and 3D matrices were prepared in order to investigate cell response to topographical differences. Designation of the prepared matrices is shown in Table 2.1 and the experimental part of the whole study is summarized in Figure 2.2.

Table 2.1. Designation of 2D and 3D matrices prepared from PEU

Designation	**Matrices**
	2D
SF	Smooth film
MF	Micropatterned film
SF-Fn	Fibrinogen coated smooth film
MF-Fn	Fibrinogen coated micropatterned film
SF-P	Plasma treated smooth film
	3D
SP0	Freeze dried
SP5	Freeze dried and salt leached with salt/polymer ratio: 5/1
SP10	Freeze dried and salt leached with salt/polymer ratio: 10/1
BP-B	Bioplotted with basic configuration
BP-O	Bioplotted with offset configuration

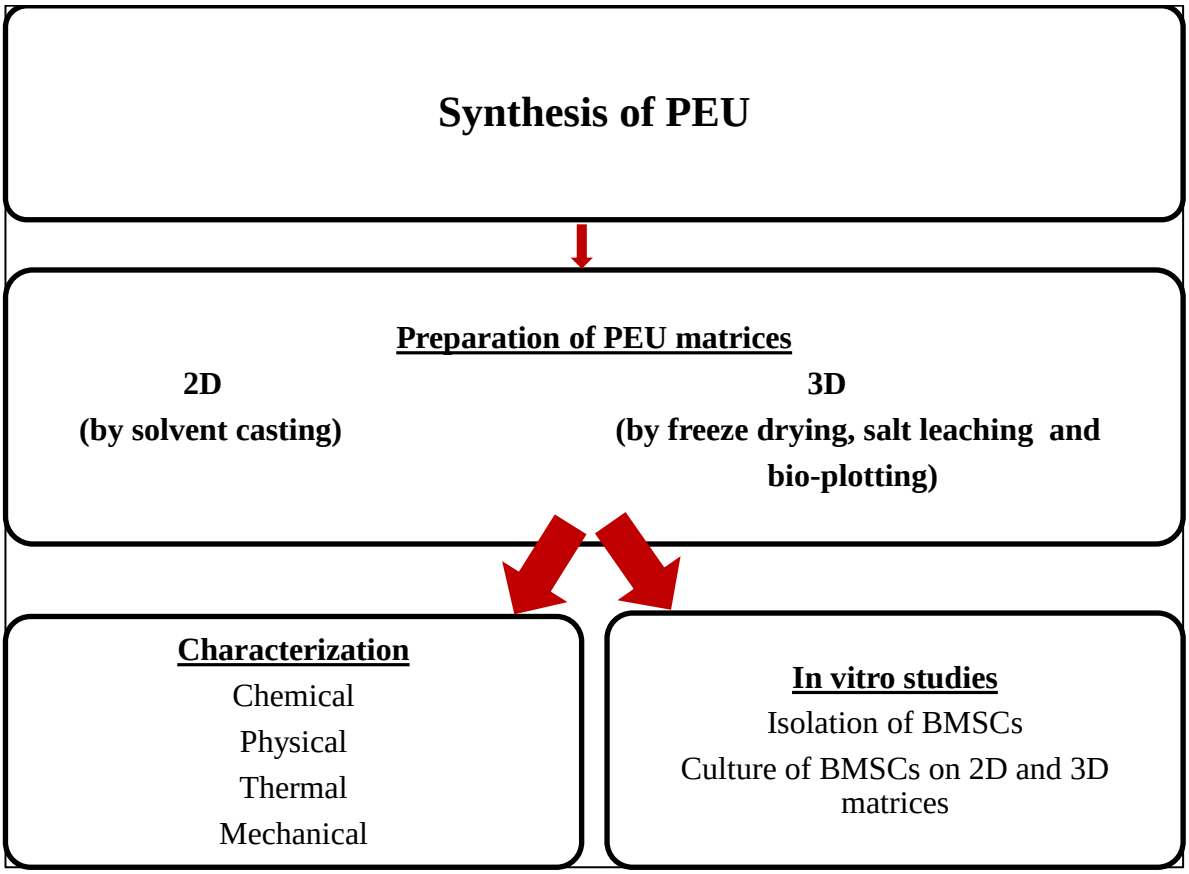

Figure 2.2. Summary of experimental study.

2.3.1 Preparation of PEU Films

Polymer films were obtained by solvent casting on glass petri dishes of a 15% w/v solution of PEU in chloroform and by drying first at room temperature and then in a vacuum oven for 48 h. The films were about 150 – 250 μm thick. Samples for characterization were cut from films, unless otherwise stated. Films without surface modification was referred as smooth film (SF).

Micropatterned film were obtained with the same approach on micropatterned polydimethylsiloxane (PDMS) templates (groove width: 4 µm, ridge width: 10 µm, depth: 4 µm, wall angle: 90^{o}) which themselves were obtained on micropatterned silicon wafers (Figure 2.3). After solvent evaporation, the films were peeled off from the templates. Film thickness ranged from 150 µm to 250 µm for both type of films. In order to improve cell adhesion on the films, fibrinogen (Fn) was adsorbed on the films. Briefly, 250 µL Fn solution (1mg/mL in PBS) was pipetted on ethanol-sterilized dry films. After 10 min, excess Fn solution was removed by pipetting and allowed to dry at ambient temperature in a laminar flow.

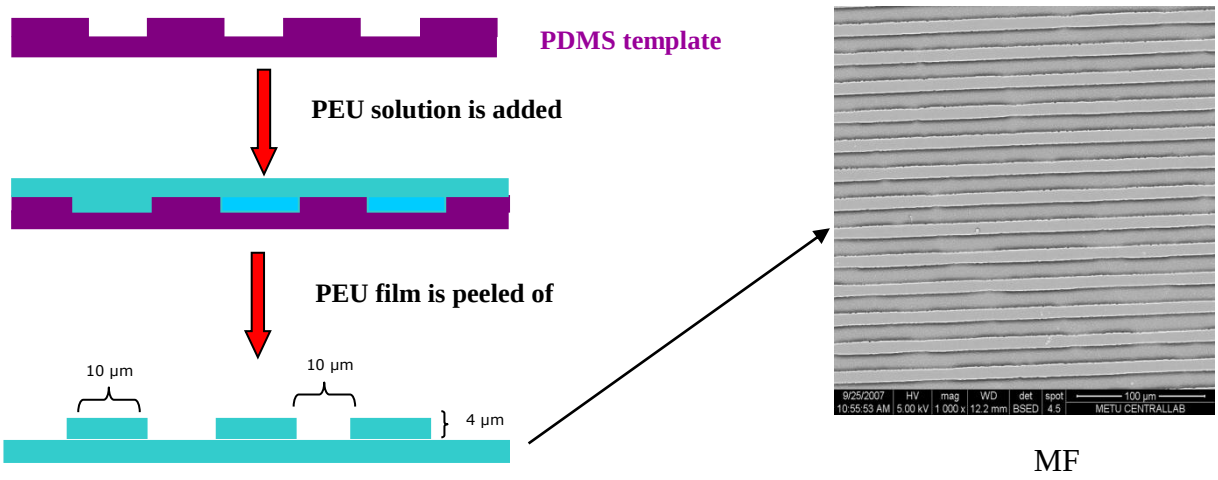

Figure 2.3. Schematic presentation of micropatterned polymeric film preparation.

2.3.2 Preparation of PEU Sponges

PEU solution (15%, w/v) was prepared in 1,4 dioxane and poured into glass petri dishes, frozen at -20^{o}C and then lyophilized in a freeze dryer (Labconco Freeze Dry, Model 78680, Missouri, USA).

In order to obtain a highly porous matrix, sieved salt crystals (180 - 300 μm) were added into PEU solution in 1,4 dioxane (polymer/salt ratio: 1:5 or 1:10 w/w). Then, solution-salt mixture was poured into glass petri dishes and processed as described above. Preparation steps of PEU sponges are illustrated in Figure 2.4. After drying, the samples were cut with a puncher (d = 6 mm) and the salt containing samples were immersed in distilled water in order to leach the salt particles. Prepared salt leached sponges were designated as SP5 and SP10 for the samples with polymer/salt ratio = 1:5, or polymer/salt ratio = 1:10, respectively.

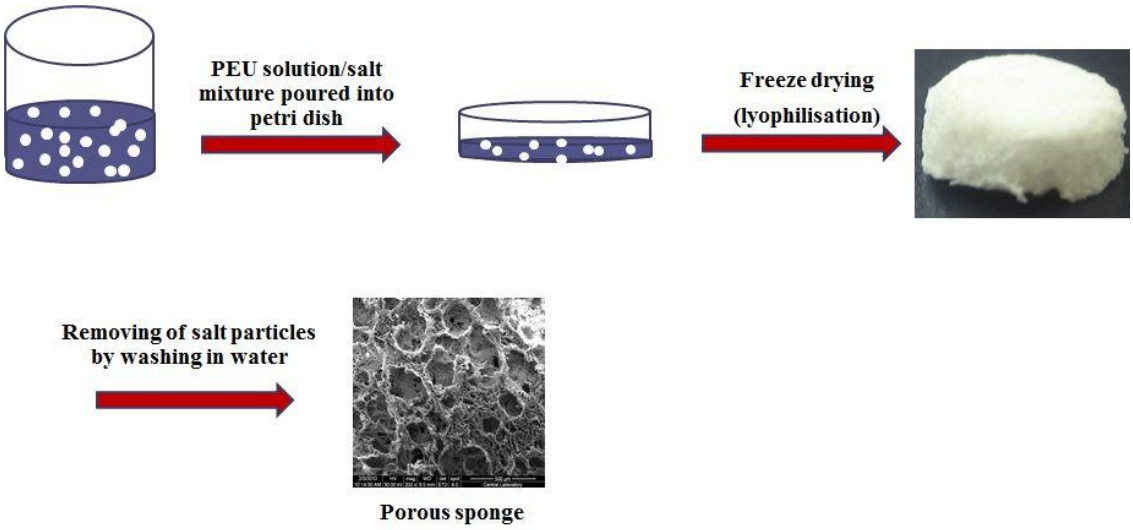

Figure 2.4. Steps of salt leaching for porous foam fabrication.

2.3.3 Fabrication of PEU Scaffolds by 3-D Plotting

PEU scaffolds were fabricated layer by layer using a Bioplotter® (Envisiontec GmbH, Germany) (

Figure **2.5**). In order to prepare polymer cartridges, ~ 5 g of polymer was manually compressed in plastic tubes and then heated at 50^{o}C for 15 min in oven where the

polymer slightly melts and no gaps were left within the polymer bulk. Then the polymer cartridges were removed from the oven and put in freezer (-20^{o}C) for another 15 min. After cooling, one polymer cartridge was placed in the stainless steel syringe of the equipment (needle length 28.1 mm, needle inner diameter 0.5 mm) and heated to 105^{o}C in the heated cartridge unit. When the polymer melted, CO_2 pressure (5 mm Hg) was applied to the syringe through a pressurized cap. Rectangular block models (20 mm x 20 mm) were uploaded on the Bioplotter CAD/CAM software and the 3D scaffold was plotted up to 8 layers, through the extrusion of polymer as fibers (Figure 2.6 a). Each layer was 20 mm x 20 mm with a thickness of 0.45 mm yielding a final 8 layered scaffold of 20 mm x 20 mm x 30 mm.

Scaffolds with different architectures were produced by changing the respective orientation of the deposited fibers using the CAD/CAM software. PEU scaffolds were produced by bioplotter to have two different standard architectures, named as: basic (BP-B), and offset (BP-O). The BP-B architecture was produced by the consecutive deposition of the layers, where each layer (N) was plotted orthogonally to the layer below (N-1), and was plotted in the same relative position of layer N-2 (Figure 2.6 b). The BP-O architecture was similar to BP-B, but layer N is plotted with in an offset distance relative to layer N-2 (Figure 2.6 c). Finally, the scaffolds were cut using a circular punch with 5 mm of diameter.

Figure 2.5. Bioplotter instrument.

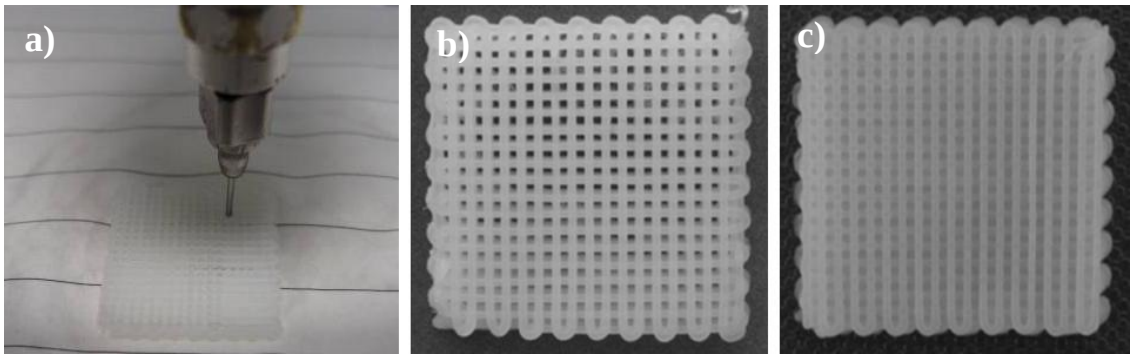

Figure 2.6. Plotting of melted PEU a) layer by layer, b) BP-B, c) BP-O (dimensions: 20 mm x 20 mm x 3 mm).

2.3.4 Modification of PEU Matrices with Oxygen Plasma

All 3D scaffolds were treated with oxygen plasma in order to enhance wettability of the samples prior to cell culture tests. For this purpose, 3D scaffolds were placed in a plasma chamber (Advanced Plasma Systems, with a SEREN IPS R 300 13.56 MHz power supply, St. Petersburg, USA) and subjected to oxygen plasma (100 W) for 3 min. Samples were then sterilized and used in cell culture tests.

2.4 Characterization of Matrices

2.4.1 Composition and Molecular Weight

The chemical structure of the poly(ester-urethane) was determined by liquid state NMR and ATR-FTIR study. ^{13}C-NMR spectra were recorded in $CCl_4/CDCl_3$ (2/3, v/v) solvent system on a Bruker Spectrospin Avance DPX 400 spectrometer. FTIR-ATR analysis was performed by Perkin Elmer Spectrum BX-FTIR Spectrometer (USA). The molecular weight of the polymer was determined by gel permeation chromatography (GPC, Polymer Laboratories, UK) with PL-GPC 220 with tetrahydrofuran (THF) as the carrier solvent. The Universal Calibration method was used during the GPC analysis.

2.4.2 Thermal Characterization

The thermal properties of the polymer were determined by differential scanning calorimetry (DSC) and thermogravimetric analysis (TGA). DSC was used to determine the glass-transition temperature (Tg) and crystalline melting temperatures (T_m) under nitrogen atmosphere by using DuPont 2000 Differential Scanning Calorimeter at a rate of 10°C/min in the temperature range between -100°C and 100°C. Thermal stability and thermal decomposition were studied by thermogravimetry using a Perkin Elmer Pyris 1 TGA instrument (USA) under N_2 atmosphere.

2.4.3 Determination of Porosity and Pore Size Distribution of PEU Matrices

Scaffold porosity was determined using liquid displacement method by pycnometer. The pycnometer is a glass vessel with a close-fitting ground glass stopper with a capillary hole through it. First, the sample and the empty pycnometer with glass stopper was weighted and recorded as m_s and $m_{p,}$ respectively. Second, the pycnometer was filled with decane (nonsolvent for the samples), weighted and recorded as m_1. Then, the sample was immersed and the total weight (pycnometer + n-decane + sample) was recorded as $m_{2.}$ Mass of decane (m_d) was found by subtracting (m_s + m_p) from $m_{2.}$ Volume of n-decane that fills an empty pycnometer was calculated as follow:

$$V_1 = \frac{m_S - m_p}{\rho_d}$$

Where, ρ_d is density of n-decane. V_1 gives the volume of the pycnometer.

Volume of n-decane that added (V_d) was obtained by dividing its mass (m_d) by its density (726.28 kg/m^3) and the volume of the sample (V_s) was found as;

$$V_s = V_1 - V_d$$

The percent porosity (P) of each scaffold was determined according to the following equation:

$$\text{P (\%)} = \frac{V_a - V_s}{V_a} \times 100$$

Where V_a is apparent volume of the sample calculated from simple formula for cylinders: $V_a = \pi r^2 h$

Each step was repeated two times for each individual scaffold.

Pore size distributions of the freeze dried and salt leached scaffolds were determined by Mercury intrusion Porosimeter (Quartachrome Corporation, Poremaster 60, Florida, USA).

Porosity of bioplotted scaffolds were assessed by using micro-computed tomography (μCT) (m-CT 20, SCANCO Medicals, Switzerland). Scanner settings were 40 keV and 248 mA. Entire scaffolds were scanned in around 200 slices. CT Analyser and CTVolRealistic 3D Visualization (SkyScan, Belgium) softwares were used for image processing in CT reconstructions, and to create and visualize the 3D representations.

2.4.4 Mechanical Properties of PEU Matrices

The mechanical properties of PEU matrices were studied by using Lloyd LRX 5K Mechanical Tester, controlled by a computer running program (WindapR). For tensile testing, the PEU samples were cut from prepared films as sheets (thickness = 0.20±0.07 mm, width = 10.0 mm, length = 40.0 mm) and attached to the holders of the instrument with a free length of 10 mm. A constant extension rate of 10 mm/min was applied to all samples.

For compression tests, 3D scaffolds in cylindrical shape were placed between compression presses. The compressive speed was arranged as 2 mm/min. The compressive modulus was evaluated from the initial linear elastic region of the stress – strain curve.

The load deformation curve was printed for each specimen. The tensile and compressive strengths were obtained from equation $\rho = F/A$, where ρ is the tensile or compressive strength (MPa), F is the maximum load applied (N) before rapture, and A is the initial area (m^2) of the specimen. The load deformation curve was converted to

stress–strain curve, where stress is the load applied per unit area (F/A) and strain is the deformation per unit length. Slope of straight line (elastic region of the stress-strain curve) is accepted as the Young's modulus of the specimen. Average of five experiment values was taken.

2.4.5 Dynamical Mechanical Analysis (DMA) of PEU Films

Dynamic mechanical analysis (DMA) was carried to determine the viscoelastic relaxation transition temperature of the PEU films with sample thickness around 200 μm. The measurements were carried out using a Perkin Elmer Pyris Diamond DMA (USA). The samples were measured over a temperature range from -103°C to 29°C at a heating rate of 3°C.min^{-1} under nitrogen atmosphere. The oscillation frequencies of 1 Hz, 2 Hz, 4 Hz, 10 Hz and 20 Hz were used and the analyses were carried out with oscillatory tension mode. The storage modulus (E′), and tan delta ($\tan\delta$) values were recorded against temperature at different frequencies. The T_g values were obtained from the peak maxima of tan delta curves.

2.4.6 Evaluation of In Situ Degradation

The stability of the polymer was evaluated by incubating in aqueous media with and without the presence of Pseudomonas lipase enzyme. Degradation experiments were carried out according to *ASTM* F-1635 standard of U.S.A. For enzymatic degradation, various types of polymer matrices (film, freeze dried, salt leached and bioplotted) were placed into vials containing 5 mL of PBS (0.1M, pH 7.4) with 0.18 U/mL enzyme and 0.02% of sodium azide to inhibit bacterial growth and incubated at 37^{o}C within a water bath shaker. The solutions were changed everyday. Samples were removed periodically, washed with distilled water, freeze dried and weighed in order to examine the weight loss due to erosion of the samples. The weighed samples were then placed back into the fresh PBS medium containing enzyme and sodium azide. Same steps

were followed for hydrolytic degradation, except enzyme was not added into PBS solution. Three parallel experiments were carried out for samples of each type of specimen and the measured values were averaged. Percentage weight loss was calculated as follows:

$$\text{Weight loss (\%)} = [(W_0 - W_1)/W_0] \times 100$$

Where W_0 and W_1 are weight of dry samples before and after hydrolytic or enzymatic degradation test, respectively.

2.4.7 Water Contact Angle Measurements

For contact angle measurements, thin films of PEU were obtained on glass slides by solvent casting of the polymer solution (15% in chloroform). The water contact angle values of films were measured by goniometer (KSV-CAM200, Finland) by using 5 μL deionized water drops with average of five measurements. Contact angle measurements were conducted on unmodified smooth PEU film surfaces (SF), on fibrinogen coated surfaces (detailed below) and oxygen plasma treated surfaces.

2.5 In Vitro Studies

2.5.1 Isolation and Culture of Mesenchymal Osteoprogenitor Cells

The biocompatability of the polymer for the cells was tested by using rat bone marrow mesenchymal stem cells (BMSCs). BMSCs were obtained from the femurs and tibias of 6 week old, male Sprague Dawley rats and cultured as it was previously described [128]. Briefly, femurs and tibias were aseptically excised, cleaned of soft tissue and washed with Dulbecco's modified Eagle's medium (DMEM) with penicillin and streptomycin about 10 times more of normal concentration. Then, the marrow within

the midshaft was flushed out with DMEM containing 20% fetal calf serum (FCS) and 100 U/mL penicillin and 100 μg/mL streptomycin, centrifuged at 3000 rpm for 5 min, the resulting cell pellet was resuspended in medium and plated in T-75 flasks. These primary cultures were allowed to reach approximately 80% confluence (~15 days, passage 0). Then the cells were trypsinized and stored frozen in liquid nitrogen until use.

2.5.2 Cell Seeding and Culturing on PEU Matrices

Unpatterned and micropatterned 2D PEU films were cut into 1 cm x 1 cm square shapes and placed in 24-well plates. The samples were sterilized in 70% ethanol for 2 h, and then washed with phosphate buffer saline (PBS, pH 7.4) three times and left to dry under laminar flow. Cell supsension (30 μL) containing $1x10^4$ cells were seeded on each film and incubated for 2 h at 37^oC to allow cell attachment. Then osteogenic media consisted of DMEM supplemented with 10% FCS, 10 mM β-glycerophosphate, 50 μg/mL L-ascorbic acid and 10 nM dexamethasone in the presence of 100 U/mL penicillin and 100 μg/mL streptomycin was added. The cells on the films were then allowed to grown for 3 weeks at 37^oC in a humidified atmosphere containing 5% of CO_2 with changing the media every other day.

In cell culturing of 3D scaffolds; first salt leached and bioplotted 3D scaffolds were sterilized under UV for 30 min for each surface. Then 100 μL of cell supsension containing $5x10^4$ cells were seeded on each scaffold and the same culture conditions were followed as described above.

2.5.3 Microscopy and Image Analysis

2.5.3.1 Scanning Electron Microscopy

The microstructures of the 2D and 3D PEU matrices were characterized using Scanning Electron Microscope (SEM, FEI Quanta 400F, Holland). The samples were mounted on aluminum stubs, sputter-coated with gold–palladium (AuPd) under an argon atmosphere. For examination of cell morphology and deposited minerals, cell seeded samples were fixed with 2.5% glutaraldehyde in 0.14M sodium cacodylate buffer (pH 7.4) for 2 h at room temperature, rinsed in cacodylate buffer, and freeze dried.

2.5.3.2 Fluorescent Microscopy

The cell morphology and spreading at different time points were characterized by fluorescent microscope (Leica, TCS SPE, Germany). For fluorescent examination, the samples were washed twice with PBS (10 mM, pH 7.4) fixed in 4% paraformaldehyde solution in PBS for 15 min at room temperature, and treated with triton X-100 (1%) for 5 min to permeabilize the cell membrane. Samples were then incubated at 37^{o}C for 30 min in 1% bovine serum albumin (BSA)-PBS (10mM pH 7.4) solution and incubated with FITC-labeled phalloidin and DAPI to stain F-actins and the nuclei, respectively.

2.5.4 Cell Proliferation

Number of viable cells on the samples was assessed with Alamar Blue assay (US Biological) at different time points. Prior the measurement, the culture medium in the wells was discarded and the wells were washed with sterile PBS to remove any remaining medium. Then Alamar Blue solution (10%, 1 mL) in colorless DMEM was added to the wells and incubated at 37°C and 5% CO_2 for 1 h. After 1 h, 200 µL of the test solution was transferred to a 96 well plate and absorbance was determined at 570

nm and 595 nm using the plate reader (Molecular Devices, V max Microplate Reader, USA). The test medium in the wells was then discarded, washed with sterile PBS, fresh complete medium was added to the wells and the incubation was continued.

2.5.5 Determination of Osteoblastic Differentiation

2.5.5.1 Alkaline Phosphatase (ALP) Activity

ALP activity was determined on BMSC seeded 2D films by using a biochemical Randox kit (USA), based on conversion of p-nitrophenyl phosphate to p-nitrophenol. The absorbance of p-nitrophenol formed was spectrophotometrically measured at 405 nm and amount of enzyme was calculated from a calibration curve according to manufacturer's description. The analysis carried out with triplet samples.

2.5.5.2 Matrix Mineralization

Mineralization by osteoblasts on 2D film matrices was studied by labeling the calcium phosphate formed with tetracycline as described earlier [139]. The cells seeded on the TCP and films were cultured for 3 weeks. On the third day of culture the previously used antibiotics (penicillin and streptomycin) were replaced with tetracycline (10 mg/mL). At the end of third week, the cells were washed with PBS, then with 70% ethanol and fixed in 96% ethanol at 4^{o}C for 6 h. Ethanol was discarded and the films were left to dry in the dark. Mineralization was studied at an excitation wavelength of 480 nm using the fluorescence microscope (Leica, TCS SPE, Germany).

On the other hand, mineralization on 3D scaffolds was examined by von Kossa staining and SEM/EDX analysis after 5 weeks of culture. For von Kossa staining, seeded scaffolds were fixed with PFA as described before, washed with distilled water and incubated in 5% $AgNO_3$ under ultraviolet light for 30 min. After rinsing in several

changes of distilled water, samples were treated with 5% sodium thiosulphate for 5 min in order to remove unreacted silver. Then samples were rinsed in distilled water for several times before visualization under light microscopy. For SEM/EDX analysis, samples were prepared as described in section 2.5.3.1.

CHAPTER 3

RESULTS AND DISCUSSION

3.1 Characterization of PEU Matrices

In this study; a biodegradable poly(ester-urethane) (PEU) was synthesized from polycaprolactondiol (PCL) and lysinediisocyanate (LDI). The polymerization and the chemistry of the PEU were examined with FTIR-ATR, GPC and NMR and the results provided a confirmation of the successful synthesis.

3.2 Liquid State NMR, FTIR-ATR, GPC and Contact Angle Analyses

The chemical structure of the synthesized PEU polymer was verified using its ^{13}C-NMR and FTIR-ATR spectra. In ^{13}C-NMR spectrum it was seen that –OH bonded specific peaks of alkyl carbons (32 ppm ve 68 ppm) present in PCL, were not present in the PEU spectrum and a new urethane carbonyl carbon peak demonstrating the formation of PEUs appeared (157 ppm) (Figure 3.1).

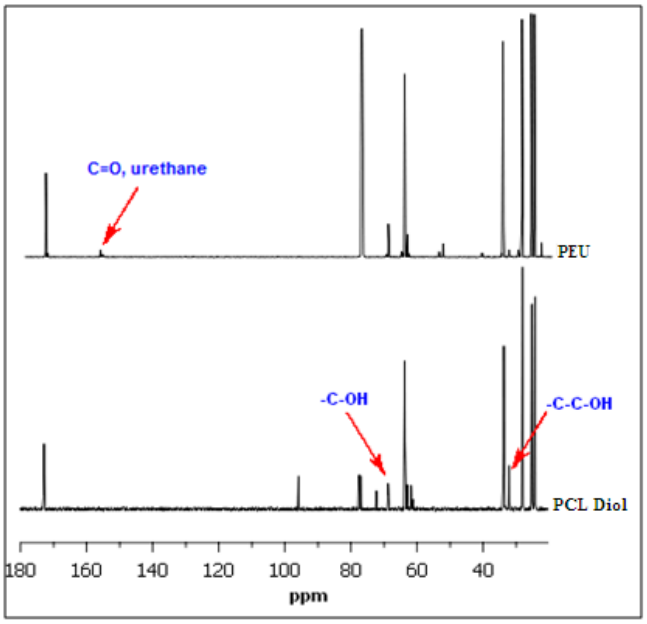

Figure 3.1. ^{13}C NMR spectrum of PEU and PCL diol.

FTIR is useful in the characterization of the functional groups present in the polymer. The IR spectra of PEU and one of its precursors, PCL are shown in Figure 3.2. In the PEU spectrum, N-H stretching and bending vibration of urethane bonds at 3362 cm^{-1} and 1524 cm^{-1} were observed. Besides, disappearance of hydroxyl peak of PCL (3500 cm^{-1}) and the NCO peak in LDI (2260 cm^{-1}) [83] are indications of successful synthesis of PEU. In addition, GPC data of PEU show that weight average and number average molecular weights were $58.3x10^3$ and $19.5x10^3$, respectively (Table 3.1).

Surface wettability of a biomaterial is very important in the sense of protein - surface interaction which eventually determines cell attachment. Contact angle is dependent on polymer surface hydrophilicity which influence cell adhesion. As seen in Table 3.1, water contact angle of the smooth PEU films decreased from 90±3° to 82±1° as a result of Fn coating. Fn adsorption led to a slight increase in hydrophilicity of smooth PEU

films which may enhanced the interaction between cells and biomaterial. There are also contrary results reported in the literature. Bumgardner et al. (2003) evaluated the contact angle, protein adsorption and osteoblast attachment to intact and chitosan coated titanium surfaces and they reported that protein adsorption was higher on chitosan coated titanium surfaces even chitosan coatings exhibited higher water contact angles (76°) than uncoated titanium controls (32°). They concluded that high amine positive charge of the chitosan promoted greater protein adsorption and enhanced cell attachment [154]. Thus, we can hypothesize that lysine based polymer (PEU) used in this study may enhance cell adhesion by promoting fibrinogen adsorption to the polymer surface.

On the other hand, a significant decrease from 90±3° to 23±1° was observed for oxygen plasma applied film surfaces (SF-P), which indicates considerable increase of surface wettability (Table 3.1). Oxygen plasma application is widely used in tissue engineering applications to enhance initial cell attachment onto hydrophobic synthetic polymers [155].

Table 3.1. The molecular weight, heterogeneity index (HI) and water contact angle values of SF

Molecular weight		**HI**	**Water contact angle (°)**		
M_w ($g.mol^{-1}$) $x10^3$	**M_n ($g.mol^{-1}$) $x10^3$**		**SF**	**SF-Fn**	**SF-P**
58.3	19.5	2.98	90 ± 3	82 ± 1	23 ± 1

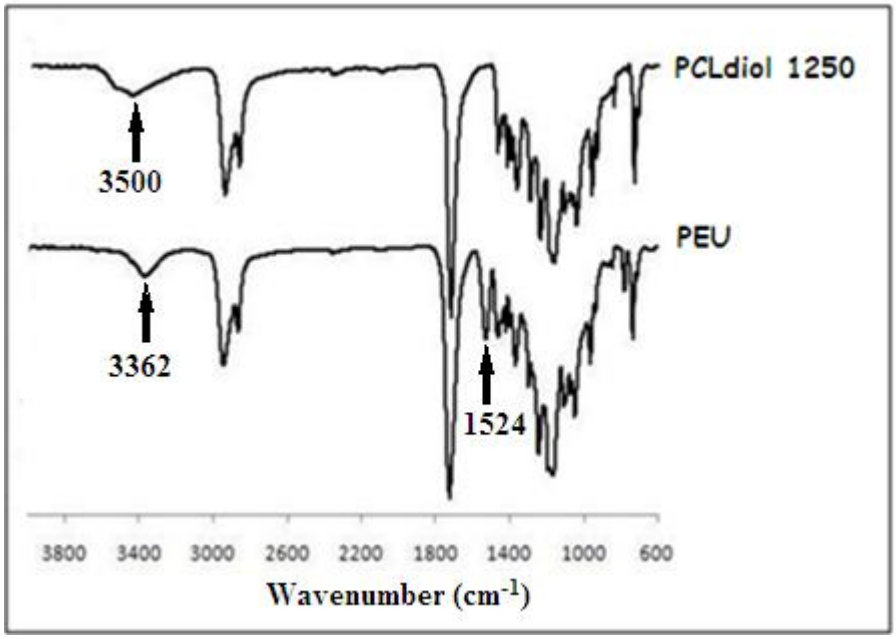

Figure 3.2. FTIR-ATR spectra of PEU and PCL diol.

3.3 Thermal Properties of PEU Matrices

In biomedical applications it is important to know thermal properties of the polymers, because they determine the physical properties of the materials. If the glass transition temperature (T_g) of the polymer is above that of body temperature, the polymer is rigid when implanted. On the other hand, if the T_g value is below the body temperature, as in the PEU synthesized in this study, it indicates the elastomeric characteristic of the polymer.

The thermal properties of the prepared PEU matrices were determined by DSC and TGA. Thermal data for processed samples are reported in Table 3.2. For DSC analysis, four samples representing different preparation methods were examined. The first-heating DSC thermograms for different specimens, namely smooth film (SF), freeze

dried sample (SP0), salt leached sample (SP10) and bioplotted basic (BP-B) samples are presented in Figure 3.3. The melting peaks (T_m) were observed at about 45^{o}C, 41^{o}C, 40^{o}C and 51^{o}C for SF, SP0, SP10 and BP-B, respectively. The thermogram of BP-B has relatively broader melting peak which is attributed to broader distribution of crystal sizes than other specimens [156]. The smaller peak near 39^{o}C is due to melting of small and imperfect crystallites formed during the solvent evaporation. This low melting point make the polymer a good candidate for processing by melting techniques; however a T_m of ~45°C make the polymer unsuitable for thermal sterilization which may be an important criterion in biomedical applications.

Although the melting thermograms differ from each other, all specimens showed close T_g values ranging from -45^{o}C to -43^{o}C. The differences in melting thermograms can be attributed to different preparation of the mentioned four specimens: The films were casted by chloroform evaporation, salt leached samples were prepared in different solvent (dioxane) and bioplotted samples were obtained by melting process. Therefore, each specimen showed different thermal responses.

The thermogravimetric analysis (TGA) was carried out for 2D SF samples and 3D SP10 and BP-B scaffolds in order to assess the thermal stability of the synthesized polymer and to define the effect of salt leaching and melt processing on thermal properties (Figure 3.4). The TGA analysis shows that the polymer is thermally stable as the degradation temperature for SF, SP10 and BP-B samples was around 300°C. It is seen that neither salt leaching process nor melting process for rapid prototyping did not cause a significant change in the degradation temperature of the polymer since TGA curves of SP10 and BP-B displayed similar weight loss phenomena as solvent casted film samples.

Table 3.2. Thermal data for different PEU matrices

Sample	T_g (^oC)	T_m (^oC)	T_d (^oC)
SF	-45.29	45.27	300
SP0	-42.70	40.66	-
SP10	-44.41	40.28	300
BP-B	-45.34	51.37	300

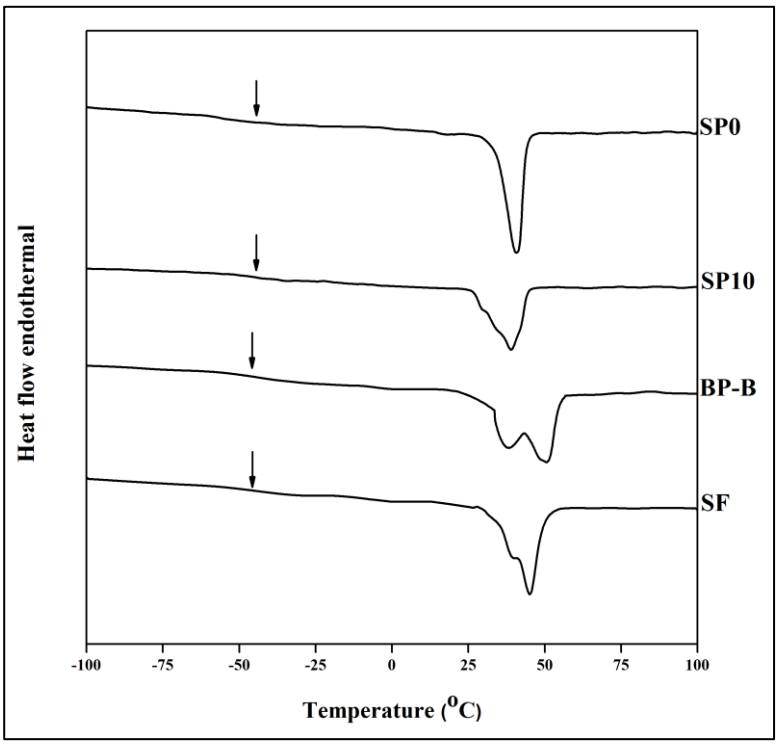

Figure 3.3. DSC thermograms of PEU matrices.

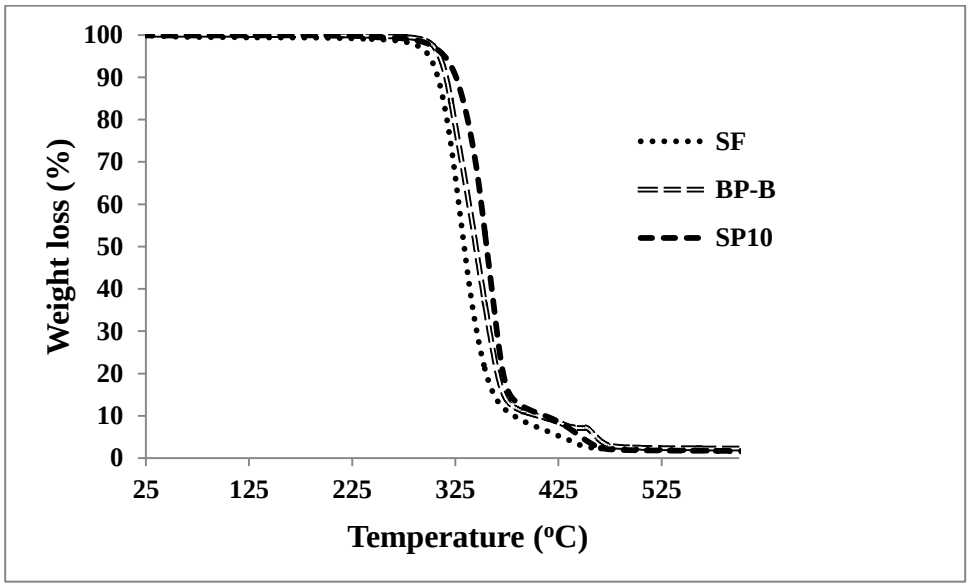

Figure 3.4. TGA curves of SF, SP10 and BP-B samples.

3.3.1 Tensile Test Results of PEU Films

The mechanical values showing the tensile strength, elastic modulus, and ultimate elongation of the PEU films are summarized in Table 3.3. The polymer was highly flexible, with ultimate tensile strength of 5.74 MPa and maximum strain about 1500%. The initial modulus was found as 11.94 MPa. The mechanical behavior of the polymer is similar to those of poly(ester-urethane)s obtained with PCL and LDI. In literature, generally higher tensile strength and lower elongation values were reported for these poly(ester-urethane)s, which resulted from use of a higher molecular weight of PCL (e.g. 2000 g/mol) and a chain extender to increase hard blocks in the polymer chains [157]. The high elongation value of synthesized PEU is due to high content of soft segment in the polymer.

Figure 3.5 shows stress –strain behavior of the prepared PEU film which is typical for viscoelastic poly(ester-urethane)s, and indicates the semi-crystalline structure of the prepared films [83,157]. As it is seen in the stress–strain curve, after a steep stress, there is a yield point where formation of a neck was visually observed. The stress increased sharply almost up to a certain small strain and then increased linearly with an incredible increase in the strain.

Table 3.3. Tensile test parameters of PEU

Mechanical Properties		
Ultimate Tensile Strength, (MPa)	**Modulus of Elasticity (E´), (MPa)**	**Elongation at Break (%)**
5.74 ± 1.33	11.94 ± 1.03	1504 ± 291

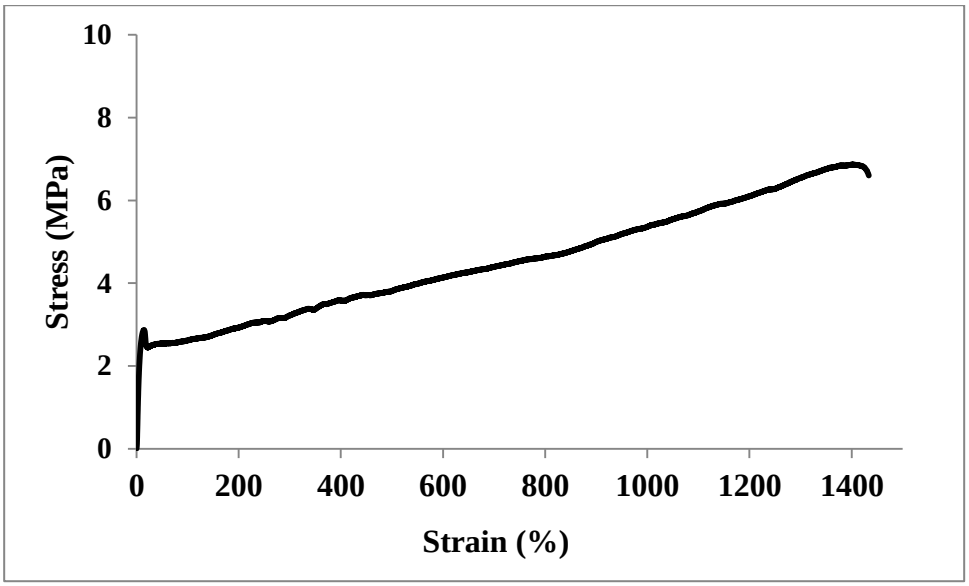

Figure 3.5. Representative stress–strain curve of the PEU synthesized in this study.

3.3.2 Dynamical Mechanical Analysis (DMA) of PEU Films

DMA analysis was carried out in order to determine the relationship between tan δ, and storage modulus (E′). DMA measures the modulus (stiffness) and energy dissipation properties of a material as the material is deformed under a periodic stress. It is particularly useful for evaluating polymeric materials that exhibit time, frequency and temperature effects on mechanical properties due to their viscoelastic nature.

DMA plots for tan delta (Figure 3.6) and storage modulus (E′) (Figure 3.7) of PEU films at different frequencies (1, 2, 4, 10 and 20 Hz) were obtained as a function of temperature. The mechanical behaviors of thermoplastic polyurethanes are known to be dependent on strain rate. Storage modulus is a measure of material stiffness and can be used to provide information about molecular weight, degree of cure and cross-link density of the polymer. The storage modulus is plotted logarithmically in order to clarify the transition regions. As seen in Figure 3.7, the storage modulus rapidly decreases above 20°C which confirms the DSC results that the synthesized polymer would be useful in low-temperature applications.

In addition to DSC analysis, DMA gave a further insight into the transition temperature (T_g). The temperature corresponding to the maximum peak of tan δ is defined as the glass transition temperature. Tan δ peaks and corresponding Tg values are given in Table 3.4. The tan δ curve displays a broad peak between -60°C and 10°C which is associated with the glass transition region of the PCL soft block of the PEU. The Tg region of the LDI hard block segment of the polymer was not obvious which is evident for relatively low amount of hard blocks in the polymer. Hassan et al. (2006) observed the Tg region of the hard block segment between 25 - 34°C for low amount and between 10 - 45°C for high amount of chain extender in LDI/PCL based poly(ester-urethane)s [157]. They also observed that the hard block Tg was more prominent for

the polymer with relatively high amount of chain extender. The Tg value observed at 1 Hz (-43.86°C) showed good correlation with the Tg value obtained by DSC (-45.29°C). As seen in Figure 3.8, Tg has shifted with strain rate (frequency). Shifting in Tg was not observed at all frequencies, but when increasing the frequency from 2 to 4 Hz and from 10 to 20 Hz (Table 3.4). Yi et al. (2006) defined this shifting as a shift in apparent Tg, which is mechanically recognized Tg by the material at a given strain rate [158]. This increase in Tg is consistent with elastomeric polymers which indicates formation of phase mixing at some degree [159].

Table 3.4. Tan δ peak magnitude and Tg values for PEU at different frequencies

Hz	**Tg (°C)**	**Tan δ**
1	- 43.86	0.23
2	- 43.86	0.23
4	- 39.88	0.26
10	- 39.88	0.29
20	- 34.56	0.37

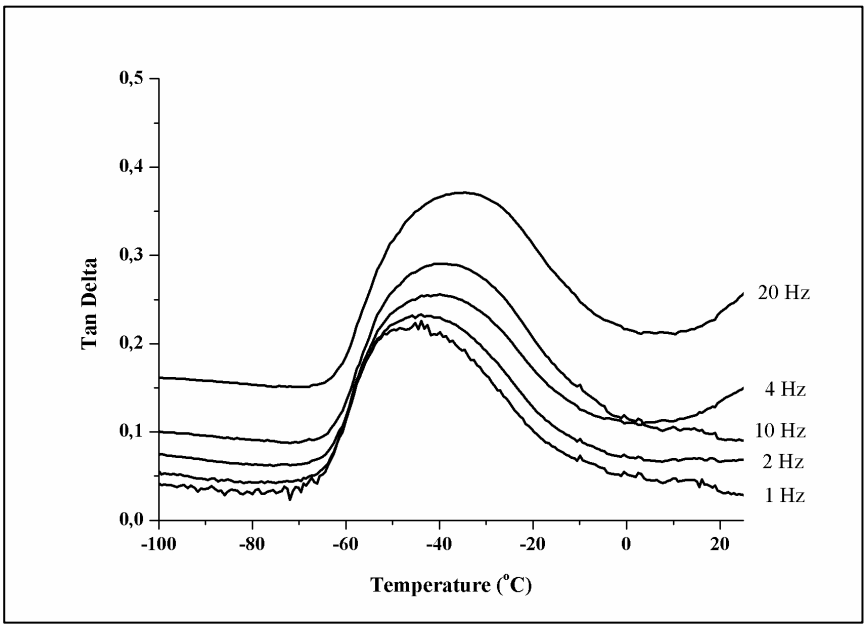

Figure 3.6. Tan δ versus temperature curve of PEU film at different frequencies.

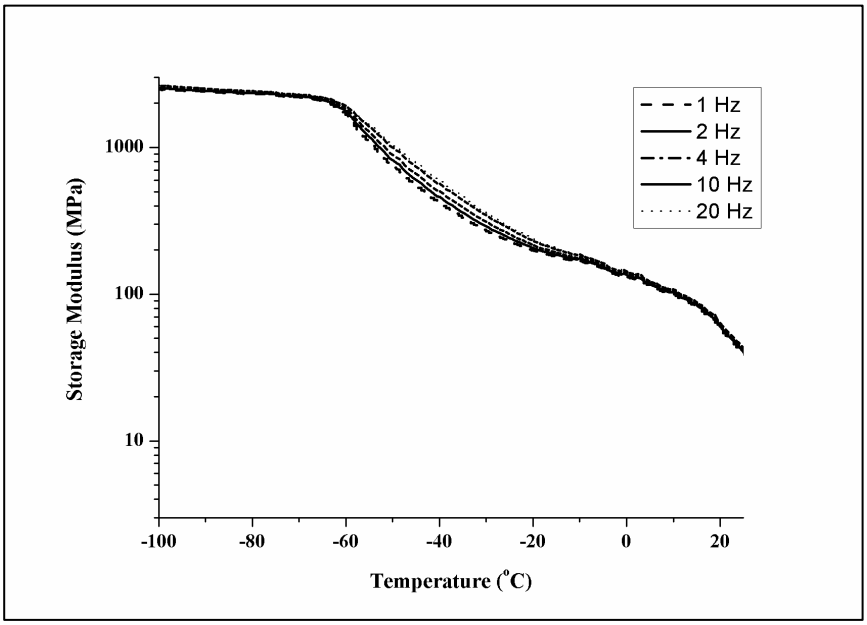

Figure 3.7. Temperature dependency of the storage modulus for PEU film at different frequencies.

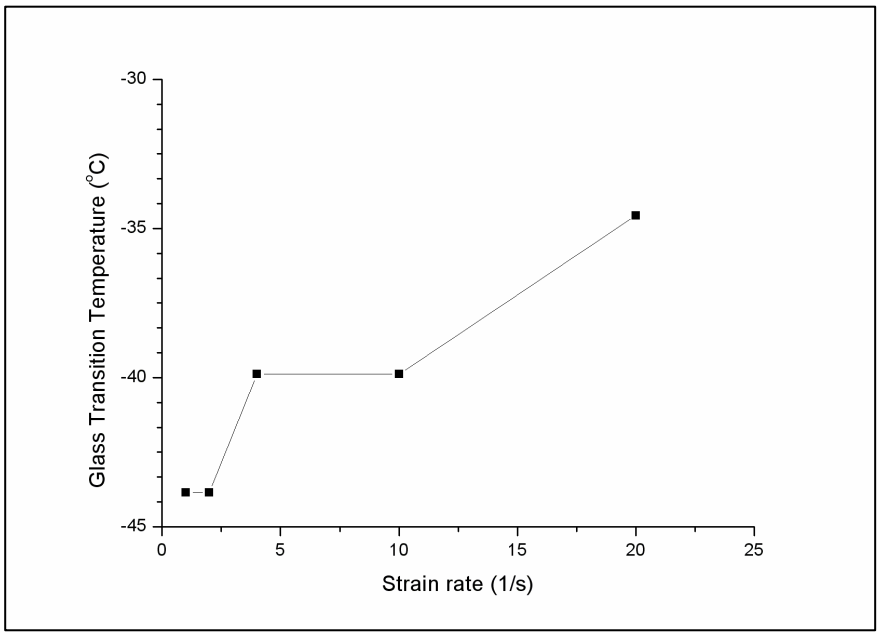

Figure 3.8. Shifting of Tg at different frequencies.

3.4 Morphology of 3D PEU Matrices

Morphology and pore interconnection of porous structures of the 3D scaffolds were observed by SEM. The synthesized PEU fabricated into scaffolds of any desired shapes with different pore sizes, either by freeze drying or by salt leaching or by bioplotting, as shown in Figure 3.9 and Figure 3.10. The bioplotted scaffolds as basic (BP-B) or as offset (BP-O) configuration had fully interconnected pore architectures with a strand diameter and strand distance and pore size of ~450 μm. The approximate pore sizes of SP0, SL5 and SL10 were in the range of 5 - 50 μm, 10 - 300 μm and 30 - 350 μm, respectively. The surface area/volume ratio of the salt leached (SP5 and SP10) sponges was greatly increased compared to SP0 sponges obtained by freeze drying. Higher surface area/volume ratio provide more area for the cells to attach, thus would increase the percentage of total cells attached and cell diffusion into the scaffold. SEM images

also revealed the presence of numerous pore interconnections with at least 5 micron sized pores in salt leached scaffolds which expected to promote vascular and tissue ingrowth when implanted.

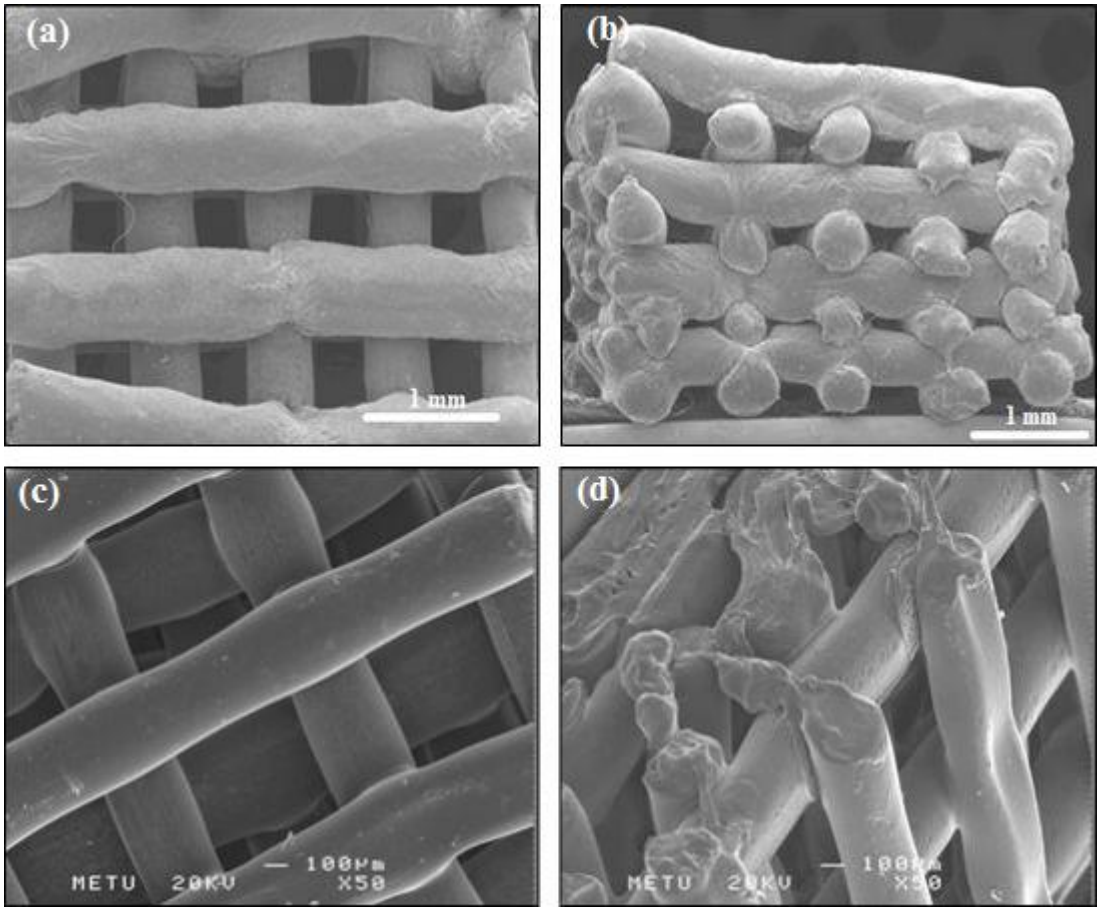

Figure 3.9. SEM images of PEU scaffolds fabricated by Bioplotter. a) BP-B top surface, b) BP-B side profile, c) BP-O top view, d) BP-O side profile.

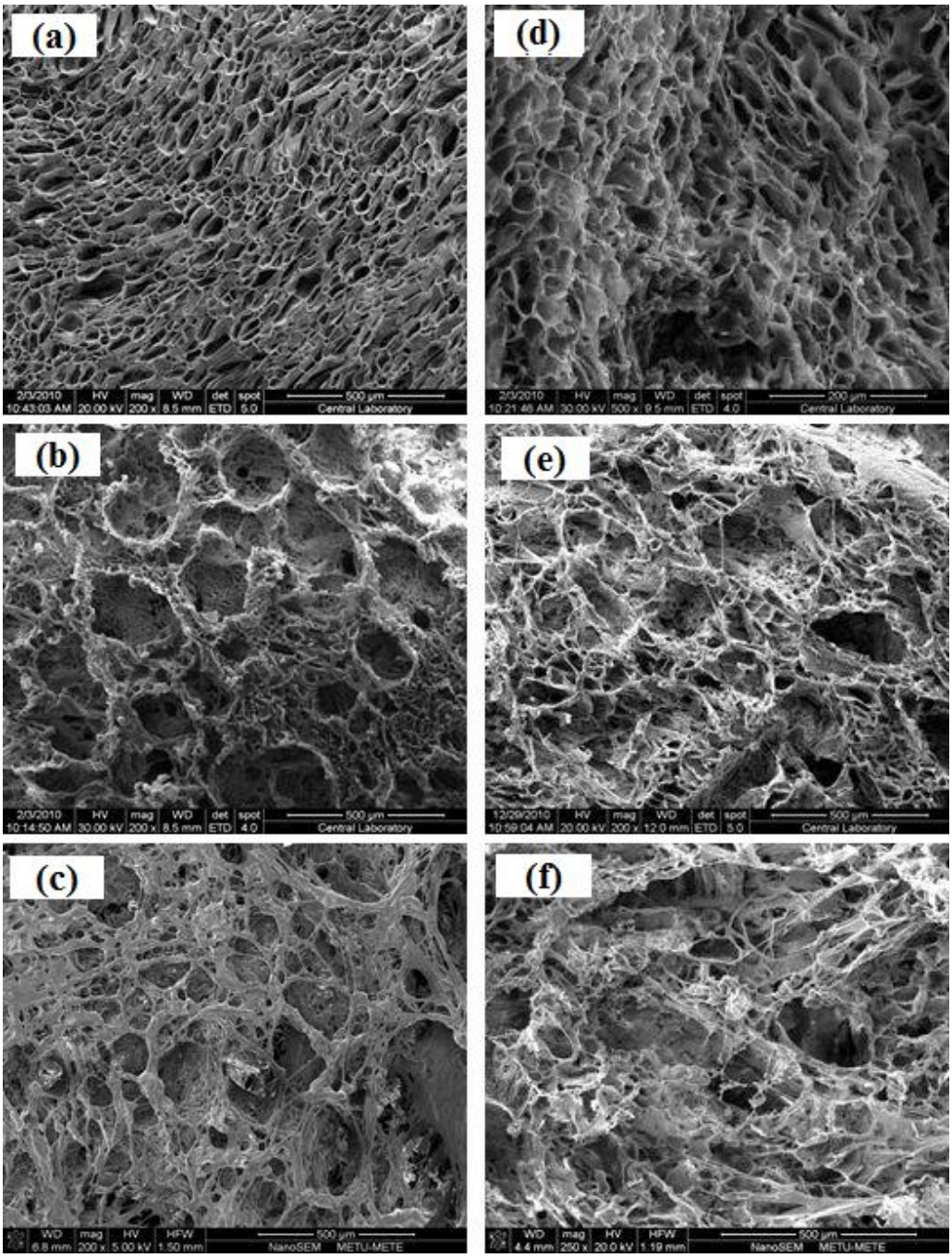

Figure 3.10. SEM images of PEU scaffolds prepared by freeze drying and salt leaching. a, d) SP0; b, e) SP5; c, f) SP10. a, b, c) Upper surface, d, e, f) Longitudinal cross-section.

3.5 Porosity and Pore Size Distribution of 3D PEU Matrices

3.5.1 Determination of Porosity

The microstructures of the scaffolds are defined by their porosity values [160]. Pore size and porosity are among the most important parameters used to characterize a scaffold. Porosity refers to the overall percentage of void space within a solid, whereas pore size indicates the diameter of individual voids in the scaffold. It is a general acceptance porosity, mean size, pore size distribution and pore interconnectivity play a critical role in scaffold design and production because of its importance for cell migration, proliferation and ECM formation [161]. Permeability of a scaffold is also important for nutrition diffusion and waste clearance. Some researchers reported the pore size as determinant for sufficient tissue ingrowth where a minimum pore size for tissue ingrowth and vascularization was indicated as 100 μm [162], while some others' studies suggested that the controlling factor is the pore interconnection size which is related to both pore size and the extent of porosity. A minimum pore diameter is important that as cells proliferate the pore diameter will eventually drop to a size where cells can not longer fit into the pores which will lead to decrease in cell viability. For bone tissue engineering, the ability of a scaffold to enhance osteogenic differentiation and support new bone formation is dependent pretty much on the pore size and porosity of the scaffold. The importance of scaffold porosity and pore size can be attributed to the native structure of bone, which itself is a porous tissue. Cortical bone is mainly a dense structure, but its small porous region (totally 10%) allows vascularization and cellular infiltration. On contrary, cancellous bone has a highly porous structure (50-90%) [163].

In an in vivo study, ceramics with a pore size range of 50 - 100 μm and 200 - 400 μm with similar porosity (60%) were compared. It has been shown that tissue ingrowth was totally achieved by specimen with small pores, whereas in larger pored specimen tissue

did not infiltrated all the pores after a couple of months. The results suggests that a well-interconnected 50 - 100 μm pores could be more suitable for rapid and sustained bone ingrowth when compared with less connected but larger pores of 200 - 400 μm with similar porosity [164].

Thus, achieving structural interconnectivity between pores is crucial in scaffold fabrication. Klawitter et al. (1971) conducted several studies about porous ceramics as bone graft substitutes. In one study, they showed that interconnection sizes at least 100 μm, 40 μm and 5 μm were required for the ingrowth of mineralized tissue, osteoid and fibrous tissue, respectively [165]. Lu et al. (1999) reported 50 μm as the critical pore interconnection size for bone ingrowth by using HAp or β-TCP in their study [166]. The minimum level for continuous bone integration was reported to be around 50-60%. All these thresholds for pore size, pore connectivity and porosity volume is generally attributed to nondegradable scaffolds as degradation leads to pore opening in the structure. Therefore, optimal degree of connectivity and porosity for degradable scaffolds may be lower than those established in literature for nondegradable ones [161].

In this study, pore size and porosity of scaffolds produced by Bioplotter were determined by using micro computed tomography (μ-CT), while porosity of sponges were obtained by using pycnometer. For the prepared scaffolds mean pore sizes are obtained from SEM images, while pore size distribution is determined by mercury porosimeter. Although SEM is useful for evaluation of pore shape and size, SEM image analysis does not give exact size distribution of the pores. In the last decade, a computer aided technology, μ-CT, has been applied specially in bone engineering studies for imaging fabricated scaffolds and constructs.

The percent porosity values of the bioplotted scaffolds were found as 65% and 56% for BP-B and BP-O, respectively (Figure 3.11). It was observed that the pores were

interconnected throughout the whole structure with controlled pore size approximately 450 μm as it was also seen in SEM images. This is especially important when most scaffolds produced by conventional methods do not have interconnectivity, and the porosity decreases towards downwards. Percent porosity of freeze dried scaffolds was found as 33% by using pycnometer. Salt particles used for producing high porosity have increased the porosity up to 85% and 96% depending on the amount of salt particles used. The porosity profiles of all 3D scaffolds are tabulated in Table 3.5.

Table 3. 5. Porosity of 3D scaffolds

Sample	Porosity (%)
SP0	33
SP5	85
SP10	96
BP-B	65
BP-O	56

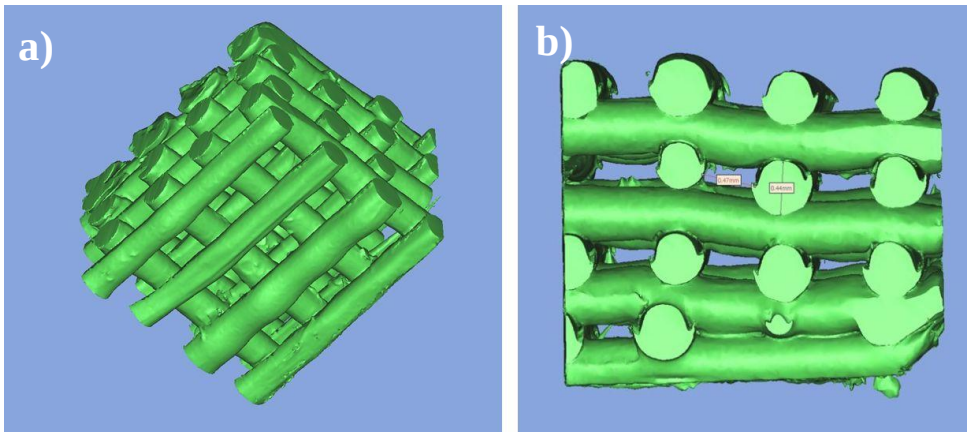

Figure 3.11. Pseudo-coloured μ-CT images of PEU scaffolds produced by Bioplotter. a) Isometric, b) Side view.

3.5.2 Pore Size Distribution

Pore sizes and porosity are usually stated in the terms of micropore, mesopore and macropore. Porous materials are classified into several kinds by their size. According to IUPAC notation, pore diameters for microporous, mesoporous and macroporous materials are: < 2 nm, 2-50 nm and > 50 nm, respectively [167]. Mercury porosimetry is the most common technique for porosimetry analysis; however it does not measure pore sizes over 200 μm. Pore size distribution analysis was not applied for bioplotted scaffolds since they were produced with homogenous pore sizes. For the samples prepared by freeze drying and salt leaching; pore size distribution plots also confirm SEM observations that pores are inhomogeneous and pores as small as five microns are present within scaffolds even for the highest content of salt which provide pore interconnections. In Figure 3.12, distributions of pore sizes of spongy scaffolds in the range of 5 – 200 μm are shown, as measured by a mercury porosimeter. From the plots it is seen that overall macroporosities of SP5 and SP10 were higher than that of SP0, as expected. In SP5 and SP10, fraction of bigger pores increased with the addition of salt

particles. For SP0, the fraction of pores over 20 μm is very low, while for SP5 and SP10 the fraction of pores over 20 μm is high. Almost no pores with diameter over 50 μm were present in SP0. The volume fraction of pores between 20 - 300 μm was much closer to each other in SP10 when compared to SP5, indicating existence of relatively more homogenous pore distribution in SP10.

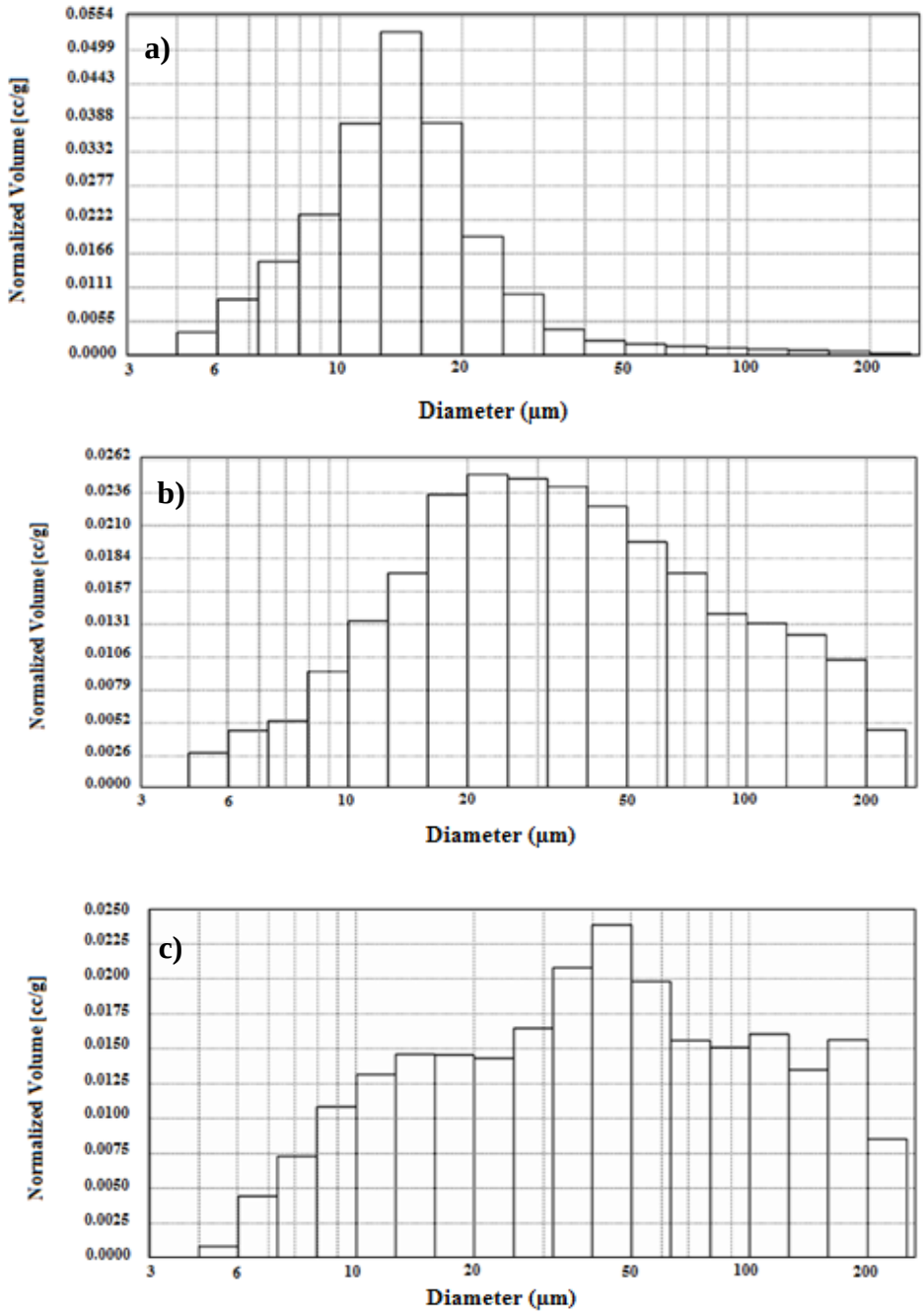

Figure 3.12. Pore size distributions of freeze dried spongy scaffolds. a) Freeze dried (SP0), b) Low salt leaching (SP5), c) High salt leaching (SP10).

3.6 In situ Degradation Profiles of PEU Matrices

PEU matrices obtained by solvent casting, freeze drying, salt leaching and bioplotting were incubated in PBS either in the presence or absence of lipase.

Lipase is an enzyme presents in human serum responsible for hydrolysis of ester bonds in polyesters, and several studies have shown that PCL degrades in the presence of lipase [168,169]. PCL is a hydrophobic crystalline polymer that degrades slowly in vitro and in vivo in the absence of enzymes. The in vitro degradation can be enhanced with the addition of the enzyme lipase. There are various commercial lipases which obtained from different sources. It is indicated that lipases from *Pseudomonas* species show the best effect on degradation of PCL [170]. Enzymatic degradation can be also used in order to increase porosity and pore interconnectivity of the scaffolds prepared for the aim of tissue engineering [171]. Degradability allows newly synthesized tissue to replace the scaffold both physically and functionally as the scaffold resorbs within the natural tissue.

In this study, PEU matrices which immersed in PBS with no enzyme addition did not show any significant weight loss up to 30 days. On the other hand, under enzymatic condition different forms of PEU matrices showed different weight loss profiles as shown in Figure 3.13. The order of weight remained obtained after 15^{th} days of enzymatic incubation were found as: SP10 (46%) < SP5 (65%) < SF (81%) < SP0 (86%) < BP-B (91%). The salt leached scaffolds immersed in lipase containing solution presented greatest weight loss among five specimens due to higher porosity, thus higher surface area for enzymatic attacks. Rate of degradation is directly proportional to the surface area to volume ratio. But, the same trend was not observed with the bioplotted scaffolds. Lower degradation rate of BP-B scaffolds with respect to films can be explanied by fiber thickness and higher crystallinity due to polymer chain orientation which formed during melting of the polymer, and this inversely affected the

degradation rate. The higher the crystallinity, the lower is the biodegradation rate. It has been shown that degradation rate in the amorphous regions could be twenty times faster than that of crystalline regions [156].

Controlling the degradation rates of synthetic polymer scaffolds is one of their advantages over natural materials. Scaffolds produced from synthetic polymers such as PCL could preserve their structure without showing any degradation when incubated in PBS for months, due to their hydrophobicity [96]. Some studies have reported that the biodegradation rate of PCL depends on the shape and inherent surface area: volume ratio of the PCL matrix, with films being slowly degraded, whereas nano- and microparticles are quickly degraded [172].

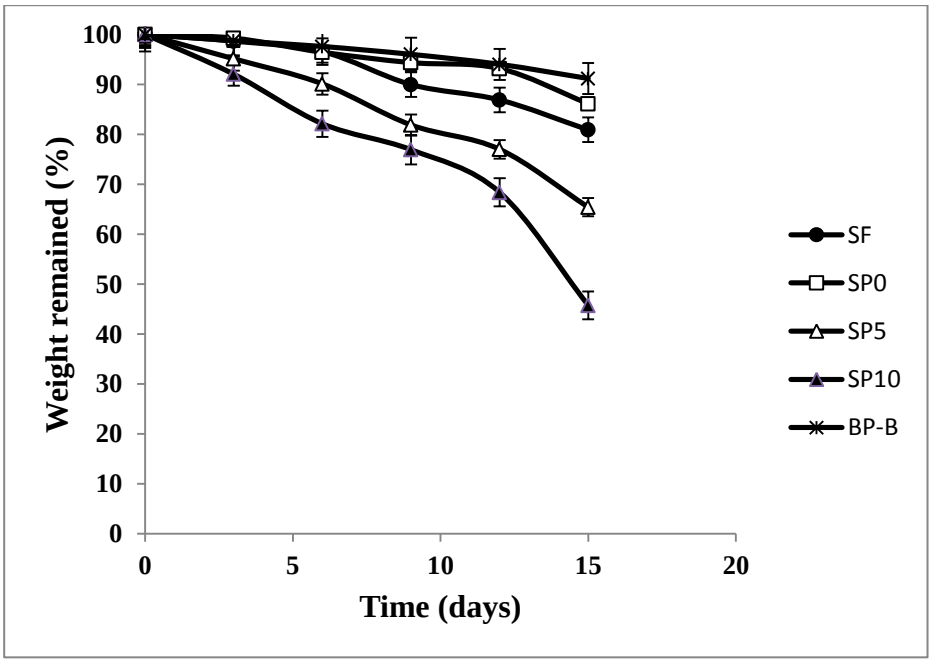

Figure 3.13. Degradation profiles of 2D films and 3D scaffolds in PBS with 0.18 U/mL of lipase (n=3).

3.7 Compressive Modulus of 3D PEU Matrices

Tissue engineering scaffolds acts as a physical support structure as an analog for ECM of natural tissues. Beside necessity for mechanical functionality within natural tissue, adequate mechanical strength of a scaffold is required for facility during in vitro cell culture and implantation applications [173]. Scaffold features, such as pore structure, mechanical strength and degradation properties, play important roles in cellular growth and function since specific cells need mechanical stimuli generated by the scaffold to mediate cell stiffening due to cell focal adhesions attachment [174]. Thus, parameters like, molecular weight, crystallinity, microstructure (porosity, mean pore size, pore shape, interconnectivity and specific surface area) and preparation method that influence scaffold stiffness would inherently influence the cell response. Different cells show varying responses. For example, mesenchymal stem cells (MSCs), fibroblasts and epithelial cells have been shown to exhibit better cell spreading, adhesion and proliferation on stiffer scaffolds [118].

Compressive elastic modulus is a measure of material stiffness. In present study, the effect of microstructure on the elastic modulus of the scaffolds which were obtained by freeze drying, by salt leaching and by bio-plotting were evaluated by compressive tests. Representative compressive stress-strain curves for sponges and bioplotted scaffolds are shown in Figure 3.14 and Figure 3.15, respectively. Spongy scaffolds (SP0, SP5 and SP10) exhibited similar stress–strain behavior characteristic of low-density, elastomeric open-cell foams as defined by Harley et al (2007) [173]. The compression curve of these types of scaffolds is typically characterized by three distinct zone. The first zone is a linear elastic regime (bending), the second is a collapse plateau regime (pores start to collapse) and the third one is a densification regime (complete collapsing of pores) (distinct zones are shown on curve of SP0 in Figure 3.14).

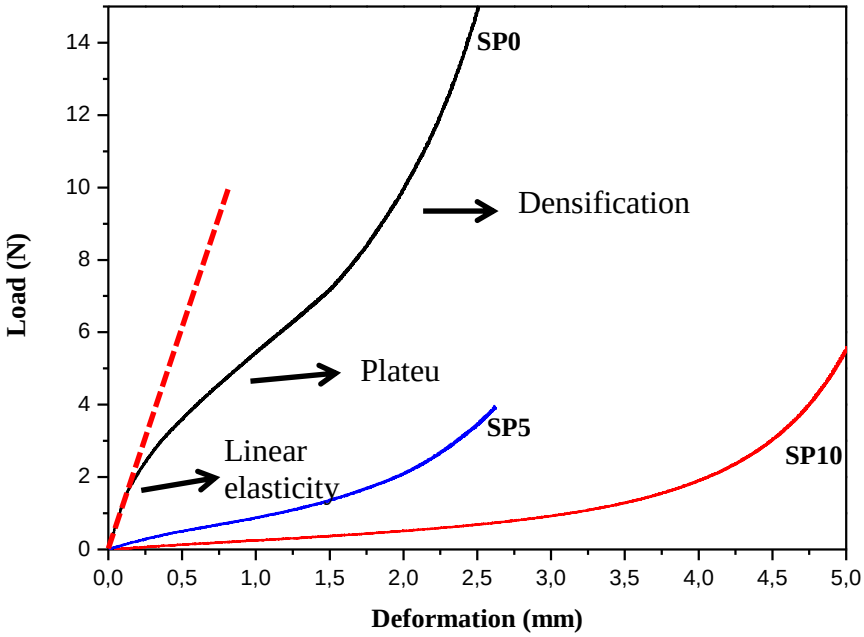

Figure 3.14. Representative load- deformation curves of freeze dried and salt leached scaffolds.

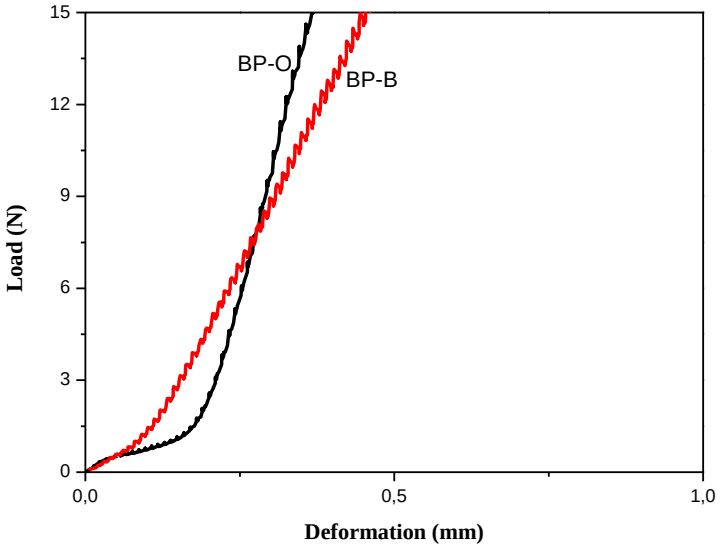

Figure 3.15. Representative load-deformation curve of bioplotted scaffolds

As seen in Table 3.6, bioplotted scaffolds (BP-B and BP-O) displayed significantly higher compressive stiffness than the spongy scaffolds obtained by freeze dried (SPO) and salt leached (SP5 and SP10) samples. Addition of leaching particles decreased the compressive elastic modulus of SP0 from 584±67 kPa to 148±6 kPa for SP5 and to 38±2 kPa for SP10, under dry conditions. In the case of bioplotted scaffolds, it was observed that alteration of fiber orientation from basic (BP-B) to offset (BP-O) architecture leaded a decrease in compressive modulus from 4720±540 kPa to 3450±610 kPa due to juxtaposition of sequential fibers along the Z axis. Yilgor et al. (2008) also showed that scaffolds with basic configuration exhibited higher mechanical strength [128]. Mechanical properties can be attributed to differences in microarchitecture and porosity. SP10 had the highest porosity with a value of 96%, thus showed lowest mechanical strength. Although SP0 displayed the lowest porosity, BP-B and BP-O had the highest elastic modulus. This can be explained by re-orientation of PEU chains during melt processing to form more crystalline structure as confirmed by DSC and degradation studies. Increase of crystalline amount leads to increase in mechanical strength.

As a supportive matrix for cell culture, a scaffold must have appropriate mechanical strength. Generally, the optimum value for mechanical strength is correlated with the strength of target tissue, but a strength of at least 100 kPa is reported to be necessary [175]. Compressive moduli for cancellous bone are given as 50 - 500 MPa depending on anatomical location [54]. When compared to natural bone, it is seen that compressive moduli of all prepared scaffolds including bioplotted ones were lower than this reported range. On the other hand, prepared scaffolds seem to have potential mechanical stiffness to support osteogenic differentiation. It has been indicated that scaffold stiffness plays an important role to induce differentiation into osteogenic lineage. Pek et al. (2010) showed that human MSCs differentiated into osteogenic phenotypes on 2D substrates with elastic modulus higher than 34 kPa; below which MSCs differentiated into neural or myogenic phenotypes [176]. They further confirmed

the effect of matrix stiffness on the differentiation of human MSCs in 3D scaffolds. These findings showed that PEU based scaffolds are not useful for load bearing applications, but can be used for bone defects which demand only low compressive strength and for soft tissue applications.

Table 3.6. Compressive modulus values of 3D scaffolds

Sample	E´ (kPa)
SP0	584 ± 66
SP5	147 ± 6
SP10	38 ± 2
BP-B	4720 ± 540
BP-O	3450 ± 610

3.8 In Vitro Studies

3.8.1 In Vitro Cell Culture on 2D PEU Films

3.8.1.1 Cell Morphology

The effect of surface chemistry and micro-patterned topography of the films on cell morphology and cytoskeleton organization were studied by SEM and fluorescence microscopy

In view of the fact that responses are cell type-dependent, cells are generally aligned in the direction of the groove on the substrates, known as contact guidance. It is well known that contact guidance by grooves/ridges structures induces many cell types to

align along the groove direction. In several studies it is indicated that the degree of cell orientation was significantly affected by groove depth rather than groove width [164, 165]. Yucel et al. (2010) reported that groove depths greater than 2 μm promoted alignment of neurites [62]. Jeon et al. (2010) found that a height threshold of nearly 1 μm influences fibroblast alignment on both parallel line and orthogonal mesh patterns [179]. In several studies it has been demonstrated that cell shape alterations due to surface topography may influence differentiation [180]. Cairns et al. (2010) investigated the influence of surface topography on osteoblast adhesion, proliferation and differentiaon in the presence an adsorbed fibronectin layer. They reported that presence of fibronectin on the surface improve cell adhesion and early osteoblastic differentiation [181].

In this study, SEM and fluorescence microscope images showed that the cells attached very well with flattened morphology on both modified and unmodified PEU film surfaces which indicate cell compatability of the synthesized polymer. Cells were extended in the direction of grooves on both Fn-free (MF) and Fn- coated (MF-Fn) surfaces, while cells were spreaded in a random fashion on smooth surface (SF and SF-Fn) as seen in Figure 3.16 and Figure 3.17. Orientation angles of the cells were calculated from the measured values of thirty representative cells. The orientation angle was found to be within 10° of the groove direction which indicates very good alignment of the cells. Cells with 45° orientation angle are considered as randomly dispersed [105].

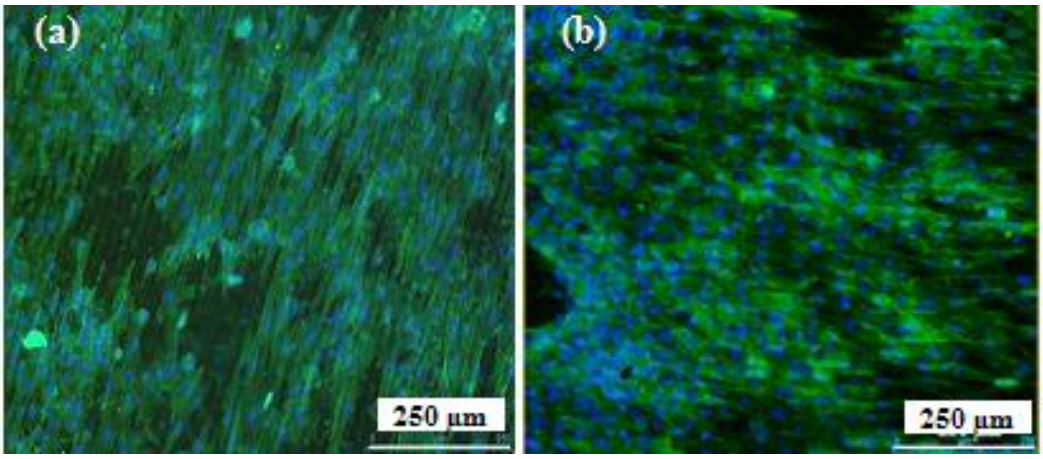

Figure 3.16. Fluorescence images of BMSCs seeded on a) MF-Fn, b) MF (mag. x10, day 3). Actin microfilaments (green) were visualized by FITC-labeled phalloidin. Cell nuclei were visualized by DAPI (blue).

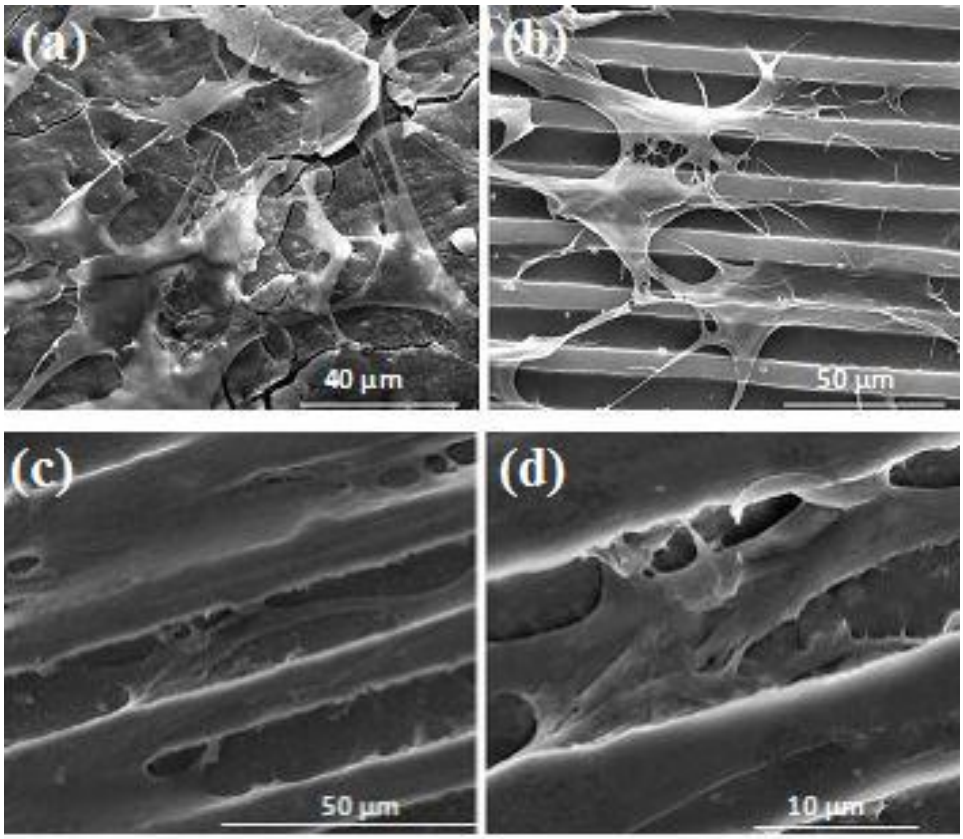

Figure 3.17. SEM images of BMSCs seeded on a) SF, b) MF. c) and d) Closer views of alignment within the groove (day 3).

3.8.1.2 Cell Proliferation

Proliferation of BMSCs on unpatterned and micro-patterned PEU films with or without Fn coating was studied by Alamar blue assay after 21 days with TCPS serving as the control (Figure 3.18). This study confirmed that the novel PEU polymer synthesized in this study was not cytotoxic. On the contrary, the proliferation rates were very similar to those on TCPS and this is quite a success. The initial attached cell numbers on Fn-coated surfaces were significantly higher than on Fn-free surfaces. The initial attached

cell numbers on Fn-coated surfaces were significantly higher than on Fn-free surfaces.This might partially be due to a slight increase in the hydrophilicity of PEU film surfaces upon Fn adsorption which was was also indicated by Kenar et al. (2006) [139]. Increase in cell population was higher on Fn coated surfaces regardless of the presence of micro-patterns. Actually, presence of micro-patterns did not have significant influence in terms of attachment or proliferation.

An increase was observed in the proliferation on each sample up to day 14, followed by a decrease towards day 21. The decrease in proliferation was probably due to confluency; after two weeks cells covered the whole film surfaces forming a cell sheet which led to cell death or cell migration to the well plate. Moreover, a decreased proliferation rate is expected, since during differentiation phase the bone marrow stem cells induced to differentiate into osteocytes stop dividing and start to express osteogenic markers.

There is not a certain hydrophilicity value for optimum cell-material interaction. Cell type and matrix surface determine the cell adhesion strength. Ardhaoui et al. (2008) investigated the effects of water contact angle on cell adhesion strength and cell viability of various cell types on polystyrene surfaces having different contact angles. They found that some cell types attached better on moderately hydrophilic surfaces while others adhered better on more hydrophilic surfaces [183]. In our study; contact angle values are found to be 90° and 82° for SF and SF-Fn samples, respectively; and Fn coated samples demonstrated better cell attachment.

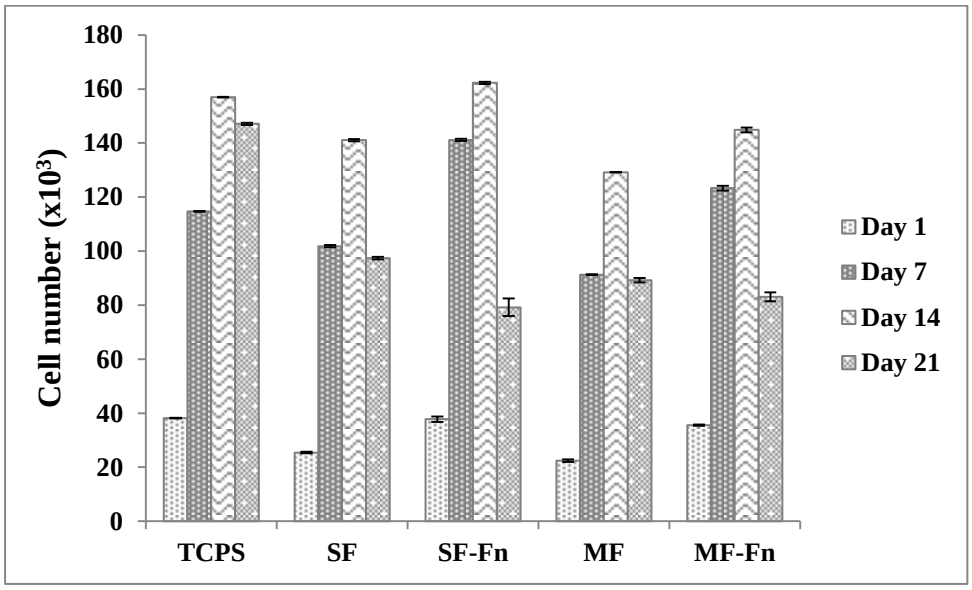

Figure 3.18. Cell proliferation of BMSCs on PEU films and tissue culture plate (control) quantified using Alamar Blue assay on days 1, 7, 14 and 21 (n=3).

3.8.1.3 Osteoblastic Differentiation

The osteogenic differentiation capability of BMSCs was studied by determining alkaline phosphatase (ALP) activity and calcium deposition which are correlated with osteoblastic phenotype. Differentiation on different PEU surfaces was evaluated at the end of three weeks an the results are consistent with proliferation results; there is a significant difference between the Fn coated and uncoated samples in terms of ALP activity regardless of the presence of fibrinogen (Figure 3.19).

Mineral salts, mostly calcium phosphates constitute the inorganic matrix of bone and are responsible for the hardness and compressive strength of the bones. Deposition of calcium salts is an indication of mineralization. In the present study, mineralization of the ECM by the osteoblasts was studied by staining calcium salts with tetracycline

(Figure 3.20). It was observed that mineralization is denser on Fn coated film surfaces. Calcium minerals formed on all smooth and patterned films while for patterned films mineralization was observed within the grooves as well as on the ridges. As it was mentioned in cell proliferation study, presence of patterns on film surface showed no difference in cell proliferation and bone differentiation compared to control smooth surfaces; but alignment of cells along the grooves was observed.

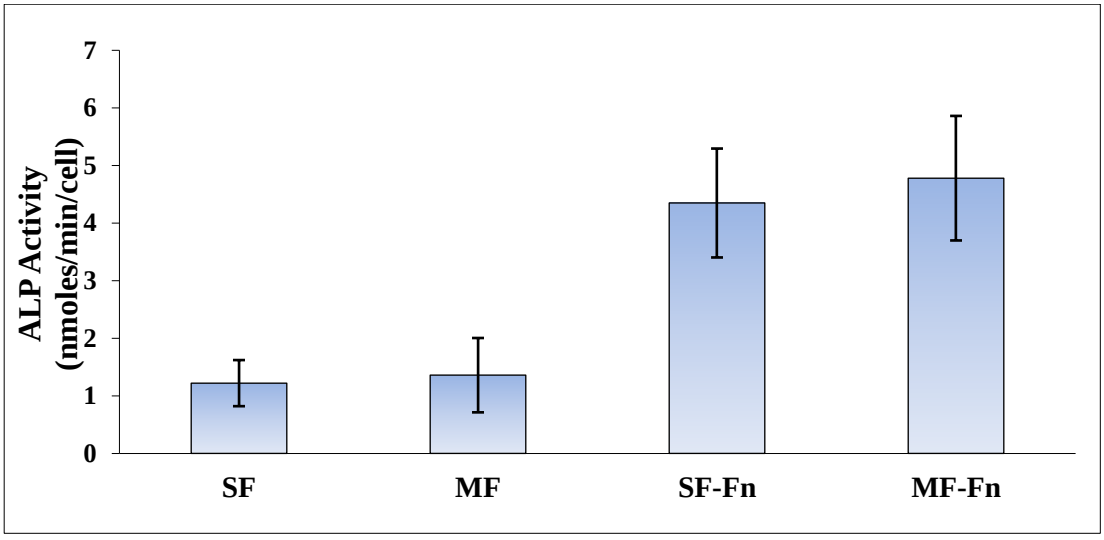

Figure 3.19. ALP activity of BMSCs for the film samples at the end of three weeks (n=3).

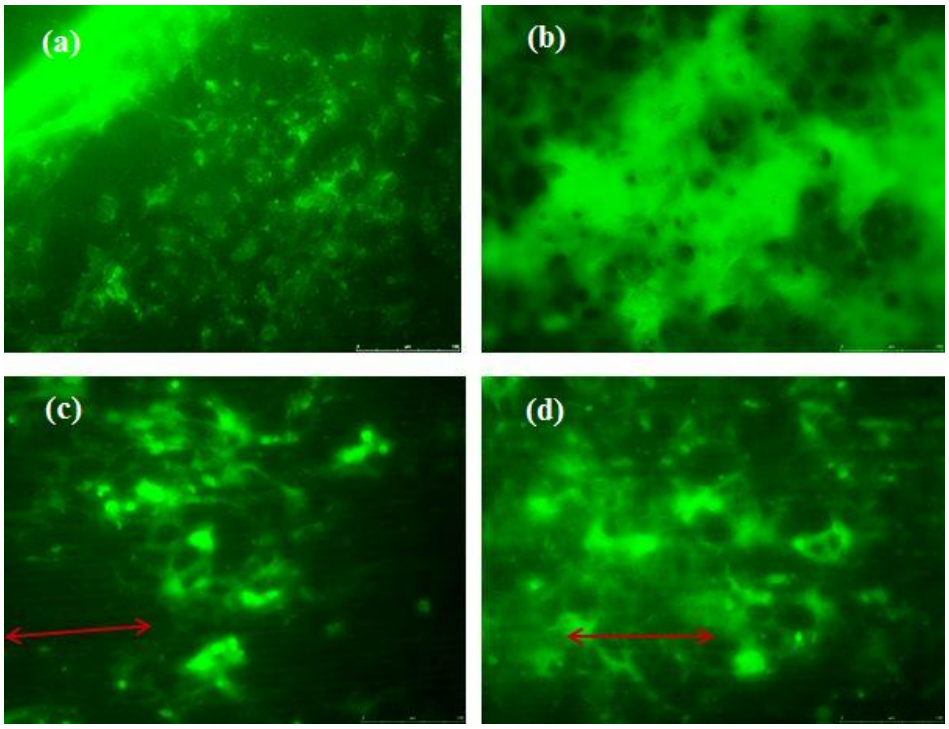

Figure 3.20. Fluorescence microscopy images showing mineralization achieved by osteoblasts on polymeric films at the end of three weeks. a) SF, b) SF-Fn, c) MF, d) MF-Fn (mag. x20). Arrows indicate the direction of parallel grooves.

3.8.2 In Vitro Cell Culture on 3D Scaffolds

3.8.2.1 Surface Modification of 3D Scaffolds

Surface topography and hydrophobicity of scaffolds play a critical role in regulating initial cell behaviors, such as cell adhesion and proliferation. Oxygen plasma treatment is widely used for surface modification of cell carrier materials to enhance cell adhesion and proliferation. In this part of study, 3D scaffolds were treated with oxygen plasma in order to increase wettability by decreasing surface contact angle. After

plasma treatment, cell suspension droplets were immediately absorbed by the scaffolds, while it continued to stay as a droplet on the surfaces of untreated samples (Figure 3.21). Thus, increasing water wettability by plasma application enhanced penetration of cells into the 3D scaffolds.

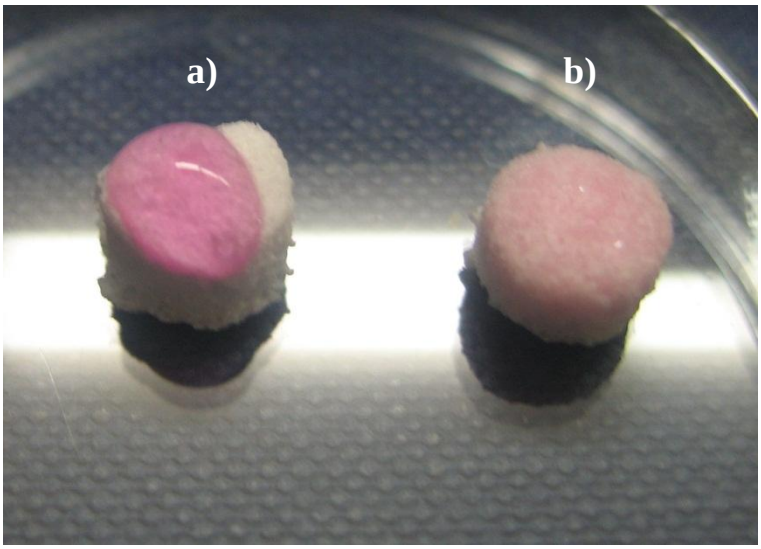

Figure 3.21. Fate of drop of cell suspension on a) untreated and b) plasma treated SP10 scaffolds. Photo was taken right after the drop was added.

3.8.2.2 Cell Morphology on 3D Scaffolds

The scaffolds which have 3D structure (SP5, SP10, BP-B and BP-0) were used in in vitro cell culture experiments. SP0 samples were not used for in vitro culture due to their relatively small pore size and low porosity.

As seen in Figure 3.22 and Figure 3.23, the BMSC showed good adherent ability on both salt leached and bio-plotted scaffolds on which a layer of cells can be detected. Cells were attached closely with neighboring cells and formed cellular network on struts as well as within the pores of salt leached scaffolds. Cell layers as well as bridging on bioplotted fibres were observed. Morphology of seeded scaffolds indicates good interaction of scaffolds with the cells.

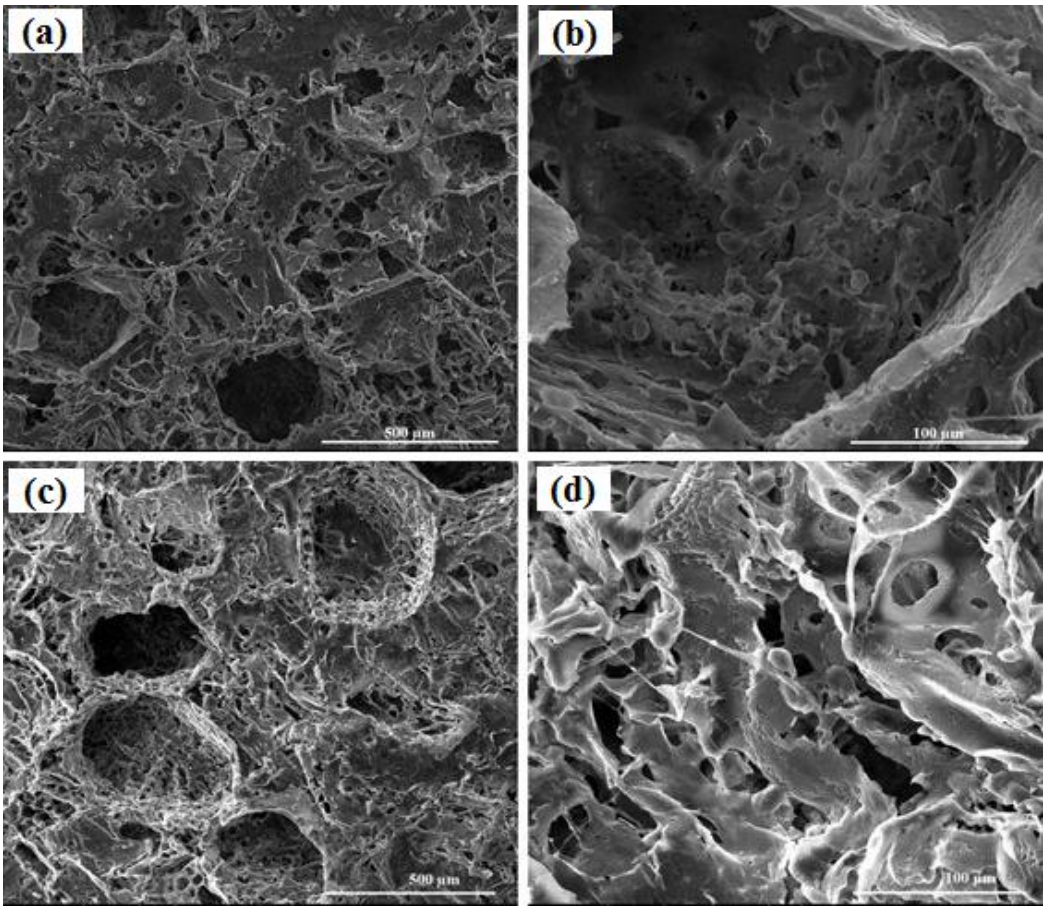

Figure 3.22. Cell attachment and spreading on salt leached spongy scaffolds on day 1. a - b) SP5 c - d) SP10.

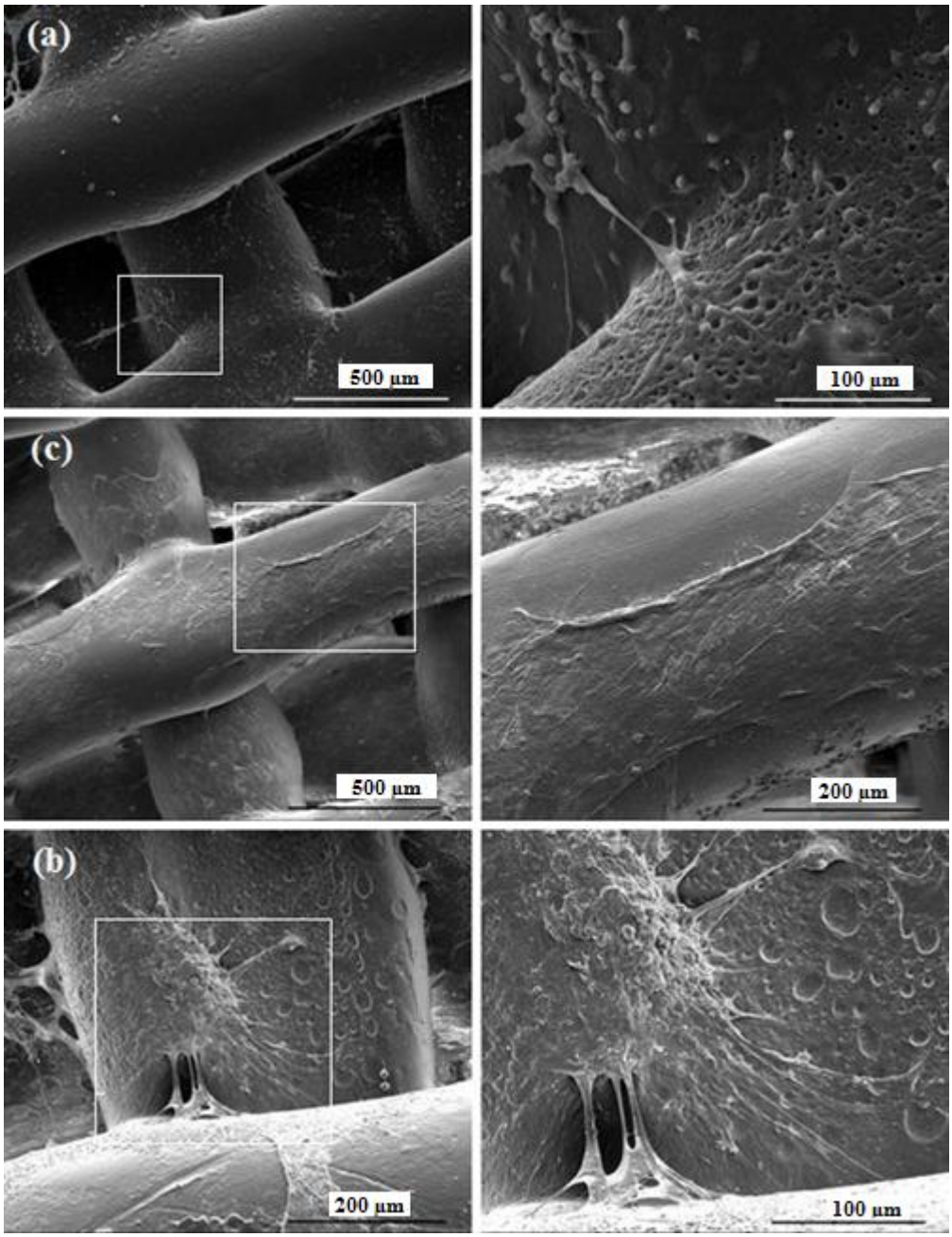

Figure 3.23. SEM micrographs of the seeded bioplotted scaffolds (BP-O) showing the interaction between the cells and scaffold fibers on a) day 1, b) day 3, c) day 7. Images on the right colons are the high magnification of the corresponding inset images.

3.8.2.3 Cell Proliferation on 3D Scaffolds

Proliferation ability of BMSCs on salt leached and bioplotted scaffolds is shown in Figure 3.24. Results of day 1 show the initial cell attachment ability on individual scaffold. It was observed that the initial attachment on SP5 and SP10 almost same, while it was relatively lower on bioplotted scaffolds (BP-B and BP-O). Cell seeding efficiency on bioplotted scaffolds was expected to be low due to very big pores which leaded to flow of cell suspension to the well plate. This is obvious when BP-B and BP-O scaffolds are compared. Initial cell attachment was influenced by whether offset architecture was present or not. The number of initially attached cells was significantly higher on BP-O scaffolds than that of BP-B scaffolds due to higher available fiber surface area on the flow path of the cell suspension. If there is no fiber positioned as offset, there is a direct open path for cells to escape from the scaffolds. On the other hand, fibers in offset position, act as a barrier to prevent cell flow which further leads to higher number of initial adhesion and proliferation. On all scaffolds, cells were able to proliferate up to 21 days, which indicate good cell-material interactions. On day 21, a small decrease in cell number was observed for SP5 which can be attributed to lower interconnectivity compared to other constructs. All scaffolds displayed a sharp increase in cell number after 7 days of culture. Based on initial cell number, bioplotted scaffolds exhibited better proliferation rate than salt leached scaffolds. BP-B and BP-O showed similar trend but, SP10 showed slightly higher proliferation rate than SP5. This is most probably due higher interconnection pore size within bioplotted scaffolds which enhanced the proliferation of cells by allowing greater diffusion of nutrients and waste. After day 7, a decrease in cell growth rate was observed for all samples. Cell proliferation rate is known to decrease during expression of differentiation factors.

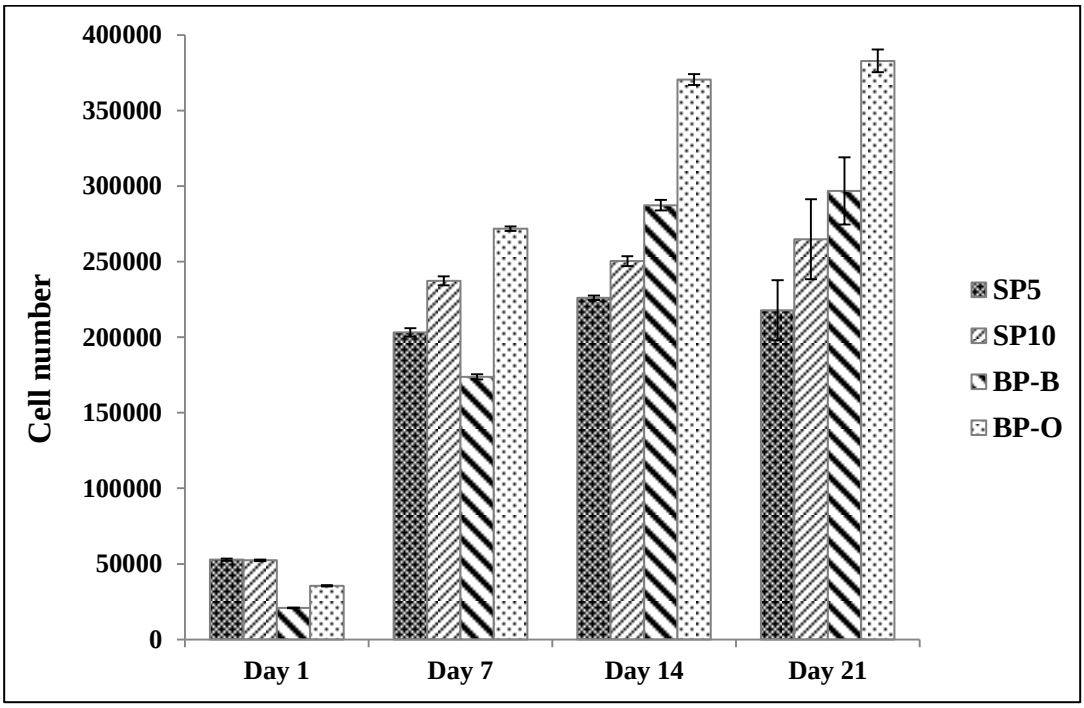

Figure 3.24. Proliferation of BMSCs on 3D scaffolds (n=3).

3.8.2.4 von Kossa Staining

The ability of cells to produce mineralised matrix and calcium nodules is an indicator for bone formation in vitro. In literature, mineralization is stated in different ways like calcification, mineral deposition, calcium salts, mineralized matrix and bone nodule formation. There are several methods used for detection of mineralization. These include von Kossa staining, haemotxylin staining, EDX analysis, FTIR and X-ray diffraction where von Kossa staining method has been widely used to examine mineralization in vitro. It is an inexpensive technique, which require only a simple light microscopy as an instrumentation. Various osteoblast and osteoblast-like cells have been reported to form matrix-mediated mineral based on von Kossa staining [184]. However, the method provide a quantitative measurement of mineralization.

In this study, von Kossa staining for mineralisation was positive for all scaffolds, with the most intense staining in bioplotted scaffolds. After staining, calcium salts are coloured as dark brown or black. Significant amounts of black-stained deposits were observed after 35 days of culture on 3D scaffolds which indicates that the seeded osteoblasts produced mineralized tissues. Light microscopy images showed that small nodules were formed on SP5, while some relatively larger nodules were observed beside small ones on SP10 (Figure 3.25 b and c, respectively).

von Kossa staining indicated more extensive mineralization of osteoblasts on bioplotted scaffolds. As seen in Figure 3.26 b-c, black deposits was covered all the surfaces of fibers at upside and underside of bioplotted scaffolds, while no apparent positive staining was observed on unseeded controls (Figure 3.26 a). These results suggest that BMSCs were able to differentiate into osteogenic lineage in vitro. This suggestion was further supported by SEM/EDX results.

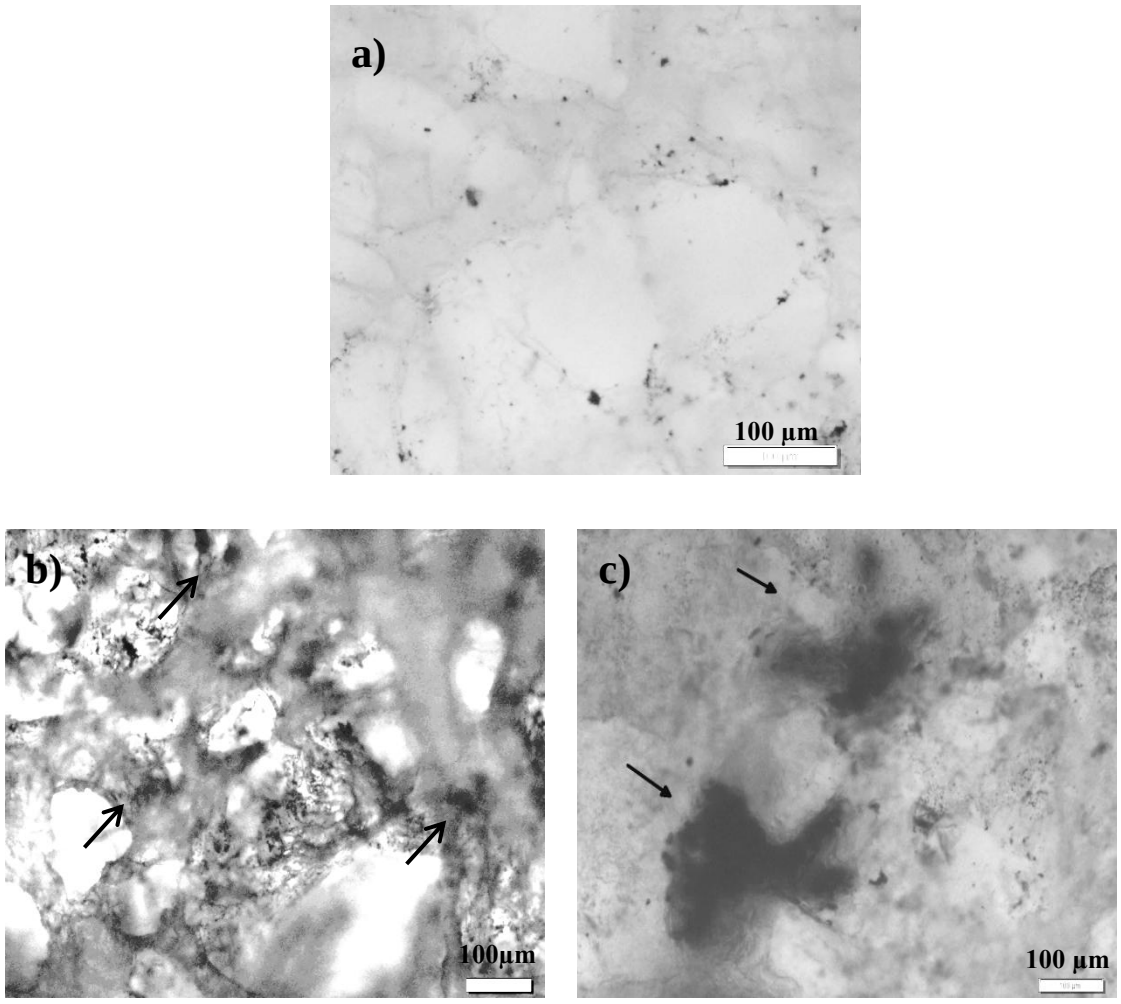

Figure 3.25. von Kossa staining of mineralization on salt leached scaffold after 5 weeks of culture. a) Unseeded negatif control (SP5), b) SP5 and c) SP10. Arrows indicate mineralized nodules.

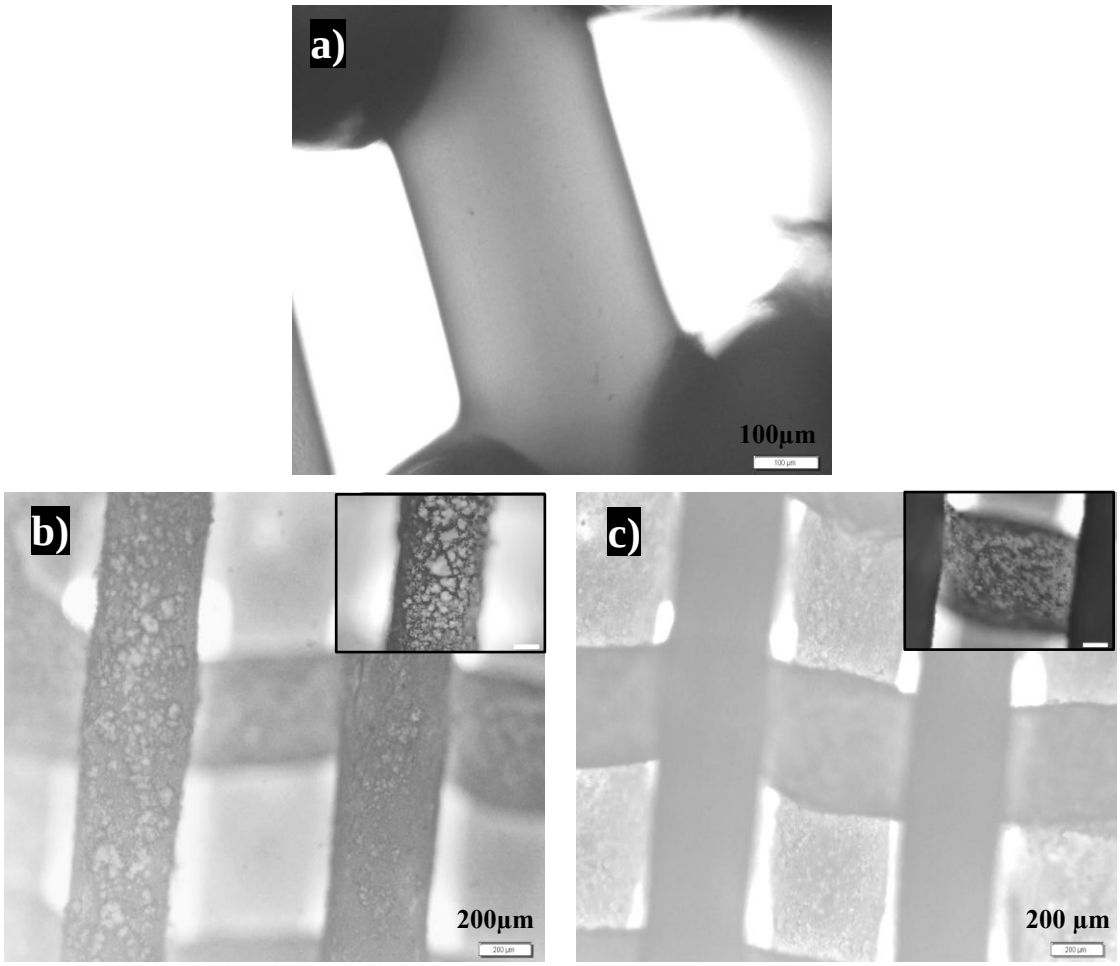

Figure 3.26. von Kossa staining of mineralization on BP-O scaffolds after 5 weeks of culture. a) Unseeded negative control, b) Focus on upside fiber surface, b) Focus on underside fiber surface (Scale bar = 200 µm, insets = 100 µm).

3.8.2.5 SEM/EDX Imaging of Mineralization on 3D Scaffolds

SEM/EDX analysis was performed in conjunction with von Kossa staining in order to confirm the mineralization. Figure 3.27 and Figure 3.28 show morphological observation of mineral deposition on salt leached spongy and bioplotted scaffolds, respectively. At the end of 5 weeks, it is noticeable that all constructs were covered with multilayers of cells and cells started filling up the pores with extracellular matrix and abundant mineral deposits, indicating well cell attachment and proliferation of osteoblasts. SEM images demonstrated that extracellular mineral deposition was higher on bioplotted scaffolds than on salt leached scaffolds, which was also confirmed by analyzing the seeded scaffolds' surfaces via SEM/EDX imaging, that provides determination of chemical composition of material surfaces (Figure 3.29). The amount of elemental Ca and P was measured from the mineral nodules synthesized by osteoblasts on surfaces of different scaffolds, and weight percentage of elements measured on day 1 and day 35 are tabulated in Table 3.7. It is known that calcium and phosphate serves as the nucleating agent for the formation of bone HAp. EDX analysis verify the presence of calcium and phosphorous on the surface of all scaffolds after five weeks of culture, while these elements were not detected on day 1, since there was no mineral deposition yet. EDX detected low level of Ca and P deposition on salt leached scaffolds compared to bioplotted scaffolds after 35 days of cultivation. Moreover, EDX analysis revealed that Ca/P ratio of BP-O (~1.60) was close to the value attributed to HAp (1.67), whereas Ca/P ratios of SP5 and SP10 (~0.55 for both) were very low compared to that of HAp.

These results indicate that higher mineralization on bioplotted scaffolds might be resulted from matrice stiffness. It has been stated that substrate stiffness can influence the morphology and cell specific protein expression. Of course, responses to mechanical stimuli vary with different cell type. For example, Flanagan et al. (2002) showed that motor neurons derived from embryonic mouse spinal cord had preferred

soft surfaces to extend branches rather than hard surfaces [185]. On the other hand, Engler et al. (2004) showed that fibroblasts spreaded well on hard surfaces but had round shape on soft materials [186].

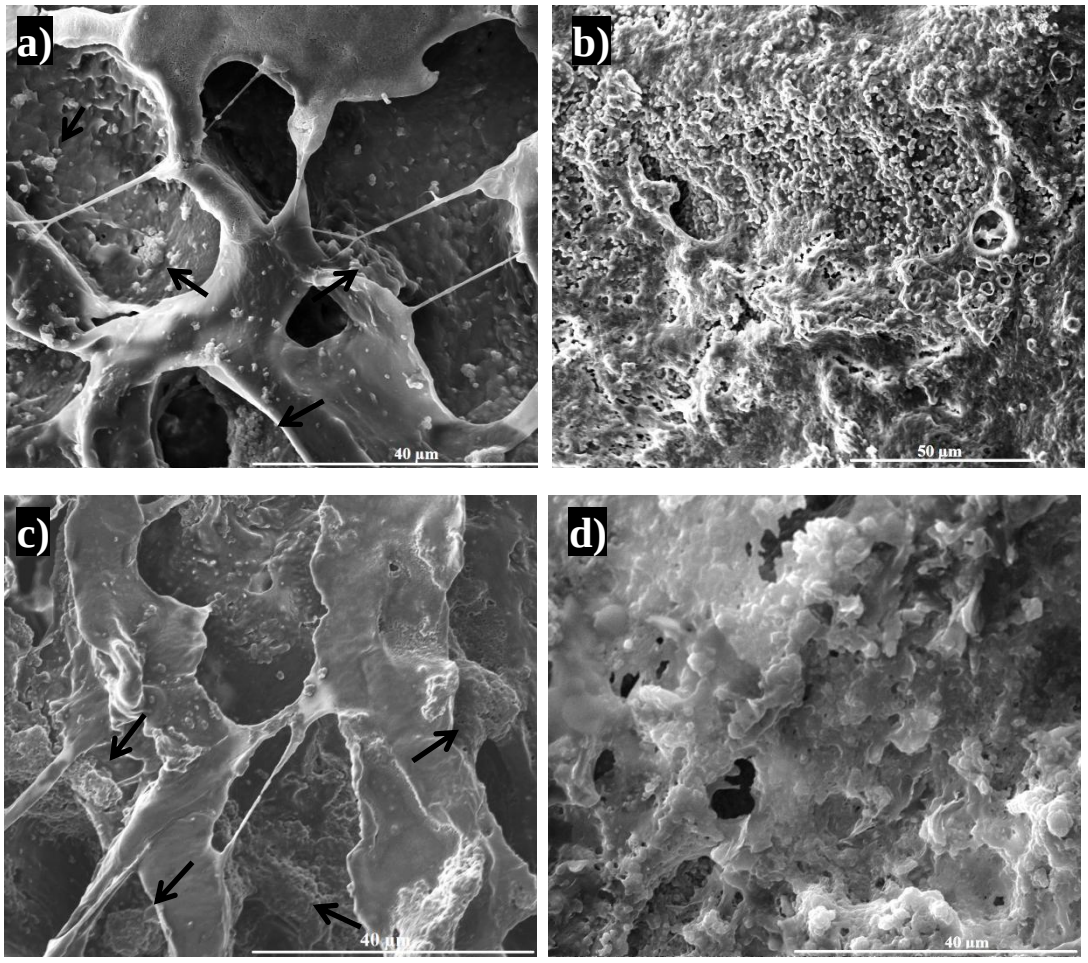

Figure 3.27. SEM micrographs showing ECM deposition and mineralisation on salt leached scaffolds after 5 weeks of culture. a-b) on SP5, c-d) on SP10. Arrows indicate mineral deposits.

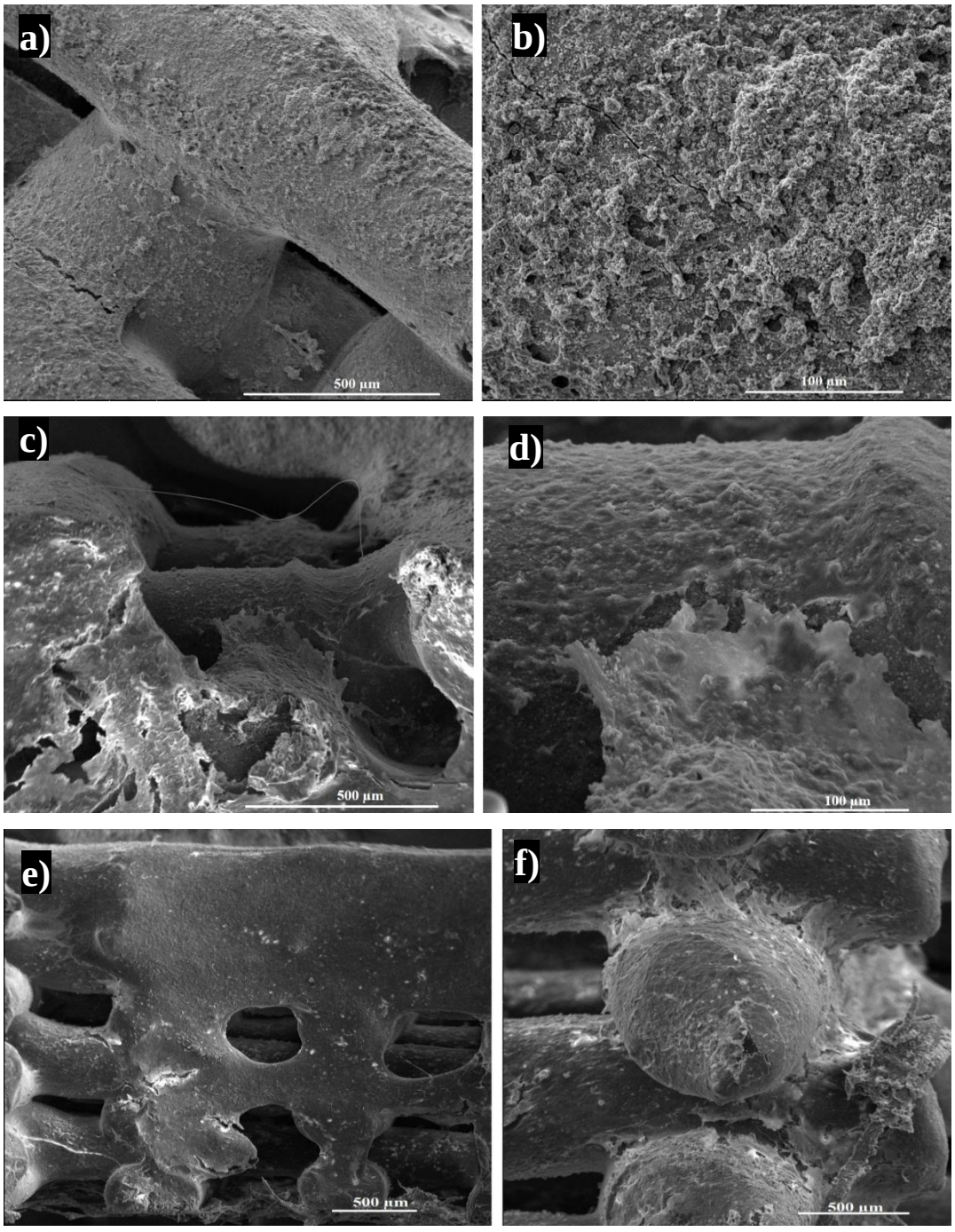

Figure 3.28. SEM micrographs showing ECM deposition and mineralisation on bioplotted scaffolds (BP-O) after 35 days of culture. a-b) Top view, c-d) and e-f) Side view of ECM deposition.

Table 3.7. Weight percentage of C, O, P and Ca elements on different scaffolds seeded with BMSCs

	SP5		SP10		BP-O	
Element	**Day 1**	**Day 35**	**Day 1**	**Day 35**	**Day 1**	**Day 35**
C	71.59	49.54	62.30	49.11	67.86	38.23
O	28.41	39.62	37.47	31.66	31.81	33.64
P	0.00	6.95	0.00	12.36	0.00	10.83
Ca	0.00	3.89	0.23	6.87	0.33	17.31

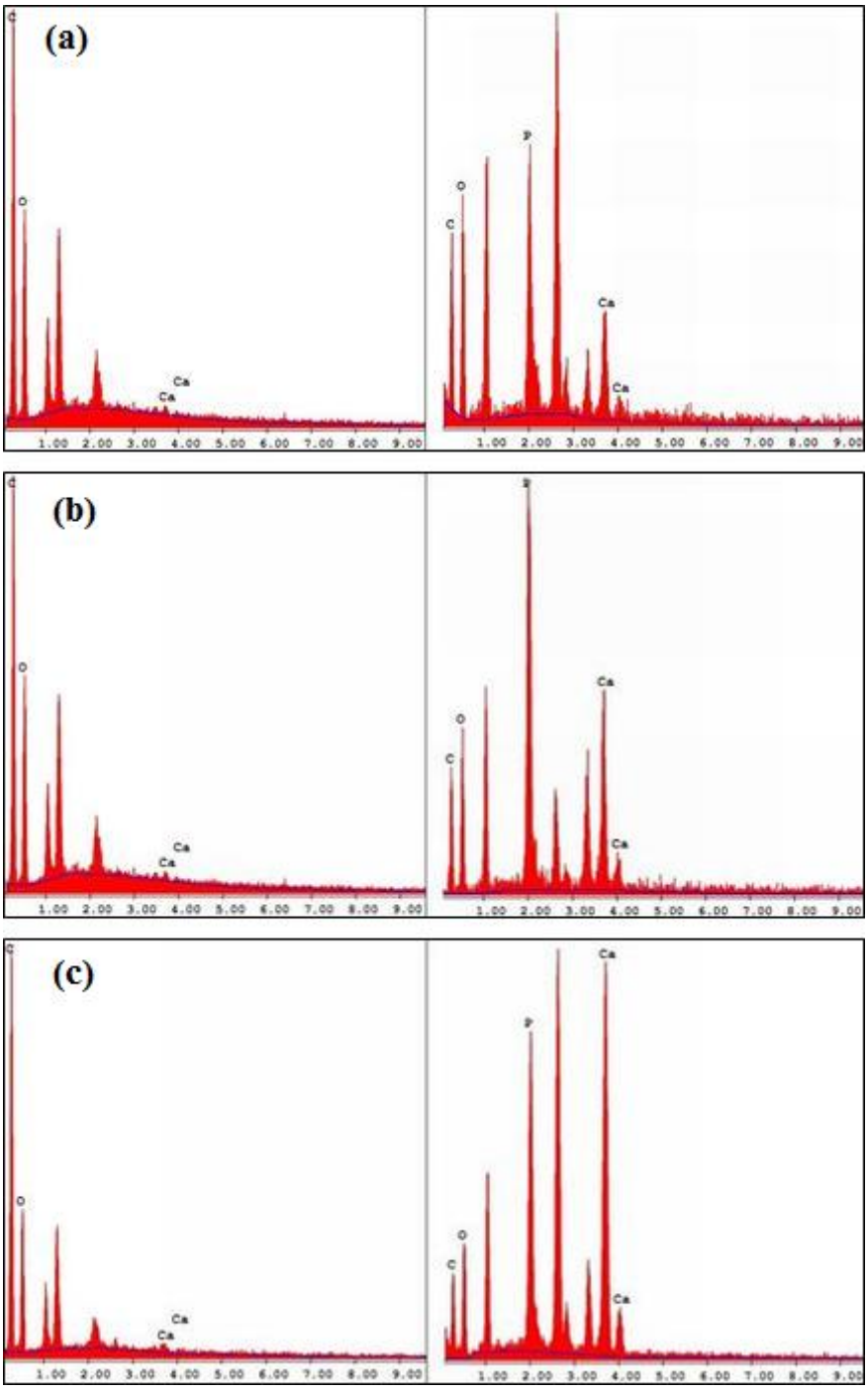

Figure 3.29. EDX measurement for the detection of mineralization on a) SP5, b) SP10), c) BP-O on day 1 (left column) and on day 35 (right column).

3.8.3 Effect of Cell Proliferation on Compressive Properties of 3D PEU Matrices

The mechanical performances of BMSC seeded 3D scaffolds were characterized under wet conditions after 1, 21 and 35 days of cultivation. In natural tissues, ECM provides compressive strength to tissues [187]. Increase of compressive stiffness of scaffolds after in vitro cell culture is an indication of ECM deposition by proliferated cells.

Figure 3.30 and Figure 3.31 show the influence of cell proliferation/matrix mineralization on salt leached and on bioplotted scaffolds, respectively. Compressive modulus of seeded scaffolds on day 1, day 21 and day 35 were compared in Table 3.8. While compressive modulus of SP5 increased from 25.6±3.83 kPa to 35.01±2.82 kPa that of SP10 changed from 16.38±3.20 kPa to 25.01±4.21 kPa after 21 days of cell culture. Moreover, compressive moduli were increased to 44.44±3.48 kPa and 37.40±3.94 kPa for SP5 and SP10, respectively, with further cultivation up to 35 days. Compressive moduli increased by 36% and 73% for SP5 and by 53% and 98% for SP10 after 21 and 35 days of cultivation, respectively. The higher increase in the mechanical properties of SP10 was most probably due to its more porous structure compared to SP5 and this might have resulted in a higher cell penetratration and proliferation throughout the scaffold, thus larger amount of ECM deposition after cell culture up to 35 days. This is in agreement with the study of Lien et al. (2010), in which they reported that chondrocyte seeded gelatin scaffolds with higher pore size showed higher compression strength after cell culture compared to scaffolds with smaller pore size [188].

For bioplotted ones, after 35 days of cultivation, compressive moduli of BP-B and BP-O were increased from 4610±520 kPa (day 1) to 5095±614 kPa (day 35) and from 3535±437 kPa (day 1) to 3893±382 kPa (day 35) for BP-B and BP-O, respectively (Table 3.8). For both BP-B and BP-O scaffolds, the increase was approximately 10%.

As is seen from these results, percent increase in compressive strength after cell culture was more remarkable in salt leached scaffolds than it was in bioplotted ones. This is because there is a big difference between the initial stiffness of salt leached scaffolds and bioplotted ones. However, when total increase was taken into consider, it is obvious that amount of increase in compressive strength was much higher on bioplotted scaffolds.

It is not true to evaluate the efficacy of osseous tissue ingrowth by taking the initial mechanical property as the only criterion. For example, it has been demonstrated that biphasic calcium phosphate ceramics (BCP) with low microporosity and high mechanical strength showed low bioresorption and bioactivity after implantation, while BCP with initially higher microporosity and lower mechanical strength, revealed two or three times mechanical increase after implantation. The researchers indicated that highly macroporous BCP promoted higher ECM deposition in vivo and better integration with native tissue [189].

Table 3.8. Change in compressive moduli of seeded 3D scaffolds by time

Sample	**E´ (kPa)**		
	Day 1	**Day 21**	**Day 35**
SP5	25.6 ± 3.83	35.01 ± 2.82	44.44 ± 3.48
SP10	16.38 ± 3.20	25.01 ± 4.21	37.40 ± 3.94
BP-B	4610 ± 520	-	5095 ± 614
BP-O	3535 ± 437	-	3893 ± 382

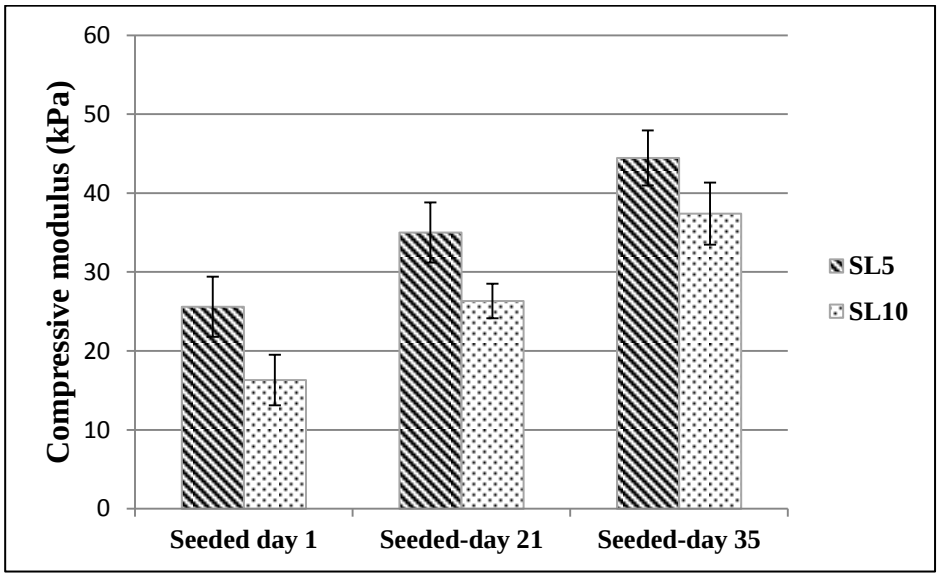

Figure 3.30. Comparison of compressive moduli of seeded salt leached scaffolds on day 1, day 21 and day 35 under wet conditions.

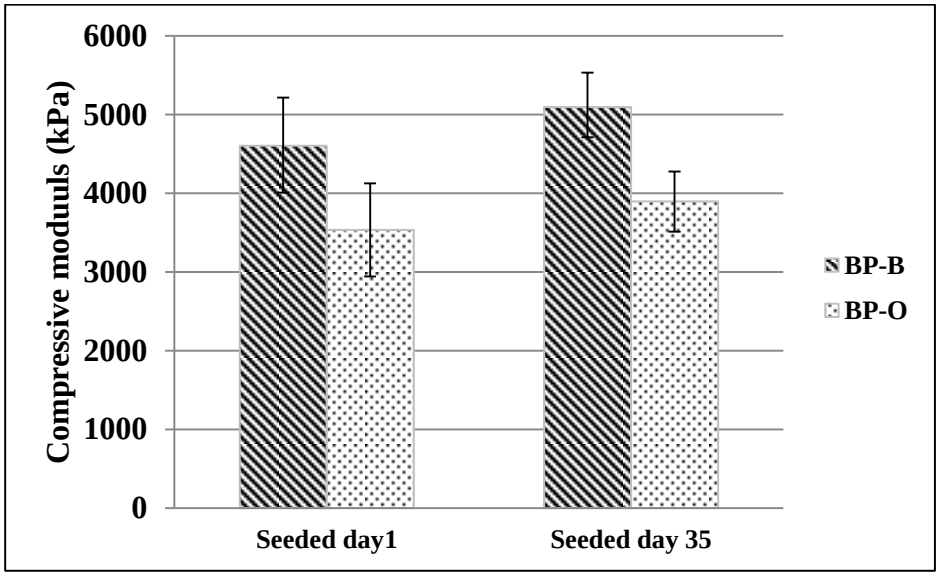

Figure 3.31. Comparison of compressive moduli of seeded bioplotted scaffolds on day 1 and on day 35 under wet conditions.

CHAPTER 4

CONCLUSIONS

With advancements in tissue engineering it has become necessary to develop polymers that meet more demanding requirements. Biodegradable synthetic polymers are attractive materials for developing scaffolds in tissue engineering because of their advantageous abilities like tailoring of mechanical properties and degradation kinetics for a target application. Therefore, quite a number of biodegradable synthetic polymers have been studied either as 2D or 3D scaffold for tissue engineering. A vast majority of them belongs to the polyesters like poly(lactide), poly(glycolide), and their copolymers. Among the wide polyester family, polyurethanes are one of the most popular group of biomaterials used for the development of medical devices, due to their versatility in chemical, physical and mechanical properties, and moderately good haemocompatibility and biocompatibility.

In tissue engineering applications, designing and fabrication of an optimum scaffold is a complex task. Depending on material properties, different manufacturing routes, and processing conditions have been utilized to fabricate three dimensional scaffolds for tissue engineering applications. In addition to other factors, these kinds of manufacturing routes, and processing conditions influence the surface texture, surface chemistry, crystallinity and microstructure of the resultant scaffolds which all influence the cell response. Beside the chemistry of the biomaterial, understanding of cell-substrate interactions is also important in the development of scaffolds for tissue engineering. The relationship of many cells with scaffold construction parameters influences expression of osteogenic factors. Parameters like fabrication factors, specifically scaffold design parameters including porosity, pore size, scaffold

interconnectivity, and mechanical strength (stiffness), may affect the osteogenic differentiation on scaffolds.

In the present study, an elastic lysine based poly(ester-urethane) (PEU) was synthesized. The resultant polymer was fully characterized in order to explore its suitability for tissue engineering applications. The polymer was assessed by fabrication smooth and micropatterned 2D film; and macroporous 3D structures. 3D structures were obtained by using traditional freeze drying and salt leaching techniques and advanced bioplotting technique.

Thermal analyses results demonstrated that 2D and 3D matrices were stable at body temperature and the synthesized polymer was suitable for melt processing. Tensile test and DMA analyses of PEU films indicated that the polymer was highly elastic and would be useful in low-temperature applications.

The 3D scaffolds had various pore sizes and porosity with different compressive modulus. The bioplotted scaffolds were obtained with almost uniform pore size, while freeze dried and salt leached scaffolds were obtained with inhomogeneous pore size distribution. The bioplotted scaffolds exhibited significantly higher compressive moduli than freeze dried and salt leached scaffolds due to stiffer nature of the bioplotted fibers. Freeze dried sponges were not evaluated for in vitro studies since they were not expected to support cell infiltration within the scaffolds because of their considerably low pore size and porosity.

In vitro culture tests were carried on both 2D and 3D structures. On 2D films effect of micropatterning and fibrinogen coating was evaluated in terms of osteoblastic function. Regardless of physical and chemical modification, PEU film surfaces demonstrated good compatability in terms of cell attachment and proliferation. Micropatterning on the film surfaces led to cell alingnment along the parallel grooves; however it did not

make any difference in the sense of osteoblastic differentiation. On the contrary, fibrinogen adsorption enhanced initial cell attachment and osteogenic activity.

Bioplotted and salt leached scaffolds were compared for their ability to promote osteogenesis of BMSCs. Alamar cell viability test showed that all scaffolds allowed cellular attachment, proliferation and osteogenic differentiation. Due to their higher pore size and interconnectivity, proliferation rate was higher on bioplotted scaffolds than that of salt leached scaffolds. Among the salt leached scaffolds, constructs with higher porosity (96%) showed better proliferation compared to constructs with lower porosity (85%) probably because of higher pore interconnectivity. SEM images demonstrated that the cells cultured on all 3D scaffolds showed good cell proliferation and mineralised extracellular matrix deposition. von Kossa staining results indicated that calcium deposition was more abundant on bioplotted scaffolds than on salt leached constructs. EDX results further supported the von Kossa staining of mineralization by qualitative and quantitative analysis of calcium and phosphate expression, with the highest calcium concentration measured on bioplotted scaffolds. It was concluded that the substrate stiffness of bioplotted scaffolds may have enhanced the osteogenic activity. As a result, all PEU based scaffolds, especially bioplotted ones possess a great potential for adhesion, proliferation and mineralization of osteoblasts and are promising for non-load bearing bone tissue engineering. However, it should be considered that substrate stiffness is an important parameter in osteoblastic differentiation. Therefore, both the underlying material and processing technique have a crucial interplay with each other and should be taken into consideration while designing a scaffold for bone tissue engineering applications.

In this study, it was shown that poly(ester-urethane) synthesized from lysinediisocyanate and polycaprolactone diol is a biocompatible polymer and can be shaped in different designs to form scaffolds. It was also shown that bone marrow stem cells can proliferate and differentiate forming osteoblasts and forming calcium

phosphate deposits on the scaffolds. The future studies should consider in vivo and further histological experiments in animals.

REFERENCES

[1] Penninger C.L., An investigation in the cellular mechanisms of bone remodeling using a hybrid cellular automation approach, PhD Thesis, University of Notre Dame, 2011.

[2] Hollinger J.O., Einhorn T.A., Doll B., Sfeir T., editors. *Bone tissue engineering*, CRC Press, Florida, 2005.

[3] http://classroom.burnet.txed.net/webs/bbarnett/upload/ap_ch_5_notes_bones.pdf (last visited on 7 July 2011)

[4] Wang X., Nyman J.S., Dong X., Leng H. *Fundamental Biomechanics in Bone Tissue Engineering.*Morgan & Claypool, Davis, 2010.

[5] Notelovitz M. Androgen effects on bone and muscle. *Science*, 77: 34-41, 2002

[6] Jäger I., Peter F. Mineralized Collagen Fibrils: A Mechanical Model with a Staggered Arrangement of Mineral Particles. *Biophysical Journal*, 79: 1737-1746, 2000.

[7] Murugan R., Ramakrishna S. Development of nanocomposites for bone grafting. *Composites Science and Technology*, 65: 2385-2406, 2005.

[8] Basu B., Katti D., Kumar A., ed., *Advanced Biomaterials: Fundamentals, Processing and Applications*, New Jersey, USA: John Wiley & Sons, 2009.

[9] M.D. Robert Proulx Heaney, M.D., G. Donald Whedon. *Encyclopædia Britannica*, 2011.

[10] Zysset P.K., Guo X.E., Ho C.E., Moore K.E., Goldstein S.A. Elastic modulus and hardness of cortical and trabecular bone lamellae measured by nanoindentation in the human femur. *Journal of Biomechanics*, 32: 1005-1012, 1999.

[11] Caplan A.I. Embryonic development and the principles of tissue engineering. *Tissue Engineering of Cartilage and Bone*, Gregory Bock and Jamie Goode, eds., Chichester, UK:, pp. 17-33, 2003.

[12] Wahl D.A., Czernuszka J.T. Collagen-hydroxyapatite composites for hard tissue repair. *European Cells and Materials*, 11: 43-56, 2006.

[13] Marquass B., Somerson J.S., Hepp P., Aigner T., Schwan S., Bader A., Josten C., Zscharnack M., Schulz R.M. A novel MSC-seeded triphasic construct for the repair of osteochondral defects. *Journal of Orthopaedic Research:Official Publication of The Orthopaedic Research Society*, 28: 1586-99, 2010.

[14] Gorokhovsky A.V., Cortes-Hernandez, D.A., Shcherbakova N.N. Composites from mixtures of potassium polytitanate and biocompatible glasses. *Glass and Ceramics*, 67: 358-360, 2011.

[15] Weiner S., Traub W. Organization of hydroxyapatite crystals within collagen fibrils. *FEBS Letters*, 206: 262-266, 1986.

[16] Landis W.J., Hodgens K.J., Arena J., Song M.J., McEwen B.F. Structural relations between collagen and mineral in bone as determined by high voltage electron microscopic tomography. *Microscopy Research and Technique*, 33: 192-202, 1996.

[17] Sasaki N., Matsushima N., Ikawa N., Yamamura H., Fukuda A. Orientation of bone mineral and its role in the anisotropic mechanical properties of bone—Transverse anisotropy. *Journal of Biomechanics*, 22: 157-164, 1989.

[18] Badylak S.F. The extracellular matrix as a scaffold for tissue reconstruction. *Seminars in Cellular and Developmental Biology*, 13: 377-383, 2002.

[19] Lutolf M.P., Hubbell J.A. Synthetic biomaterials as instructive extracellular microenvironments for morphogenesis in tissue engineering. *Nature Biotechnology*, 23: 47-55, 2005.

[20] Metcalfe A.D., Ferguson, M.W.J. Tissue engineering of replacement skin: the crossroads of biomaterials, wound healing, embryonic development, stem cells and regeneration. *Journal of the Royal Society, Interface/the Royal Society*, 4: 413-37, 2007.

[21] Fernandes H., Moroni, van Blitterswijk C. L., de Boer J. Extracellular matrix and tissue engineering applications. *Journal of Materials Chemistry*, 19: 5474, 2009.

[22] Lutter A.-H., Hempel U., Wolf-Brandstetter C., Garbe A.I., Goettsch C.,. Hofbauer L.C, Jessberger R., Dieter P. A novel resorption assay for osteoclast

functionality based on an osteoblast-derived native extracellular matrix. *Journal of Cellular Biochemistry*, 109: 1025-32, 2010.

[23] Allori W.S., Sailon AC., Biological basis of bone formation, remodeling, and repair-Part II: Extracellular matrix," *Tissue Eng Part B,* 14; 275–283, 2008.

[24] Eckstein F., Matsuura M., Kuhn V., Priemel M., Link T.M. Sex Differences of Human Trabecular Bone Microstructure in Aging Are Site-Dependent. *Journal of Bone and Mineral Research*, 22: 817-824, 2007.

[25] Stauber M., Müller R. Age-related changes in trabecular bone microstructures : global and local morphometry. *Osteoporosis International,* 17: 616-626, 2006.

[26] Bousson V., Peyrin F., Bergot C., Hausard M., Sautet A., Laredo J.-D. Cortical Bone in the Human Femoral Neck: Three-Dimensional Appearance and Porosity Using Synchrotron Radiation. *Journal of Bone and Mineral Research*, 19: 794-801. 2004.

[27] Mosekilde L. Age-related changes in bone mass, structure, and strength effects of loading. *Zeitschrift Fur Rheumatologie*, 59: 1-9, 2000.

[28] http://www.devicelink.com/news/100/2/27291.html (last visited on 7 July 2011).

[29] Stevens M.M. Biomaterials for bone tissue engineering, *Materials Today*, 11: 18-25, 2008.

[30] Hubbell J.A. Bioactive biomaterials. *Current Opinion in Biotechnology*, 10: 123-129, 1999.

[31] Bueno E.M., Glowacki J. *Biologic Foundations for Skeletal Tissue Engineering*, Davis, USA: Morgan & Claypool, 2011.

[32] Glowacki J., Mulliken J.B. Demineralized bone implants, *Clin Plast Surg*, 12: 233-241, 1985.

[33] Robertson P.A., Wray A.C. Natural history of posterior iliac crest bone graft donation for spinal surgery: a prospective analysis of morbidity. *Spine*, 26: 1473-1476, 2001.

[34] De Long W.G.D., Einhorn T.A., Koval K., Mckee M., Smith W., Sanders R., Watson T. Bone Grafts and Bone Graft Substitutes in Orthopaedic Trauma Surgery**,** A critical analysis. *J Bone Joint Surg Am,* **89:** 649-658, 2007.

[35] Saffarzadeh A., Gauthier O., Bilban M., Arc M. B. D., Daculsi G. Comparison of two bone substitute biomaterials consisting of a mixture of fibrin sealant (Tisseel) and MBCPt (TricOs) with an autograft in sinus lift surgery in sheep. *Clinical Oral Implants Research*, 20: 1133-1139, 2009.

[36] Bernhardt A., Lode A., Peters F., Gelinsky M. Novel ceramic bone replacement material Osbone in a comparative in vitro study with osteoblasts. *Clinical Oral Implants Research*, 22: 651-657, 2010.

[37] Aydin E., V. Hasirci. Biodegradable Hard Tissue Implants. *Journal of Siberian Federal University*,1: 3-17, 2010.

[38] Anderson J.M. Biological responses to materials. *Annual Review of Materials Research*, 31: 81-110, 2001.

[39] Williams D.F. *Definitions in Biocompatibility*, Amsterdam: Elsevier, 1987.

[40] Hench L.L., Wilson J., ed., *An Introduction to Bioceramics*, World Scientific, Singapore, 1993.

[41] Rakhorst G., Ploeg R.J., ed., *Biomaterials in Modern Medicine: The Groningen perspective*, London: World Scientific Publishing, 2007.

[42] Divisi D., Crisci R. Use of demineralized bone matrix and plate for sternal stabilization after traumatic dislocation. *Gen Thorac Cardiovasc Surg*, 59: 52-56,2011.

[43] Finkemeier C.G. Bone-Grafting and Bone-Graft Substitutes. *The Journal of Bone and Joint Surgery*, 84A: 454-64, 2002.

[44] Bella C.D., Dozza B., Frisoni T., Cevolani L., Donati D. Injection of Demineralized Bone Matrix With Bone Marrow Concentrate Improves Healing in Unicameral Bone Cyst. *Clinical Orthopaedics and Related Research*, 468: 3047-3055, 2010.

[45] Jayasuriya A.C., Æ.N.A. Ebraheim. Evaluation of bone matrix and demineralized bone matrix incorporated PLGA matrices for bone repair. *Journal of Materials Science: Materials in Medicine*, 20: 1637-1644, 2009.

[46] Lin H., Zhao Y., Sun W., Chen B., Zhang J., Zhao W., Xiao Z., Dai J. The effect of crosslinking heparin to demineralized bone matrix on mechanical strength and

specific binding to human bone morphogenetic protein-2. *Biomaterials*, 29: 1189-1197, 2008.

[47] Qiu Q.Q., Mendenhall H.V., Garlick D.S., Connor J. Evaluation of Bone Regeneration at Critical-Sized Calvarial Defect by DBM / AM Composite. *Journal of Biomedical Materials Research*, 81B: 516-523, 2007.

[48] Öztürk A., Yetkin H., Memis L., Cila E., Bolukbasi S., Gemalmaz C. Demineralized bone matrix and hydroxyapatite / tri-calcium phosphate mixture for bone healing in rats. *International Orthopaedics*, 30: 147-152, 2006.

[49] Peterson B., Whang P.G., Iglesias R., Wang J.C., Lieberman J.R. Osteoinductivity of Commercially Available Demineralized Bone Matrix: Preparations in a Spine Fusion Model. *J Bone Joint Surg Am*, 86A: 2243-50, 2004.

[50] Dorozhkin S.V. Calcium orthophosphates in nature, biology and medicine. *Materials*, 2: 399-498, 2009.

[51] Schieker M., Seitz H., Drosse I., Seitz S., Mutschler W. Biomaterials as Scaffold for Bone Tissue Engineering. *European Journal of Trauma*, 32: 114-124, 2006.

[52] Ogata K., Imazato S., Ehara A., Ebisu S., Kinomoto Y., Nakano T., Umakoshi Y. Comparison of osteoblast responses to hydroxyapatite and hydroxyapatite/soluble calcium phosphate composites. *Journal of Biomedical Materials Research. Part A*, 72: 127-35, 2005.

[53] Basu, B., Katti D., Kumar A., ed., *Advanced Biomaterial*s: Fundamentals, Processing, and Applications, New Jersey, USA: John Wiley & Sons, 2009.

[54] Hench L.L. Bioceramics: From Concept to Clinic. *Journal of the American Ceramic Society*, 74: 1487–1510, 1991.

[55] Le Guéhennec L., Layrolle P., Daculsi G. A Review of Bioceramics and Fibrin Sealant, *European Cells and Materials*, 8: 1-10, 2004.

[56] Demers C., Hamdy C.R., Corsi K., Chellat F., Tabrizian M. Natural coral exoskeleton as a bone graft substitute: a review. *Biomedical Materials and Engineering*, 12: 15-35, 2002.

[57] Wu Y.-C., Lee T.-M., Chiu K.-H., Shaw S.-Y., Yang C.-Y. A comparative study of the physical and mechanical properties of three natural corals based on the

criteria for bone – tissue engineering scaffolds. *Journal of Materials Science: Materials in Medicine*, 20: 1273-1280, 2009.

[58] Hejazi R., Amiji M. Chitosan-based gastrointestinal delivery systems. *Journal of Controlled Release*, 89: 151-165, 2003.

[59] Arinzeh T.L., Tran T.; Mcalary J., Daculsi G. A comparative study of biphasic calcium phosphate ceramics for human mesenchymal stem cell-induced bone formation. *Biomaterials*, 26: 3631-3638, 2005.

[60] Burg K.J.L., Porter S., Kellam J.F. Biomaterial developments for bone tissue engineering. *Biomaterials*, 21: 2347-2359, 2000.

[61] Tuan R.S., Boland G., Tuli R. Adult mesenchymal stem cells and cell-based tissue engineering. *Arthritis Research and Therapy*, 5: 32-45, 2003.

[62] Yucel D., Kose G.T., Hasirci V. Tissue engineered, guided nerve tube consisting of aligned neural stem cells and astrocytes. *Biomacromolecules*, 11: 3584-91, 2010.

[63] Ma P.X., Elisseeff J.ed. *Scaffolding in Tissue Engineering*, 2004.

[64] Sokolsky-Papkov M., Agashi K., Olaye A., Shakesheff K., Domb A.J. Polymer carriers for drug delivery in tissue engineering. *Advanced Drug Delivery Reviews*, 59: 187-206, 2007.

[65] Kuboki Y., Takita H., Kobayashi D., Tsuruga E., Inoue M., Murata M., Nagai N., Dohi Y., Ohgushi H. BMP-induced osteogenesis on the surface of hydroxyapatite with geometrically feasible and nonfeasible structures: topology of osteogenesis. *Journal of Biomedical Materials Research*, 39: 190-9, 1998.

[66] Lanza R., Langer R., Vacanti J.P., ed., *Principles of Tissue Engineering*, Burlington, MA: Elsevier Academic Press, 2007.

[67] Jin Q.M., Takita H., Kohgo T., Atsumi K., Itoh H., Kuboki Y. Effects of geometry of hydroxyapatite as a cell substratum in BMP-induced ectopic bone formation. *Journal of Biomedical Materials Research*, 52: 491-9, 2000.

[68] Vogt S., Larcher Y., Beer B., Wilke I., Schnabelrauch M. Fabrication of highly porous scaffold materials based on functionalized oligolactides and preliminary results on their use in bone tissue engineering. *European Cells and Materials*, 4: 30-8, 2002.

[69] Lin L., Tong A., Zhang H., Hu Q., Fang M. The Mechanical Properties of Bone Tissue Engineering Scaffold Fabricating Via Selective Laser Sintering. *Life System Modeling and Simulation*, 4689: 146-152, 2007.

[70] Mao, J., Mikos A.G., Gordana V.-N., Antala, A., ed., *Translational Approaches in Tissue Engineering and Regenerative Medicine*, Boston, Mass.; London: Artech House, 2007.

[71] Isikli C., Hasirci V., Hasirci N.Development of porous chitosan–gelatin/hydroxyapatite composite scaffolds for hard tissue-engineering applications. *Journal of Tissue Engineering and Regenerative Medicine*, 10.1002/term.46, 2011.

[72] Gunatillake P.A., Adhikari R. Biodegradable synthetic polymers for tissue engineering. *European Cells and Materials*, 5: 1-16, 2003.

[73] Santerre J.P., Woodhouse K., Laroche G., Labow R.S. Understanding the biodegradation of polyurethanes: from classical implants to tissue engineering materials. *Biomaterials*, 26: 7457-70, 2005.

[74] Oertel G. *Polyurethane Handbook*, Munich: Hanser Publishers, 1994.

[75] Hasirci N., Aksoy E.A. Synthesis and Modifications of Polyurethanes for Biomedical Purposes. *High Performance Polymers*, 19: 621-637, 2007.

[76] Nair L., Laurencin C. Biodegradable polymers as biomaterials. *Progress in Polymer Science*, 32: 762-798, 2007.

[77] Wheatley D.J., Raco L., Bernacca G.M., Sim I., Belcher P.R., Boyd J.S. Polyurethane: material for the next generation of heart valve prostheses? *European journal of cardio-thoracic surgery: official journal of the European Association for Cardio-thoracic Surgery*, 17: 440-8, 2000.

[78] Stokes K., Cobian K. Polyether polyurethanes for implantable pacemaker leads. *Biomaterials*, 3: 225-231, 1982.

[79] Gorman S.P., Jones D.S., Bonner, M.C., Akay M., Keane P.F. Mechanical performance of polyurethane ureteral stents in vitro and ex vivo. *Biomaterials*, 18: 1379-1383, 1997.

[80] Gogolewski S., Gorna K., Turner A.S. Regeneration of bicortical defects in the iliac crest of estrogen-deficient sheep, using new biodegradable polyurethane

bone graft substitutes. *Journal of Biomedical Materials Research Part A*, 77A: 802-810 ,2006.

[81] Huynh T.T., Padois K., Sonvico F., Rossi A., Zani F., Pirot F., Doury J., Falson F. Characterization of a polyurethane-based controlled release system for local delivery of chlorhexidinediacetate. *European Journal of Pharmaceutics and Biopharmaceutics.* 74: 255-264, 2010.

[82] Storey R.F., Wiggins J.S., Puckett A.D. Hydrolyzable poly(ester-urethane) networks from L-lysine diisocyanate and D,L-lactide/ε-caprolactone homo- and copolyestertriols. *Journal of Polymer Science Part A: Polymer Chemistry*, 32: 2345-2363, 1994.

[83] Han J., Chen B., Ye L., Zhang A.Y., Zhang J., Feng Z.G. Synthesis and characterization of biodegradable polyurethane based on poly(ε-caprolactone) and L-lysine ethyl ester diisocyanate. *Frontiers of Materials Science in China*, 3: 25-32, 2009.

[84] Guelcher S.A., Srinivasan A., Dumas J.E., Didier J.E., McBride S., Hollinger J.O. Synthesis, mechanical properties, biocompatibility, and biodegradation of polyurethane networks from lysine polyisocyanates. *Biomaterials*, 29: 1762-1775, 2008.

[85] Marcos-Fernandez A., Abraham G.A., Valentin J.L., San Roman J. Synthesis and characterization of biodegradable non-toxic poly(ester-urethane-urea)s based on poly(ε-caprolactone) and amino acid derivatives. *Polymer*, 47: 785-798, 2006.

[86] Ciardelli G., Rechichi A., Cerrai P., Tricoli M., Barbani N., Giusti P. Segmented polyurethanes for medical applications: synthesis, characterization and in vitro enzymatic degradation studies. *Macromolecular Symposia*, 169: 261-272, 2004.

[87] Gogolewski S., Gorna K. Biodegradable polyurethane cancellous bone graft substitutes in the treatment of iliac crest defects. *J Biomed Mater Res A.* 80: 94-101, 2007.

[88] Hafeman A.E., Li B., Yoshii T., Zienkiewicz K., Davidson J.M., Guelcher S.A. Injectable biodegradable polyurethane scaffolds with release of platelet-derived growth factor for tissue repair and regeneration. *Pharmaceutical Research*, 25: 2387-2399, 2008.

[89] Jian Z.Y., Chang J.K., Shau M.D. Synthesis and characterizations of new lysine-based biodegradable cationic poly(urethane-co-ester) and study on self-assembled nanoparticles with DNA. *Bioconjugate Chemistry*, 20: 774-779, 2009.

[90] Guelcher S.A. Biodegradable polyurethanes: synthesis and applications in regenerative medicine. *Tissue Eng Part B Rev.*, 14: 3-17, 2008.

[91] Zhang Y., Zhang M. Three-dimensional macroporous calcium phosphate bioceramics with nested chitosan sponges for load-bearing bone implants. *Journal of Biomedical Materials Research*, 61: 1-8, 2002.

[92] Grad S., Kupcsik L., Gorna K., Gogolewski S., Alini M. The use of biodegradable polyurethane scaffolds for cartilage tissue engineering: potential and limitations. *Biomaterials*, 24: 5163-5171, 2003.

[93] Cui T., Yan Y., Zhang R., Liu L., Xu W., Wang X. Rapid prototyping of a double-layer polyurethane-collagen conduit for peripheral nerve regeneration. *Tissue Eng Part C Methods*, 15: 1-9, 2009.

[94] Riboldi S.A., Sampaolesi M., Neuenschwander P., Cossu G., Mantero S. Electrospun degradable polyesterurethane membranes: potential scaffolds for skeletal muscle tissue engineering. *Biomaterials*, 26: 4606-4615, 2005.

[95] Kavlock K.D., Pechar T.W., Hollinger J.O., Guelcher S.A., Goldstein A.S. Synthesis and characterization of segmented poly(esterurethane urea) elastomers for bone tissue engineering. *Actabiomaterialia*, 3: 475-484, 2007.

[96] Baker S.C., Rohman G., Southgate J., Cameron N.R. The relationship between the mechanical properties and cell behaviour on PLGA and PCL scaffolds for bladder tissue engineering. *Biomaterials*, 30: 1321-1328, 2009.

[97] Mano J., Sousa R.A., Boesel L.F., Neves N.M., Reis R.L. Bioinert, biodegradable and injectable polymeric matrix composites for hard tissue replacement: state of the art and recent developments. *Composites Science and Technology*, 64: 789-817, 2004.

[98] Loh X.J., Peh P., Liao S., Sng C., Li J. Controlled drug release from biodegradable thermoresponsive physical hydrogel nanofibers. *Journal of Controlled Release*, 143: 175-182, 2010.

[99] Bruin P., Veenstra G.J., Nijenhuis A.J., Pennings A.J. Design and synthesis of biodegradable poly(ester-urethane) elastomer net- works composed of non-toxic building blocks. *Makromol Chem, Rapid Commun*, 9: 589-594, 1988.

[100] Braccini A., Wendt D., Jaquiery C., Jakob M., Heberer M., Kenins L., Wodnar-Filipowicz A., Quarto R., Martin I. Three-dimensional perfusion culture of human bone marrow cells and generation of osteoinductive grafts. *Stem Cells*, 23: 1066-1072, 2005.

[101] Pirraco R.P., Marques A.P., Reis R.L. Cell interactions in bone tissue engineering. *Journal of Cellular and Molecular Medicine*, 14: 93-102, 2010.

[102] Luu H.H., Song W.X., Luo X., Manning D., Luo J., Deng Z.L., Sharff K.A., Montag A.G., Haydon R.C., He T.C. Distinct Roles of Bone Morphogenetic Proteins in Osteogenic Differentiation of Mesenchymal Stem Cells. *Journal of Orthopaedic Research*, 25: 665-677, 2007.

[103] Basmanav F.B., Kose G.T., Hasirci V. Sequential growth factor delivery from complexed microspheres for bone tissue engineering. *Biomaterials*, 29: 4195-4204, 2008.

[104] Yilgor P., Hasirci N., Hasirci V. Sequential BMP-2 / BMP-7 delivery from polyester nanocapsules. *Journal of Biomedical Materials Research Part A*, 93: 528-536, 2010.

[105] Heinemann C., Heinemann S., Worch H., Hanke T. Development of an osteoblast / osteoclast co-culture derived by human bone marrow stromal cells and human monocytes for biomaterials testing. Eur Cell Mater. 21: 80-93, 2011.

[106] Nuttelman C.R., Tripodi M.C., Anseth K.S. Dexamethasone-functionalized gels induce osteogenic differentiation of encapsulated hMSCs. Journal of Biomedical Materials Research, 76: 183-195, 2006.

[107] Son E., Do H., Joo H.M, Pyo S. Induction of alkaline phosphatase activity by L - ascorbic acid in human osteoblastic cells: a potential role for CK2 and Ikaros. *Nutrition*, 23: 745-753, 2007.

[108] Otsuka E., Kato Y., Hirose S., Hagiwara H. Role of ascorbic acid in the osteoclast formation: induction of osteoclast differentiation factor with formation of the extracellular collagen matrix. *Endocrinology*, 141: 3006-3011, 2000.

[109] Mao J.J., Vunjak-Novakovic G., Mikos A.G., Atala A. ed. Scaffolds with designed architecture: Effect on Scaffold Function and Tissue Regeneration. *Translational Approaches in Tissue Engineering and Regenerative Medicine*, 2008.

[110] Liu X., Ma P.X. Polymeric scaffolds for bone tissue engineering. *Annals of Biomedical Engineering*, 32: 477-486, 2004.

[111] Meyer U., Wiesmann H.P., *Bone and Cartilage Engineering*, Springer, Münster, Germany, 2006.

[112] Lam C.X.F., Mo X.M., Teoh S.H., Hutmacher D.W. Scaffold development using 3D printing with a starch-based polymer *Materials Science and Engineering: C*, 20: 49-56, 2002.

[113] Sachlos E., Czernuszka J.T. Making tissue engineering scaffolds work. Review: the application of solid freeform fabrication technology to the production of tissue engineering scaffolds. *European Cells & Materials*, 5:29-40, 2003.

[114] Chung C., Burdick J.A. Engineering cartilage tissue. *Advanced Drug Delivery Reviews*, 60: 243 - 262, 2008.

[115] Mikos A.G., Bao Y., Cima L.G., Ingber D.E., Vacanti J.P., Langer R. Preparation of poly(glycolic acid) bonded fi ber structures for cell attachment and transplantation *J. Biomed. Mater. Res*, 27: 183-189, 1993.

[116] Kose G.T., Kenar H., Hasirci N., Hasirci V. Macroporous poly(3-hydroxybutyrate-co-3-hydroxyvalerate) matrices for bone tissue engineering. *Biomaterials*, 24: 1949-1958, 2003.

[117] Harris L.D., Kim B.S., Mooney D.J. Open pore biodegradable matrices formed with gas foaming. *J Biomed Mater Res*, 42: 396-402, 1998.

[118] Brien F.J.O., Harley B.A., Yannas I.V., Gibson L.J. The effect of pore size on cell adhesion in collagen-GAG scaffolds. *Biomaterials*, 26: 433-441, 2005.

[119] Ndreu A., Nikkola L., Ylikauppila H., Ashammakhi N., Hasirci V. Electrospun biodegradable nanofibrous mats for tissue engineering. *Nanomedicine*, 3: 45-60, 2008.

[120] Padeste C., Ozcelik H., Ziegler J., Schleunitz A., Bednarzik M., Yucel D., Hasirci V. Replication of high aspect ratio pillar array structures in

biocompatible polymers for tissue engineering applications. *Microelectronic Engineering*, 88: 1836-1839, 2011.

[121] Gomes M.E., Godinho J.S., Tchalamov D., Cunha A.M., Reis R.L. Alternative tissue engineering scaffolds based on starch : processing methodologies , morphology, degradation and mechanical properties. *Materials Science and Engineering: C*, 20: 19- 26, 2002.

[122] Yilgor P., Sousa R.A., Reis R.L., Hasirci N., Hasirci V. Effect of scaffold architecture and BMP-2/BMP-7 delivery on in vitro bone regeneration. *Journal of Materials Science. Materials in medicine*, 21: 2999-3008, 2010.

[123] Liulan L., Qingxi H., Xianxu H., Gaochun X., Design and Fabrication of Bone Tissue Engineering Scaffolds via Rapid Prototyping and CAD. *Journal of Rare Earths*, 25: 379-383, 2007.

[124] Hutmacher D.W., Sittinger M., Risbud M.V. Scaffold-based tissue engineering: rationale for computer-aided design and solid free-form fabrication systems. *Trends in Biotechnology*, 22: 354-362, 2004.

[125] Reignier J., Huneault M. Preparation of interconnected poly(ε-caprolactone) porous scaffolds by a combination of polymer and salt particulate leaching. *Polymer*, 47: 4703-4717, 2006.

[126] Giannatsis J., Dedoussis V. Additive fabrication technologies applied to medicine and health care: a review. *The International Journal of Advanced Manufacturing Technology*, 40: 116-127, 2007.

[127] Engelmayr G.C., Papworth G.D., Watkins S.C., Mayer J.E., Sacks M.S. Guidance of engineered tissue collagen orientation by large-scale scaffold microstructures. *Journal of Biomechanics*, 39: 1819-1831, 2006.

[128] Yilgor P., Sousa R.A., Reis R.L., Hasirci N., Hasirci V. 3D Plotted PCL Scaffolds for Stem Cell Based Bone Tissue Engineering. *Macromolecular Symposia*, 269: 92-99, 2008.

[129] Masood S.H., Singh J.P., Morsi Y. The design and manufacturing of porous scaffolds for tissue engineering using rapid prototyping. *International Journal of Advanced Manufacturing Technology*, 27: 415-420, 2005.

[130] Giordano R.A., Wu B.M., Borland S.W., Cima L.G., Sachs E.M., Cima M.J. Mechanical properties of dense polylactic acid structures fabricated by three dimensional printing. *J Biomater Sci Polym Ed*, 8: 63-75, 1996.

[131] Kim S.S., Utsunomiya H., Koski J.A., Wu B.M., Cima M.J., Sohn J., Mukai K., Griffith L.G., Vacanti J.P. Survival and Function of Hepatocytes on a Novel Three-Dimensional Synthetic Biodegradable Polymer Scaffold With an Intrinsic Network of Channels. *Annals of Surgery*, 228: 8-13, 1998.

[132] Yeong W.Y., Chua C.K., Leong K.F., Chandrasekaran M. Rapid prototyping in tissue engineering: challenges and potential. *Trends in Biotechnology*, 22: 643-652, 2004.

[133] Landers R., Mulhaupt R. Desktop manufacturing of complex objects, prototypes and biomedical scaffolds by means of computer-assisted design combined with computer-guided 3D plotting of polymers and reactive oligomers. *Macromolecular Materials and Engineering*, 282: 17-21, 2000.

[134] Bignon A., Chouteau J., Chevalier J., Fantozzi G., Carret J.P., Chavassieux P., Boivin G., Melin M., Hartmann D. Effect of micro- and macroporosity of bone substitutes on their mechanical properties and cellular response. *Journal of materials science. Materials in Medicine*, 14: 1089-1097, 2003.

[135] Zeltinger J., Sherwood J.K., Graham D.A., Mueller R., Griffith L.G. Effect of pore size and void fraction on cellular adhesion, proliferation, and matrix deposition. *Tissue Engineering*, 7: 557-572, 2001.

[136] Lu Q., Wang X., Lu S., Li M., Kaplan D.L., Zhu H. Nanofibrous architecture of silk fibroin scaffolds prepared with a mild self-assembly process. *Biomaterials*, 32: 1059-1067, 2011.

[137] Flemming R.G., Murphy C.J., Abrams G.A., Goodman S.L., Nealey P.F. Effects of synthetic micro- and nano-structured surfaces on cell behavior. *Biomaterials*, 20: 573-88 1999.

[138] Solchaga L.A., Gao J., Dennis J.E., Awadallah A., Lundberg M., Caplan A.I., Goldberg V.M. Treatment of osteochondral defects with autologous bone marrow in a hyaluronan -based delivery vehicle *Tissue Engineering*, 8: 333-347, 2002.

[139] Kenar H., Köse G.T., Hasirci V. Tissue engineering of bone on micropatterned biodegradable polyester films. *Biomaterials*, 27: 885-895, 2006.

[140] Hasirci N., Endogan T., Vardar E., Kiziltay A., Hasirci V. Effect of oxygen plasma on surface properties and biocompatibility of PLGA films. *Surface and Interface Analysis*, 42: 486-491, 2010.

[141] Walboomers X.F., Jansen J.A. Cell and tissue behavior on micro-grooved surfaces. *Odontology*, 89: 2-11, 2001.

[142] Lim J.Y., Hansen J.C., Siedlecki C.A., Runt J., Donahue H.J. Human foetal osteoblastic cell response to polymer-demixed nanotopographic interfaces. *Journal of the Royal Society, Interface*, 2: 97-108, 2005.

[143] Berry C.C., Campbell G., Spadiccino A., Robertson M., Curtis A.S. The influence of microscale topography on fibroblast attachment and motility. *Biomaterials*, 25: 5781-5788, 2004.

[144] Van Kooten T.G., Whitesides J.F., von Recum A. Influence of silicone (PDMS) surface texture on human skin fibroblast proliferation as determined by cell cycle analysis. *Journal of Biomedical Materials Research*, 43: 1-14, 1998.

[145] Park J., Berthiaume F., Toner M., Yarmush M.L., Tilles A.W. Microfabricated grooved substrates as platforms for bioartificial liver reactors. *Biotechnology and Bioengineering*, 90: 632-644, 2005.

[146] Kanamori Y., Sato J., Shimano T., Nakamura S., Hane K. Polymer microstructure generated by laser stereo-lithography and its transfer to silicon substrate using reactive ion etching. *Microsystem Technologies*, 13: 1411-1416, 2007.

[147] Mcbeath R., Pirone D.M., Nelson C.M., Bhadriraju K., Chen C.S. Cell Shape, Cytoskeletal Tension, and RhoA Regulate Stem Cell Lineage Commitment. *Dev Cell*, 6: 483-495, 2004.

[148] Su W.T., Chu I.M., Yang J.Y., Lin C.D. The geometric pattern of a pillared substrate influences the cell-process distribution and shapes of fibroblasts. *Micron*, 37: 699-706, 2006.

[149] Khang G., Lee S.J., Jeon J.H., Lee J.H., Lee H.B. Interaction of fibroblast cell onto physicochemically treated PLGA surfaces. *Polymer (Korea)*, 24: 869-876, 2000.

[150] Bhati R.S., Mukherjee D.P., Mccarthy K.J., Rogers S.H., Smith D.F., Shalaby S.W. The growth of chondrocytes into a fibronectin-coated biodegradable scaffold. *J Biomed Mater Res*, 56: 74-82, 2001.

[151] Prime K.L., Whitesides G M., Self-assembled organic monolayers: model systems for studying adsorption of proteins at surfaces. *Science*, 252: 1164-1167, 1991.

[152] Athanasiou K.A., Darling E.M., Hu J.C. *Articular Cartilage Tissue Engineering*, Davis, USA: Morgan & Claypool, 2010.

[153] Hasirci V., Tezcaner A., Hasirci N., Suzer S. Oxygen plasma modification of poly(3-hydroxybutyrate-co-3-hydroxyvalerate) film surfaces for tissue engineering purposes. *Journal of Applied Polymer Science*, 87: 1285-1289, 2003.

[154] Bumgardner J.D., Wiser R., Elder S.H., Jouett R. Contact angle , protein adsorption and osteoblast precursor cell attachment to chitosan coatings bonded to titanium. *J Biomater Sci Polym Ed.*, 14: 1401- 1409, 2003.

[155] Hasirci V., Tezcaner A. Yaszemski M.J., Trantolo D.J, Lewandrowski K., Hasirci V, Altobelli D.E., Wise D.L., ed. Surface Properties of Polymeric Biomaterials and Their Modification for Tissue Engineering Applications. *Tissue Engineering and Novel Delivery Systems,* CRC Press, 2003

[156] Hong S., Lin Y.C., Lin C.H. Crystallization and degradation behaviors of treated polyhydroxybutyrates," *Reactive and Functional Polymers*, 68: 1516-1523, 2008.

[157] Hassan M.K., Mauritz K.A., Storey R.F., Wiggins J.S. Biodegradable Aliphatic Thermoplastic Polyurethane Based on Poly (e-caprolactone) and L -Lysine Diisocyanate. *Journal of Polymer Science Part A-polymer Chemistry*, 44: 2990-3000, 2006.

[158] Yi J., Boyce M., Lee G., Balizer E. Large deformation rate-dependent stress – strain behavior of polyurea and polyurethanes. *Polymer*, 47: 319-329, 2006.

[159] D.M. Crawford, Bass R.G., Haas T.W. Strain effects on thermal transitions and mechanical properties of thermoplastic polyurethane elastomers," *Thermochimica Acta*, 323: 53-63, 1998.

[160] "Standard Guide for Assessing Microstructure of Polymeric Scaffolds for Use in Tissue Engineered Medical Products," *ASTM F2450 - 10*.

[161] Hing K.A. Bioceramic Bone Graft Substitutes: Influence of Porosity and Chemistry. *International Journal of Applied Ceramic Technology*, 2: 184-199, 2005.

[162] Hing K.A., Best S.M., Bonfield W. Characterization of porous hydroxyapatite. *Journal of Materials Science: Materials in Medicine*, 10: 135-145, 1999.

[163] Mistry M.A., Mikos A.G. Tissue engineering strategies for bone regeneration. *Adv Biochem Eng Biotechnol*, 94: 1-22, 2005.

[164] Eggli P.S., Müller W., Schenk R.K. Porous hydroxyapatite and tricalcium phosphate cylinders with two different pore size ranges implanted in the cancellous bone of rabbits. A comparative histomorphometric and histologic study of bony ingrowth and implant substitution. *Clinical Orthopaedics and Related Research*, 232: 127-138, 1988.

[165] Klawitter J. J., Hulbert S.F. Application of porous ceramics for the attachment of load bearing internal orthopedic applications. *Journal of Biomedical Materials Research*, 2: 161-229, 1971.

[166] Lu J.X., Flautre B., Anselme K., Hardouin P., Gallur A., Descamps M., Thierry B. Role of Interconnections in Porous Bioceramics on Bone Recolonization In Vitro and In Vivo. *J. Mater. Sci. Mater. Med.*, 10: 111-120, 1999.

[167] Sing K.S.W. International union of pure and applied chemistry reporting physisorption data for gas / solid systems with special reference to the determination of surface area and porosity. *Pure & Appl. Chem.* 54: 2201-2218, 1982.

[168] Calil M.R., Gaboardi F., Bardi M.A.G., Rezende M.L., Rosa D.S. Enzymatic degradation of poly (ε-caprolactone) and cellulose acetate blends by lipase and α-amylase *Polymer Testing*, 26: 257-261, 2007.

[169] Gan Z., Yu D., Zhong Z., Liang Q., Jing X. Enzymatic degradation of poly (ε-caprolactone)/ poly (dl-lactide) blends in phosphate buffer solution. *Polymer*, 40: 2859-2862, 1999.

[170] Gan Z., Liang Q., Zhang J., Jing X. Enzymatic degradation of poly(ε-caprolactone) film in phosphate buffer solution containing lipases. *Polymer Degradation and Stability*, 56: 209-213, 1997.

[171] Martins A.M., Pham Q.P., Malafaya P.B., Sousa R.A., Gomes M.E., Raphael R.M., Kasper F.K., Reis R.L., Mikos A.G. The role of lipase and alpha-amylase in the degradation of starch/poly(epsilon-caprolactone) fiber meshes and the osteogenic differentiation of cultured marrow stromal cells. *Tissue Engineering. Part A*, 15: 295-305, 2009.

[172] Zeng J., Chen X., Liang Q., Xu X., Jing X. Enzymatic degradation of poly(L-lactide) and poly(epsilon-caprolactone) electrospun fibers. *Macromolecular Bioscience*, 4: 1118-1125, 2004.

[173] Harley B.A., Leung J.H., Silva E.C., Gibson L.J. Mechanical characterization of collagen-glycosaminoglycan scaffolds. *Acta Biomaterialia*, 3: 463-474, 2007.

[174] Klein-Nulend J., Bacabac R.G., Mullender M.G. Mechanobiology of bone tissue. *Pathologie-Biologie*, 53: 576-580, 2005.

[175] Zhang J., Zhang H., Wu L., Ding J. Fabrication of three dimensional polymeric scaffolds with spherical pores. *Journal of Materials Science*, 41: 1725-1731, 2006.

[176] Pek Y.S., Wan A.C., Ying J.Y. The effect of matrix stiffness on mesenchymal stem cell differentiation in a 3D thixotropic gel. *Biomaterials*, 31: 385-391, 2010.

[177] Teixeira A.I., McKie G.A., Foley J.D., Bertics P.J., Nealey P.F., Murphy C.J. The effect of environmental factors on the response of human corneal epithelial cells to nanoscale substrate topography. *Biomaterials*, 27: 3945-3954, 2006.

[178] Clark P., Connolly P., Curtis A.S., Dow J.A., Wilkinson C.D. Topographical control of cell behaviour: II. Multiple grooved substrata. *Development*, 108: 635–644, 1990.

[179] Jeon H., Hidai H., Hwang D.J., Grigoropoulos C.P. Fabrication of arbitrary polymer patterns for cell study by two-photon polymerization process. *Journal of Biomedical Materials Research. Part A*, 93: 56-66, 2010.

[180] Hayes J.S., Khan I.M., Archer C.W., Richards R.G. The role of surface microtopography in the modulation of osteoblast differentiation. *European Cells and Materials*, 20: 98-108, 2010.

[181] Gil E.S., Park S.H., Marchant J., Omenetto F., Kaplan D.L. Response of human corneal fibroblasts on silk film surface patterns. *Macromolecular Bioscience*, 10: 664-673, 2010.

[182] Cairns M.L., Meenan B.J.,. Burke G.A, Boyd A.R. Biointerfaces Influence of surface topography on osteoblast response to fibronectin coated calcium phosphate thin films. *Colloids and Surfaces B: Biointerfaces*, 78: 283-290, 2010.

[183] Ardhaoui M., Nassiri M., Rubaei, M., Dowling D. Influence of water contact angle on cell adhesion on polystyrene surfaces. *Nanotech*, 2008.

[184] Bonewald L.F., Harris S.E., Rosser J., Dallas M.R., Dallas S.L., Camacho N.P., Boyan B., Boskey A. von Kossa staining alone is not sufficient to confirm that mineralization in vitro represents bone formation. *Calcified Tissue International*, 72: 537-547, 2003.

[185] Flanagan L.A., Ju Y.E., Marg B., Osterfield M., Janmey P.A, Neurite branching on deformable substrates. *Neuroreport*, 13: 2411-2415, 2002.

[186] Engler A., Bacakova L., Newman C., Hategan A., Griffin M., Discher D. Substrate compliance versus ligand density in cell on gel responses. *Biophysical Journal*, 86: 617-628, 2004.

[187] Chan B.P., Leong K.W. Scaffolding in tissue engineering : general approaches and tissue-specific considerations. *Biomaterials*, 17: 467-479, 2008.

[188] S.-M. Lien, L.-Y. Ko, and T.-J. Huang, "Effect of crosslinking temperature on compression strength of gelatin scaffold for articular cartilage tissue engineering," *Materials Science and Engineering:* 30: 631-635, 2010.

[189] E.G. and G.D. M. Trécanta, J. Delécrina, J. Royerb, "Mechanical changes in macro-porous calcium phosphate ceramics after implantation in bone," *Clinical Materials*, 15: 233-240,1994

APPENDIX A

CALIBRATION CURVE

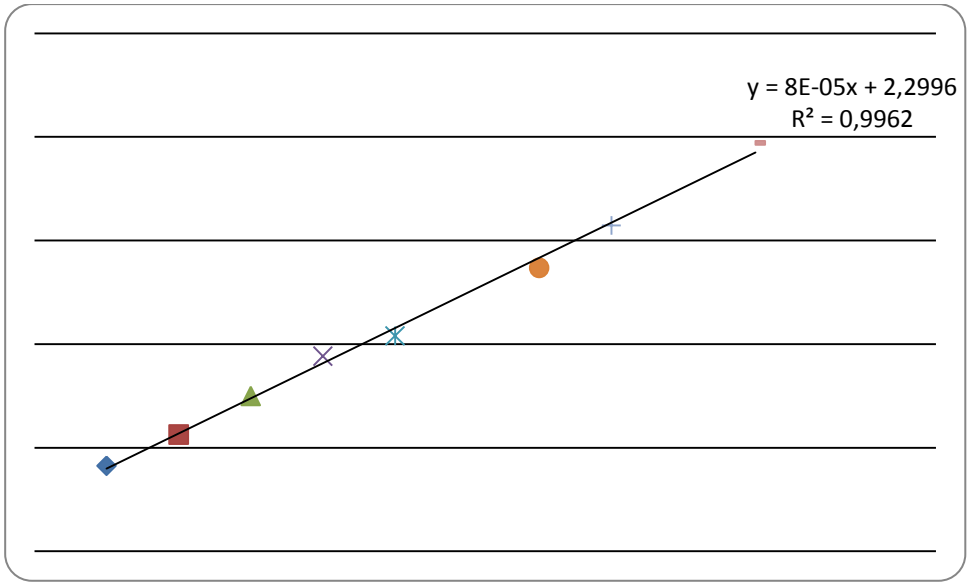

Figure A. 1. Calibration curve of BMSC with Alamar Blue assay

CURRICULUM VITAE

PERSONAL INFORMATION

Surname, Name: Kızıltay, Aysel

Nationality: Turkish Republic of Northern Cyprus, TRNC

Date and Place of Birth: 08 August 1976, Cyprus

Marital Status: Single

Phone: +90 312 210 76 14

Fax: +90 312 210 32 00

E-mail: e121000@metu.edu.tr, akiziltay@gmail.com

EDUCATION

Degree	Institution	Year of Graduation
MS	METU Biotechnology Dept.	2003
BS	Hacettepe University	1998
High School	Türk Maarif College	1994

FOREIGN LANGUAGES: Advanced English

ACADEMIC EXPERIENCE

Year	Place	Enrollment
2004-20011	METU, Department of Biotechnology, Biomaterial Research Lab	Full time Researcher
2009 (1 month)	Institute for Science & Technology in Medicine, Keele University, Hartshill Stoke-on-Trent, England	Visiting Researcher
2009 (1 month)	Department of Otorhinolaryngology, University of Ulm, Germany	Visiting Researcher
2006 (1 month)	3B's Research Group, Department of Polymer Engineering, Univ.Minho, Portugal	Visiting Researcher
2006 (1 month)	CSIC, Institute of Polymer Science and Technology, Madrid-Spain	Visiting Researcher
2000-2003	METU, Department of Biotechnology, Biomaterial Research Lab	Full time Researcher

PUBLICATIONS

1) N. Hasirci, T. Endogan, E. Vardar, **A. Kiziltay** and V. Hasirci. Effect of oxygen plasma on surface properties and biocompatibility of PLGA films. ***Surface and Interface Analysis*** 42: 486-491, 2010

2) M. A. Karahan, H. Kulacoglu, D. Seker, Z. Ergul, **A. Kiziltay**, D. Yilmazer, O. Captug, A. Yavuz, K. Serbetci,H. Bilgili, N. Hasirci. How safe is the use of prosthetic materials in the repair of abdominal-wall defects in malnourished subjects? ***Central European Journal of Medicine***. 4: 331-336, 2009

3) Dogan S., Demirer S., Kepenekci I., Erkek B., **Kiziltay A.** Hasirci N., Muftuoglu S., Nazikoglu A., Renda N., Dincer UD., Elhan A., Kuterdem E. Epidermal growth factor-containing wound closure enhances wound healing in non-diabetic and diabetic rats. ***International Wound Journal*** 6: 107–115, 2009

4) Uguralp S. , Akin M., Bay Karabulut A. , Harma B. , **Kiziltay A**., Kıran T. R. and Hasirci N. Reduction of peritoneal adhesions by sustained and local administration of epidermal growth factor , ***Pediatric Surgery International*** 24: 191-197, 2008

5) Karakayali F., Haberal N., Tufan H., Hasirci N., Basaran O., Sevmis S., Akdur A., **Kiziltay A**., Haberal M. Evaluation of Neointimal Hyperplasia on Tranilast-Coated Synthetic Vascular Grafts: An experimental Study. ***Journal of Investigative Surgery***, 20: 167-173, 2007

6) Ulubayram K., **Kiziltay A**., Yilmaz E., Hasirci N., Desferrioxamine release from gelatin based sytems. ***Biotechnology and Applied Biochemistry***, 42: 237-245, 2005

7) Uguralp S., Karabulut A. B., Mizrak B. , Kaymaz F., **Kiziltay A**. and Hasirci N. , The effect of sustained and local administration of epidermal growth factor on improving bilateral testicular tissue after torsion. ***Urological Research***,32: 323-331, 2004